Title
Design and Optimization of Monitoring and Feedback Systems in Wireless Health

Author
Rofouei, Mahsan

Publication Date
2012

Peer reviewed|Thesis/dissertation

UNIVERSITY OF CALIFORNIA
Los Angeles

Design and Optimization of Monitoring and Feedback Systems in Wireless Health

A dissertation submitted in partial satisfaction
of the requirements for the degree
Doctor of Philosophy in Computer Science

by

Mahsan Rofouei

2012

ABSTRACT OF THE DISSERTATION

Design and Optimization of Monitoring and Feedback Systems in Wireless Health

by

Mahsan Rofouei

Doctor of Philosophy in Computer Science

University of California, Los Angeles, 2012

Professor Majid Sarrafzadeh, Chair

The emergence of low cost micro-electronics and wireless systems has enabled the practical application of wearable monitoring systems that promote health and well-being of individuals. This area of research which is in the intersection of medical sciences and engineering is known as Wireless/Mobile Health. It uses the knowledge from medical sciences and employs low-cost micro-electronics and wireless systems along with powerful and sensor-rich handheld devices to enable a new dimension of health care which introduces pervasive monitoring and early diagnosis at low costs. Wireless Health introduces new opportunities to augment functional independence and daily activities of people with physical impairments, serve as monitoring and diagnostic devices and to perform feedback reinforcement. However, wearable medical systems are not yet in widespread use due to a variety of constraints including cost, energy, semantic complexity, required precision levels, reliability and many more. In this dissertation I will discuss challenges associated with design of such systems and develop new methods that can enable widespread use of these systems to address the recently growing demand of accessible health care services. Specifically, I will focus on the most significant challenges which are energy consumption and accuracy vs. cost of these systems.

Most wireless health systems are wearable and therefore operate on battery power. On the other hand, in order to enable real-time monitoring round the clock, long life-time is required. In this dissertation I will look at intelligent sampling and data aggregation strategies which are often tied

with application level understanding of the semantics of the system in order to minimize energy consumption. In addition, for these systems to be widely exploited in large populations, they need to be designed in-expensively and also sometimes even disposable due to hygiene constraints. But the main limitation is the precision levels required by these systems. I will look into this problem by either taking advantage of sensors already existing on hand-held devices that people carry with the addition of minimal add-ons or by using inexpensive material for system production but taking into account the inaccuracies at different levels of system design. The work in this dissertation can be described in the two categories of: (1) Sensor and algorithm design for medical monitoring systems that ubiquitously collect medical data; and (2) Feedback systems that could enforce awareness, deliver therapies in real-time and increase adherence to rehabilitation and medical instructions with minimal intrusion and cost.

The dissertation of Mahsan Rofouei is approved.

Mario Gerla

Michael J. Sinclair

Jennifer Wortman Vaughan

Alex Anh-Tuan Bui

Majid Sarrafzadeh, Committee Chair

University of California, Los Angeles

2012

To my parents Narges and Kazem

and my lovely brother Kasra

TABLE OF CONTENTS

LIST OF FIGURES

LIST OF TABLES

ACKNOWLEDGMENTS

I could not begin any other way but by expressing my gratitude to my parents Narges and Kazem. My parents, at a young age, afforded me an inspiring environment that helped me grow and instilled within me the desire to advance both in knowledge and in my contribution towards society. Despite the physical distance, they continued to be there for me, believing in me every step of my career. Their teachings and love for me continue to shape my goals in life, and I am forever grateful to have them be a part of my life. I also want to thank my younger brother Kasra for being a brother that I can always count on.

There were a number of exceptionally bright people in academia that provided a foil against which I grew-technically and creatively. At the head of the list is my adviser Prof. Majid Sarrafzadeh, to whom Id like to express my gratitude. I was honored and pleased to have worked under his supervision. His thoughts and comments, stemming from rich experience and vision in research, planted within me fruitful ideas and innovations. He taught me that innovation in research comes from within and by continuously challenging and questioning the limits of ones knowledge and understanding. Without his guidance my dissertation and ultimately my research would not have been possible.

I would also like to extend my appreciation to the following Ph.D. committee members for their guidance, insightful comments and feedback towards my research: Prof. Mario Gerla, Prof. Alex Bui, Prof. Jennifer Wortman Vaughan and Mike Sinclair (from Microsoft Research). Other UCLA faculty members were also an essential element in my career, helping me throughout my Ph.D. track: Prof. Zhuowen Tu and Prof. Kaiser. Among them Prof. Miodrag Potkonjak taught me many things and had an essential role in my Ph.D. research.

I would like to single out my mentor, role model and good friend Mike Sinclair of Microsoft Research (MSR). Mike exemplifies the true meaning of a research scientist. A great deal of my dissertation is owed to his guidance. I want to thank him for his continued support in my Ph.D. research, for mentoring me during my internship at MSR, for his patience, enthusiasm, and insights in knowledge. I consider him a role model both in character and research.

I would also like to thank the following people that believed in me and my abilities and provided

opportunities for me to grow during varying stages of my career: Prof. Zain Navabi for advising me in my undergraduate studies, Prof. Luca Benini for his continued support dating back to my research experience with him in Italy and Dr. Kristin Tolle who was the one that made my two internships at MSR possible.

I was also very fortunate to have the support and inspiration of my extended family. I would specifically like to thank my aunt Badri for her generous love and continued support, making me always feel like Im home. I was inspired by my uncle Ali Asghar Rofouei who was a figure of knowledge for me from my early childhood, my grandmother Fatemeh Madani who started to write fine poetry at the age of sixty and my aunt Nazli for her pure and everlasting love that taught me can overpower everything else in life.

Finally I would like to thank my friends who helped me both intellectually and emotionally during my Ph.D. program. I would like to especially thank Farshideh Kordi, Sedigheh Hashemi, Pardis Rofouei, Mohammad Ali Ghodrat, Pooya Monajemi, Khatereh Khodaverdi and my labmates: Foad Dabiri, Diane Myung-kyung Suh, Bobak Jack Razavi, Nabil Alshurafa, Zohreh Karimi, Hassan Ghasemzadeh and Ani Nahapetian.

VITA

2007	B.S. Computer Engineering , University of Tehran.
2007–2012	Teaching Assistant, Computer Science Department, University of California, Los Angeles (UCLA).
2007–2012	Researcher, Wireless Health Institute, University of California, Los Angeles (UCLA).
2009	M.S. Computer Science, University of California, Los Angeles (UCLA).
2009	Visiting Researcher , University of Bologna, Micrel Lab.
2010	Research Intern, Microsoft Research.
2011	Research Intern, Microsoft Research.

PUBLICATIONS

Mahsan Rofouei, Pooya Monajemi Mike Sinclair, Majid Sarrafzadeh, ”Arterial Pressure Pulse Palpation with the Haptic Lens”, IEEE International Conference on Biomedical and Health Informatics (BHI), 2012. Accepted for Publication.

Mahsan Rofouei, Mohammad Ali Ghodrat, Alfosono Martinez Nova, Miodrag Potkonjak, ”Optimization Intensive Energy Harvesting in Medical Shoes”, Design, Automation & Test in Europe Conference (DATE), 2012, pp. 272-275, 12-16.

Mahsan Rofouei, Andrew Wilson, A.J. Brush, Stewart Tansley, ”Your Phone or Mine? Fusing

Body, Touch and Device Sensing for Multi-User Device-Display Interaction", Proceedings of the 2012 ACM/SIGCHI Conference on Human Factors in Computing Systems (CHI), 2012. pp. 1915-1918.

Yiran Huang, Mahsan Rofouei, Majid Sarrafzadeh, "Automated Wolf Motor Function Test for Upper Extremities Rehabilitation", The 9th International Conference on Wearable and Implantable Body Sensor Networks (BSN), 2012. pp. 91-96. (Runner-up Best Paper Award)

Myung-kyung Suh, Ani Nahapetian, Jonathan Woodbridge, Mahsan Rofouei, Majid Sarrafzadeh, "Machine Learning-Based Adaptive Wireless Interval Training Guidance System", Journal on Mobile networks and applications (MONET), pp. 163-177. 2012.

Mahsan Rofouei, Majid Sarrafzadeh, Miodrag Potkonjak, "Detecting Local Events Using Global Sensing", IEEE Conference on Sensors , pp.1165-1168, 28-31 Oct. 2011.

Mahsan Rofouei, Majid Sarrafzadeh, Miodrag Potkonjak, "Energy Efficient Collaborated Sensing-based E-Textile Sensing", 2011 International Symposium on Low Power Electronics and Design (ISLPED), pp.339-344, 1-3 Aug. 2011.

Mahsan Rofouei, Mike Sinclair, Ray Bittner, Tom Blank, Nick Saw, "A Non-invasive Wearable Neck-cuff System for Real-time Sleep Monitoring", 8th International Conference on Body Sensor Networks (BSN), pp.156-161, 23-25 May 2011.

Mahsan Rofouei, Wenyao Xu, Majid Sarrafzadeh, "Computing with Uncertainty in a Smart Textile Surface for Object Recognition", IEEE International Conference on Multi-sensor Fusion and Integration for Intelligent Systems (MFI), pp. 174-179, 5-7 Sept. 2010.

Mahsan Rofouei, E. Farella, D. Brunelli, Majid Sarrafzadeh, Luca Benini, "Battery-Aware Power Management Techniques for Wearable Haptic Nodes", The Fifth International Conference on Body

Area Networks (BodyNets), pp. 227-232, 2010.

Diane Sue, Mahsan Rofouei, Ani Nahapatian, William Kaiser, Majid Sarrafzadeh, ”Optimizing Interval Training Protocols using Data Mining Decision Trees”, Sixth International Conference on Wearable and Implantable Body Sensor Networks (BSN), pp.318-323, 3-5 June 2009.

Mars Lan, Mahsan Rofouei, Stefano Soatto, Majid Sarrafzadeh, ”DWS: A Robust and Scalable Lane Departure Warning System for the Smartphones”, 12th International IEEE Conference on Intelligent Transportation Systems (ITSC), pp. 1-6, 4-7 Oct. 2009.

Mahsan Rofouei, Thanos Stathopoulos, Sebi Ryffel, William Kaiser, Majid Sarrafzadeh, ”Energy-Aware High Performance Computing with Graphic Processing Units”, Conference on Power Aware Computing and Systems (HOTPOWER), 2008.

Mahsan Rofouei, Maryam Moazzeni, Majid Sarrafzadeh, ”Fast GPU-Based Space-Time Correlation for Activity Recognition in Video Sequences” IEEE Workshop on Embedded Systems for Real-Time Multimedia (ESTImedia, part of ESWeek), pp.33-38, 23-24 Oct. 2008.

Foad Dabiri, Navid Amini, Mahsan Rofouei, Majid Sarrafzadeh, ”Reliability-Aware Optimization for DVS Enabled Real-Time Embedded Systems”, Proceedings of 9th International Symposium on Quality Electronic Design, (ISQED), pp.780-783, 17-19 March 2008.

CHAPTER 1

Introduction

The emergence of low cost micro-electronics and wireless systems has enabled the practical application of wearable monitoring systems that promote individual′s health. This area of research which is in the intersection of medical sciences and engineering is known as Wireless/Mobile Health. It uses the knowledge from medical sciences and employs low-cost micro-electronics and wireless systems along with powerful and sensor-rich handheld devices to enable a new dimension of health care that introduces pervasive monitoring and early diagnosis at low costs. Such systems introduce a new paradigm that significantly improve the quality of life for large segments of the population and enable conceptually new types of applications by engaging individuals in their own health care. Physicians will no longer need to rely solely on the information gathered through patient interviews and on-site observations, but now have the ability to gather data from the normal day to day routine of every aspect of daily life of the patient, further assisting disease diagnosis. Wireless Health systems merge data, medical knowledge, data presentation and wireless communication technologies to provide health care and medical services such as prevention, diagnosis, and rehabilitation outside of the traditional healthcare framework.

Wireless Health systems can augment functional independence and daily activities of people with physical impairments, disabilities, chronic diseases and the accumulative impairments associated with aging. These home-health and mobile-health technologies can serve as monitoring devices of health and activity, feedback reinforcement for risk factor management, and outcome measures for individual care and large clinical trials.

Figure 1.1 demonstrates the architecture of a Wireless Health system. The patient and the doctor interface with the system at two different ends. At one end, the patient communicates with the system through a set of sensors that gather several physiological signals from the person or

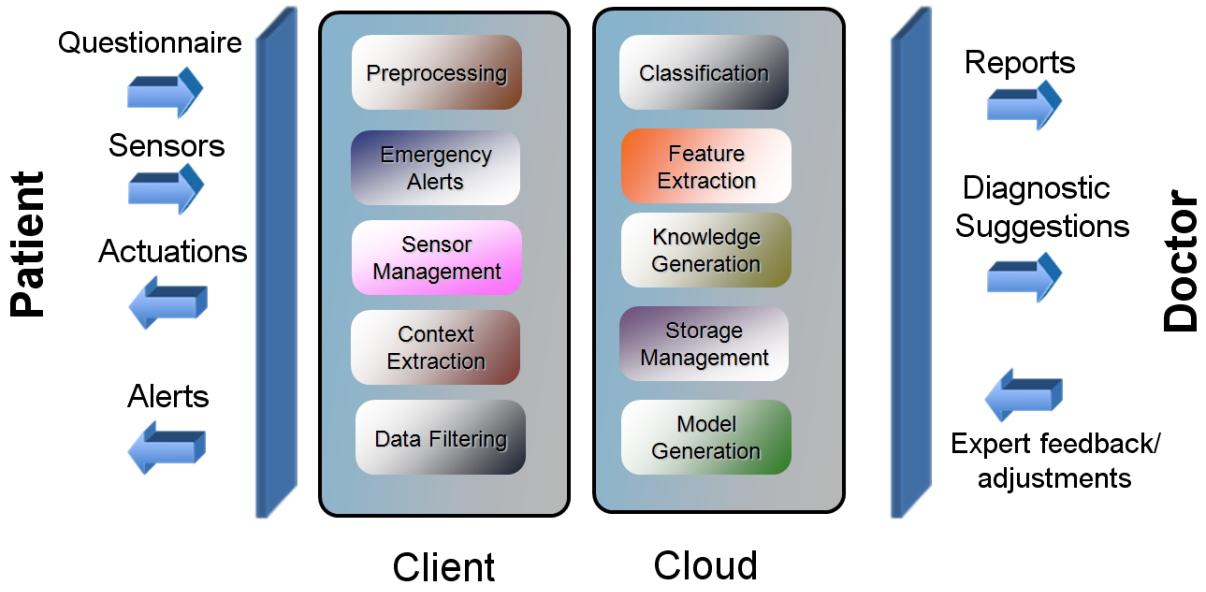

Figure 1.1: Wireless Health System Architecture

the environment around the person and short questionnaires that are usually answered through the patient's cell-phone. The patient receives feedback from the system in various forms such as alerts on their carry-on devices or actuations that provide a system for feedback reinforcement. On the other end, the doctor receives diagnostic suggestions in the form of reports from the system and enters his/her expert feedback or adjustments to the diagnostic suggestions back to the system if necessary.

The system itself is composed of two parts of client and server/cloud. Less computation intensive tasks such as preprocessing and data filtering is performed on the client part. Emergency alerts which need to be detected and reported in a timely manner are also processed on the client part. These alerts are reported to the patient or an emergency contact in the form of text messages or alarms. More computation intensive tasks such as model and knowledge generation, feature extraction and storage management are performed on the cloud.

It is worthy to mention that there is not a distinct line between the client and the cloud in wireless health systems. Different tasks might take place on either the client or the cloud based on system needs. In addition, not all wireless health systems have the two parts of client and cloud. Some systems where the amount of processing is insignificant and data is not stored are only composed of the client part.

However, wearable embedded sensing systems are not yet in widespread use. This is due to a variety of issues, including *system complexity*, *cost*, *energy*, *semantic complexity*, *required accuracy levels* and the need for *changes in consumer behaviour*. Limitations in processing power, battery life, communication bandwidth and memory constrain the applicability of existing complex medical analysis algorithms and require new methods and approaches to be proposed. For these systems to be widely exploited at communities and by large populations they need to become inexpensive but at the same time *accurate*, *reliable*, *secure* and *low power*.

This has motivated the work in this dissertation to develop new methods that can be used to serve the recently growing demand of low cost and widely accessible health care services. This work focuses on designing new end-to-end systems, from sensor design and data collection, to data analysis and data presentation to users in a ubiquitous way. The work in this dissertation can be described in the two categories of (1) Sensor and algorithm design for medical monitoring systems that ubiquitously collect medical data; and (2) Feedback systems that could enforce awareness, deliver therapies in real-time and increase adherence to rehabilitation and medical instructions with minimal intrusion and cost.

Designing low cost systems is also a major key technological constraint in designing systems. As mentioned, for these systems to be widely exploited at large populations, we need to design inexpensive systems that are sometimes even disposable due to hygiene constraints. But the main limitation is that these systems still need to provide accurate and reliable measurements. In this dissertation I look at methods that either take advantage of sensors already existing on hand-held devices with the addition of minimal add-ons or use inexpensive material for system production but takes into account the inaccuracies at different levels of system design.

In Chapter 2, I present an example of a system of Figure 1 to demonstrate the different components of a Wireless Health monitoring system. The Chapter describes a wearable neck-cuff system for sleep monitoring measuring multiple physiological parameters of the body.

Traditionally, early stages of diagnosis are performed by vision and/or sense of touch of doctors or even subjects themselves. More accurate evaluations are then performed with devices such a MRI and Ultrasound. The sense of touch is used by physicians in different diagnostic scenarios

to enhance their perception of a medical condition (palpation). It is used in palpating arteries, cysts, tumors, monitoring progress of medical conditions (such as thyroids) and etc. However palpation measurements are subjective and results may differ among different physicians and can change with experience. Chapter 3 describes efforts for quantifying the sense of touch by designing in-expensive, while accurate sensors and systems and developing new metrics and interactions techniques. It also demonstrates the use of the proposed method to enable Pulse Wave Analysis (PWA) which is the study of the waveform characteristics of pressure pulses and can provide diagnostic medical information.

Sensor-based medical systems are on a brink of revolutionizing many tasks in diagnosis, tracking, treatment, rehabilitation and many other medical activities. These systems provide unprecedented comprehensive and real-time data collection with high convenience and reliability. However as mentioned, one of the major obstacles for their more widespread application is energy supply. In Chapter 4 we propose a solution using energy harvesting for medical shoes. The approach presented in this chapter can also be adapted to other pressure-based monitoring systems.

Most of the wireless medical systems are wearable and therefore operate on battery power. On the other hand, in order to enable real-time monitoring round the clock, long life-time is required. This requires design of intelligent sampling and data aggregation strategies which is often tied with application level understanding of the semantics of the system. Focusing on medical features that are crucial in real-time monitoring and optimizing for detection of such events can result in energy efficient sampling strategies. Chapter 5 studies this problem in the design of Electronic Textile (E-Textile)-based wearable wireless health systems.

Recently technology enables us to weave computation, communication and memory into fabrics that look and feel like the fabric of clothing that we wear every day. E-Textile is an inexpensive composite yarn made of fibers coated with conductive polymer. This material enables the design and development of a wide range of pervasive systems that we have developed such as smart sheets used on beds or other surfaces such as chairs, garments, gloves, insoles in medical shoes and etc. In Chapter 5 I have looked at designing efficient sensor structures that would inherently minimize the number of samples required and therefore increase the life time of these systems. I have also looked at designing efficient sampling techniques that use the semantic knowledge about the

application to perform less and on-time samplings.

Finally, Chapter 6, focuses on designing and developing practical methods for providing feedback or guidance to individuals in the form of haptic feedback. Power minimization techniques are described that enable the practical use of these systems in home/mobile-based care.

CHAPTER 2

Sleep Monitoring: A Case Study for Medical Monitoring Systems

Sleep is clinically linked to several serious conditions including diabetes, obesity and a number of heart diseases [Mil07, Rei05]. Furthermore, sleep data such as from the respiratory system can be indicators of worsening in diseases such as Chronic Obstructive Pulmonary Disease (COPD). It is also true that Obstructive Sleep Apnea (OSA) in diabetes patients can be a severe complication [Aro09]. Despite this, gathering sleep data and tracking an individual's sleep has been mostly limited to sleep labs with high costs for limited time or hospitals for some severe cases.

In addition researchers have found correlations between sleep data and several diseases such as asthma, Alzheimer's disease, Chronic Heart Failure (CHF) and COPD [McC99, RJ79, McN00]. These findings have been possible through expensive tests and monitoring. Being able to monitor an individual's sleep continuously and at low-cost in a non-invasive method would benefit future advances in new findings and possibly enable earlier diagnosis of candidates of diseases. This would also enable knowledge on how lifestyle and environmental factors can affect sleep and sleeping disorders.

In this Chapter, a non-invasive platform for monitoring vital signs throughout sleep is presented. Here, I revisit the monitoring system Figure presented in Chapter 1 (See Figure 2.1).Here, the patient is interfaced with the system through a neckcuff. Our method is a multi-signal technique for monitoring sleep in which a set of physiological sensors are incorporated inside a soft neck-cuff and are recorded continuously. Data transmission is wireless via Bluetooth to either a Bluetooth enabled cell phone or a near-by desktop machine for ease and comfort to the wearer. Emergency situations such as not breathing, is detected on the client and alarm messages are gen-

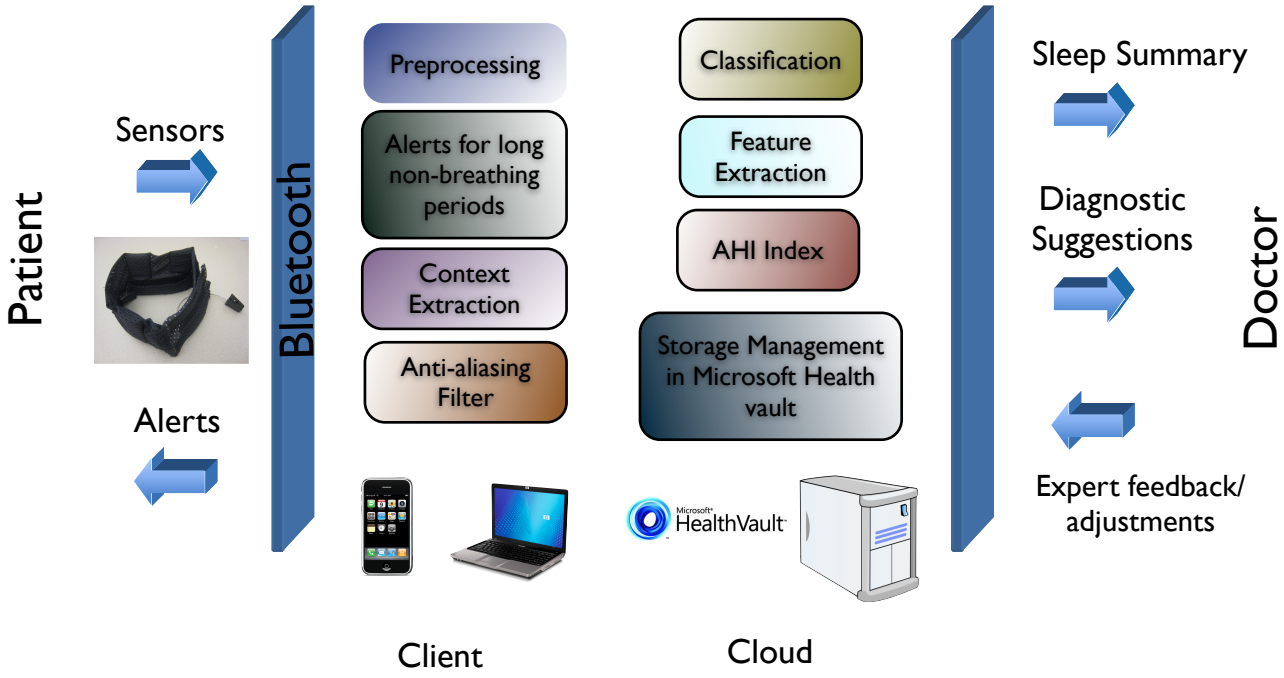

Figure 2.1: Sleep Monitoring System Architecture

erated. This information is then analyzed for detecting known sleep disorders and also stored to build a large database for further investigations such as data mining to establish a wellness baseline and possibly diagnosing other diseases. Data can also be uploaded on cloud services such as Microsoft HealthVault which is a secure platform for storing and maintaining health related information. Patients/clinicians have access to this data based on permission levels.

We have implemented the above-mentioned system and have tested it on a common sleep disorder: Obstructive Sleep Apnea (OSA). Currently 4% of the male and 2 % of the female adult population in the United States suffer from sleep apnea [sleep2].

People suffering from OSA have episodes of blocked breathing during sleep despite respiratory efforts. OSA is characterized by periods of interrupted breathing and reduced breathing (apnea and hypopnea). Each apnea event can last from seconds to minutes [Sle09]. These pauses in breathing must last at least 10 seconds to be considered an apnea event. Apnea events may occur 5 to 30 times an hour.

Individuals with sleep apnea are more prone to heart attacks and strokes relative to others. Symptoms of sleep apnea include depression, learning and memory difficulties, fatigue, poor con-

centration and daytime sleepiness. Untreated obstructive sleep apnea may lead to high blood pressure, cardiovascular diseases such as heart failure, stroke and heart arrhythmias. Therefore diagnosis of this disorder is critical.

The gold standard method for diagnosis of obstructive sleep apnea is overnight polysomnography (PSG) where the patient stays in a sleep laboratory while multiple sensors are attached to them. Many physiologic variables such as brain electrical activity, leg muscle movement, respiratory effort, airflow, heart rhythm, eye movement, oxygen saturation, etc. are monitored and recorded. This whole process is complex, time-consuming, costly and relatively invasive.

With the above mentioned neck-cuff we perform an early analysis of the sleep data to identify possible OSA candidates according to accepted standards. The system will provide a summary of possible apnea events detected and quantify the severity of sleep apnea and from that make recommendations if more accurate diagnosis is needed.

2.1 Related Work

Recently a range of systems have been developed for monitoring physiological variables with applications for medical, assisted living and sports by the means of physiological sensors. There has been some work done in the sleep context. Harada et al. use a single sensor approach to monitor respiration and body movement using a pressure sensor sheet laid under the pillow [HSM00a]. Nishida and Hori, use a different approach by building a living space shaped system with multiple sensors in furniture to monitor respiration and by analyzing breath curve estimate oxygen desaturation frequency [NH02].

In [YM09] the authors use an acoustic method using only tracheal sound and SpO2. They use a laptop to record and analyze the data connected to the sensors. [Sle99] uses a single signal analysis only using blood oximetery data to detect sleep apnea.

Based on the mentioned related works in this area, our contributions in this work can be listed as: (a) development of a non-invasive multi-signal platform for sleep monitoring and pre-diagnosis of sleep apnea; (b) development of an automatic system which will collect, save and upload sleep

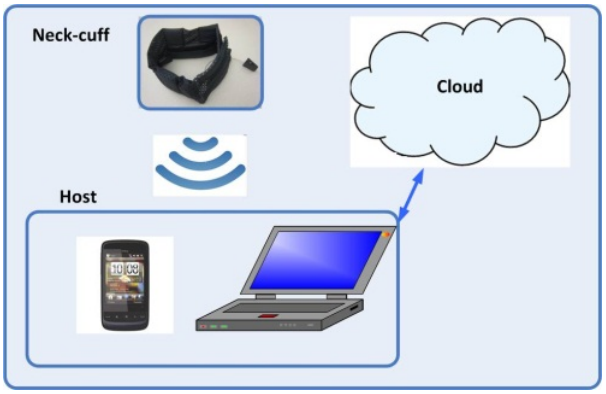

Figure 2.2: System Overview

data by the means of a Bluetooth enabled cell-phone, and (c) collecting a large set of sleep data for later investigation.

2.2 System Design

Below an overview of system architecture, the different sensing elements incorporated in the system and a demonstration of the visualization system are provided.

2.2.1 System Overview

Our platform is composed of several sensor nodes, a microprocessor and a Bluetooth transceiver arranged in a neck-cuff together with a cell phone or a desktop machine. The data from the cell phone or a laptop can be uploaded to a cloud, for data aggregation. This is depicted in Figure 2.2. Figure 2.3.a shows the neck-cuff system from outside- and against-user views and shows the different components of the system. These components are described in full detail in Section 2.2.2.

We use a low-power MSP430 micro-controller for collecting and pre-processing the data and transmitting it via a Bluetooth radio module. The operating voltage is 3.3v. The system is powered by a rechargeable 1000 mAh battery which allows the system to operate continuously for 9 hours. The Bluetooth module used in this design is the Roving Networks RN-41-SM.

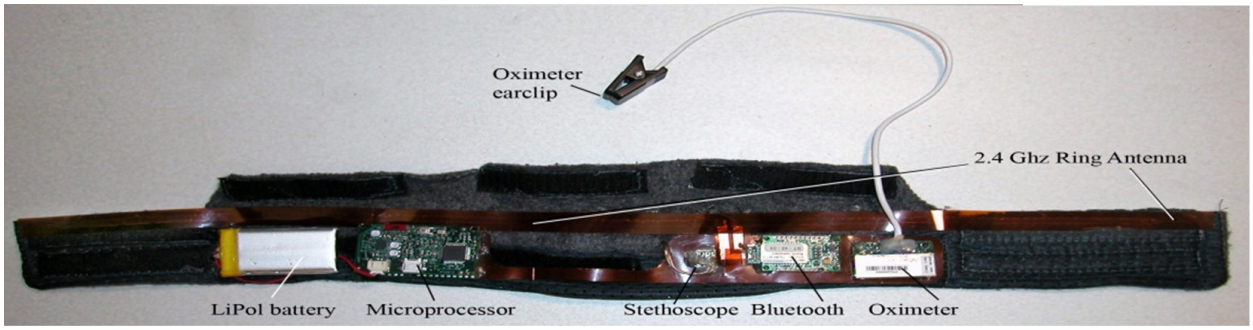

(a)

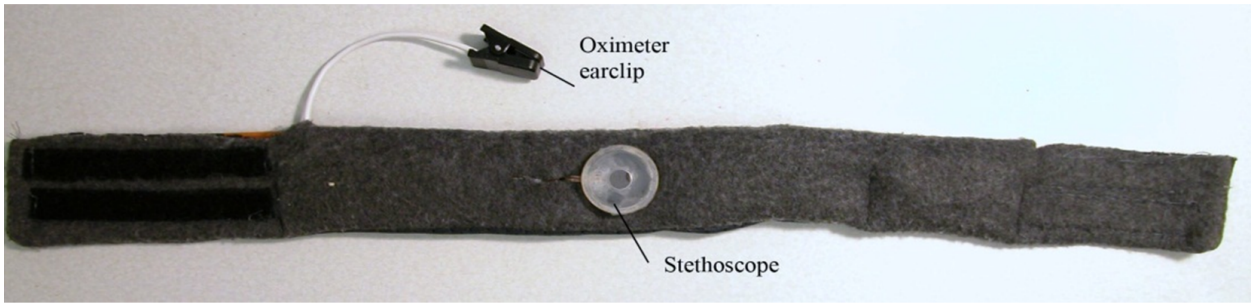

(b)

Figure 2.3: Neck-cuff (a) Outside-User View (b) Against-User View

2.2.2 System Components

Our sensing system is composed of the following components described in detail below. The arrangement of these components in the neck-cuff is shown in Figure 2.3.a.

2.2.2.1 Oximetry Sensor

Pulse oximetry is a non-invasive method which allows monitoring of the oxygen saturation level of the blood. It is placed on a thin translucent part of the body, usually a fingertip or an earlobe. Red and infrared light is alternately passed from one side to the other. The processed ratio of absorption of the red to infrared light determines the SpO2 value.

We use a pulse oximeter module model OEM III from Nonin [Sle] which takes continuous SpO2 and pulse rate (BPM) measurements from a sensor connected to a Nonin 8000Q earlobe transducer. The OEM III module is a low power device that is integrated in our neck-cuff system.

It sends a serial stream composed of SpO2 and BPM to the micro-controller. The sampling rate for the pulse oximeter is 1 Hz. The Nonin Oximeter with 8000Q earlobe sensor is company certified to be accurate to +/- 4 digits in SpO2 and +/- 3 BPM in pulse rate.

2.2.2.2 Microphone

We have integrated a small microphone with a large stethoscope-like diaphragm inside the neck-cuff which is placed against the neck and records breathing sounds. The data passes through an anti-aliasing filter at 1 KHz and the micro-controller samples this data at 2 KHz. The frequency of the optimal breath sounds we discovered is between 200 and 800 Hz. Frequency domain analysis is performed on the receiver side to capture this information and detect breathing. A low-power analog filter may be able to be used in future designs to lower the sample rate, record data size and power requirements. Figure 2.3.a shows the microphone which is visible from the back of the neck-cuff. This is done so that the microphone is placed with direct contact to the neck.

2.2.2.3 Accelerometer

Body movement can cause variation in the pulse oximetry readings [Mol93, Tob02]. Subjects go through many involuntarily movements throughout their sleep which affect the accuracy of the pulse oximetry readings and in turn the accuracy of our sleep analysis. With the use of an accelerometer we are able to detect most movements.

Other valuable information that can be extracted with the use of an accelerometer is the position of the head during each suspected OSA apnea event; whether the patient is lying on their back, left side or right side. The relationship between head position and apnea events is useful in the treatment of sleep apnea. We use a tri-axial analog accelerometer from Analog Devices: ADXL327 in the neck-cuff. The sampling rate for accelerometer data is 1 Hz.

2.2.2.4 Antenna

To maintain continuous communication between the Bluetooth neck-cuff antenna and a cell phone antenna, the neck-cuff antenna needs to provide omnidirectional radiation. Even though positioned just a few feet from the cell phone or PC, the antenna that is embedded on the Bluetooth module of the neck-cuff had many instances of lost connectivity throughout a sleeping event. This was due to the absorption of radiation from the lossy human neck depending on the orientation of the neck-cuff during sleeping. Therefore, an omnidirectional antenna which includes the neck will ensure the orientation of the individual sleeping will not have a major effect on the communication link. A suitable candidate is a circular loop antenna.

Since the operation of the neck-cuff does not allow a continuous loop antenna to be implemented, a circular dipole antenna is utilized instead. The first iteration of this antenna was simulated, designed, and constructed by placing two copper strips along the length of the neck-cuff that are connected to the signal and ground terminals of the circuit. The antenna has a gap in the area where the Velcro is used to keep the neck-cuff around the neck. Figure 2.4 shows an illustration of how the antenna performance was modeled using CST Microwave Studio, a 3D full-wave solver that solves for electromagnetic waves in the time domain. In this oversimplified model, the neck was modeled as a water body with a dielectric constant of 81. Since this antenna is a dipole instead of a circular loop, the radiation pattern will not exhibit complete omnidirectional characteristics. In addition, the neck, modeled as a lossy dielectric, contributes to the radiation pattern degradations as well. Nevertheless, this antenna implementation is better suited for this application than the smaller, factory installed antenna.

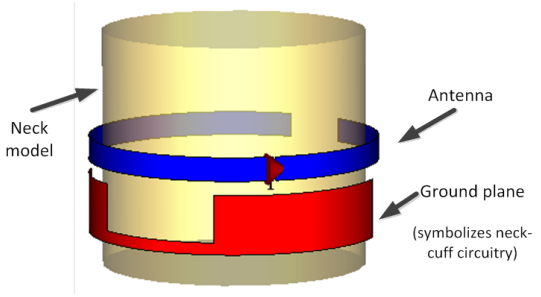

Figure 2.4: Illustration of Antenna Surrounding the Neck Model

2.2.3 Visualization

The sensor data from the neck-cuff system can be streamed to a number of standard personal devices such as cell phones, PDAs, or laptop/desktop computers. Based on application needs, we have defined different views of the system.

2.2.3.1 End-User View

In the end-user view which is displayed on the individual's cell-phone, the user would be able to see the status of the neck-cuff, e.g. if it is connected correctly and information about signal integrity of the oximeter module. The user will be notified by a beep sound if the sensors are not collecting good data so that the neck-cuff can be repositioned. In addition, sensor data is displayed for real-time monitoring. Figure 2.5 shows this view.

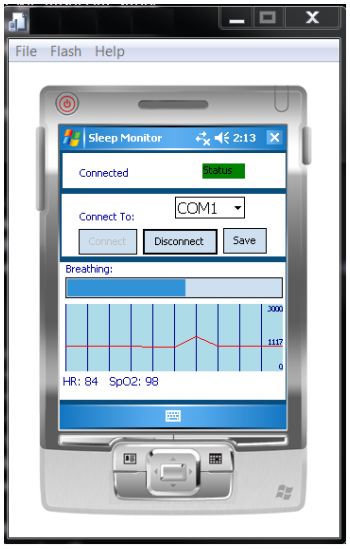

Figure 2.5: End-User View on a Mobile Phone

2.2.3.2 Clinician View

In the clinician view of the software, a clinician can access data of a specific sleep recording. Each sensor data is shown in its corresponding graph.

The clinician can zoom in/out to either view changes in a specific time/date or to view a whole

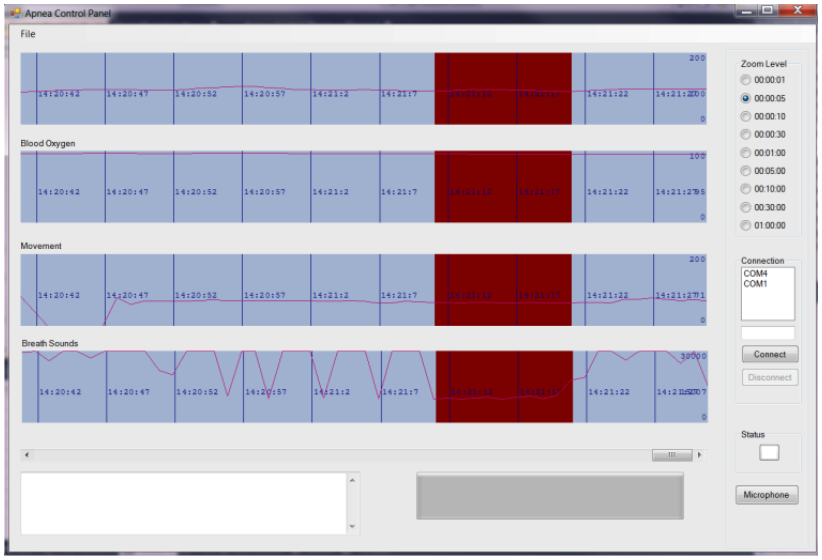

Figure 2.6: Clinician View

night. Apnea/hypopnea events detected by our system are highlighted on the graphs depicted in Figure 2.6. A sleep summary together with AHI measures (an accepted apnea index), time of events and head positioning are also listed.

2.3 Data Analysis

Apnea events are associated with drops of 4 % or more in oxygen saturation level and at least 10 seconds of cessation of air flow to the lungs. One of the common methods for measuring the severity of sleep apnea is Apnea Hypopnea Index (AHI). It is calculated as the total number of episodes of apnea and hypopnea during sleep, divided by the hours of sleep.

As described in Section III, we use a multi-signal method for probable sleep apnea detection. Figure 2.9 shows the steps of the data processing algorithm that detects events. Sound data is sampled at 2 KHz. This data is anti-aliased and sent to the host side. Frequency of breathing is different among people but based on our experiments falls between frequencies 200-800 Hz. Figure 2.7 shows a spectrogram of breathing and non breathing of an individual.

Therefore, to obtain each individual's breathing frequency, we perform a calibration phase on the first two minutes of recorded breath data. In the calibration phase we perform frequency domain

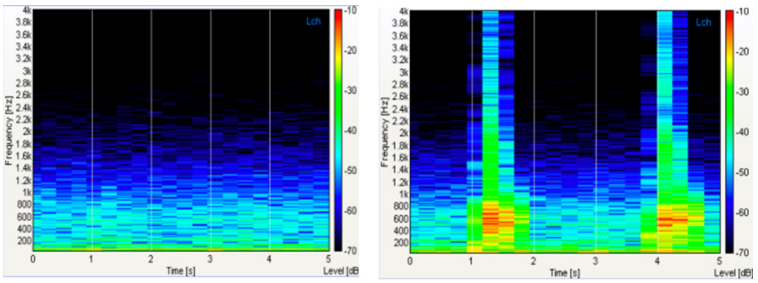

Figure 2.7: Spectogram Analysis on Sound Data (a) No Breathing (b) Breathing at Seconds 1 and 4

analysis to find breathing frequency and its energy level. We use this information to perform classification on the remaining sleep data. Sound data which has frequencies around the found breathing frequency with similar energy levels are classified as breathing. Higher energy levels indicate snoring or some vocalizing in sleep which is included in the sleep summary log.

Figure 2.8 shows breathing and non breathing periods for two subjects collected through our system. This figure shows how signal energy level and dominant frequency is different among subjects and the role of the calibration phase.

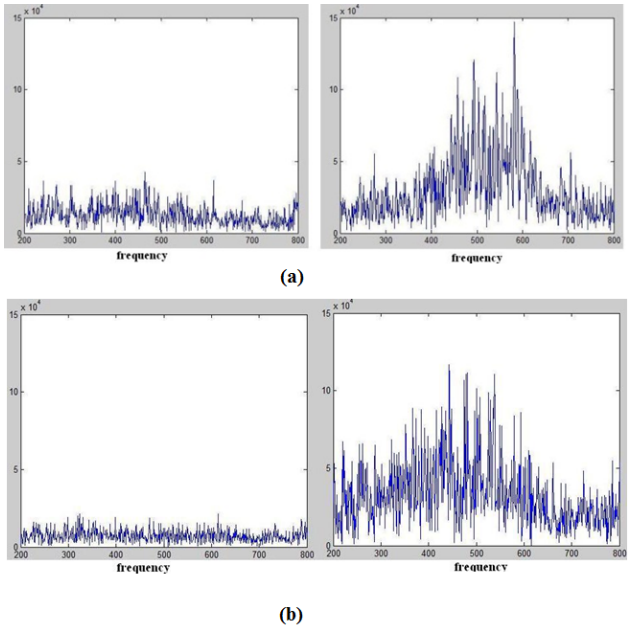

Figure 2.8: Frequency Domain Data of Two Subjects in Non-Breathing and Breathing States (a) Subject 1 (b) Subject 2

Different analysis is performed on SpO2 data to obtain apneas. A baseline for SpO2 data is

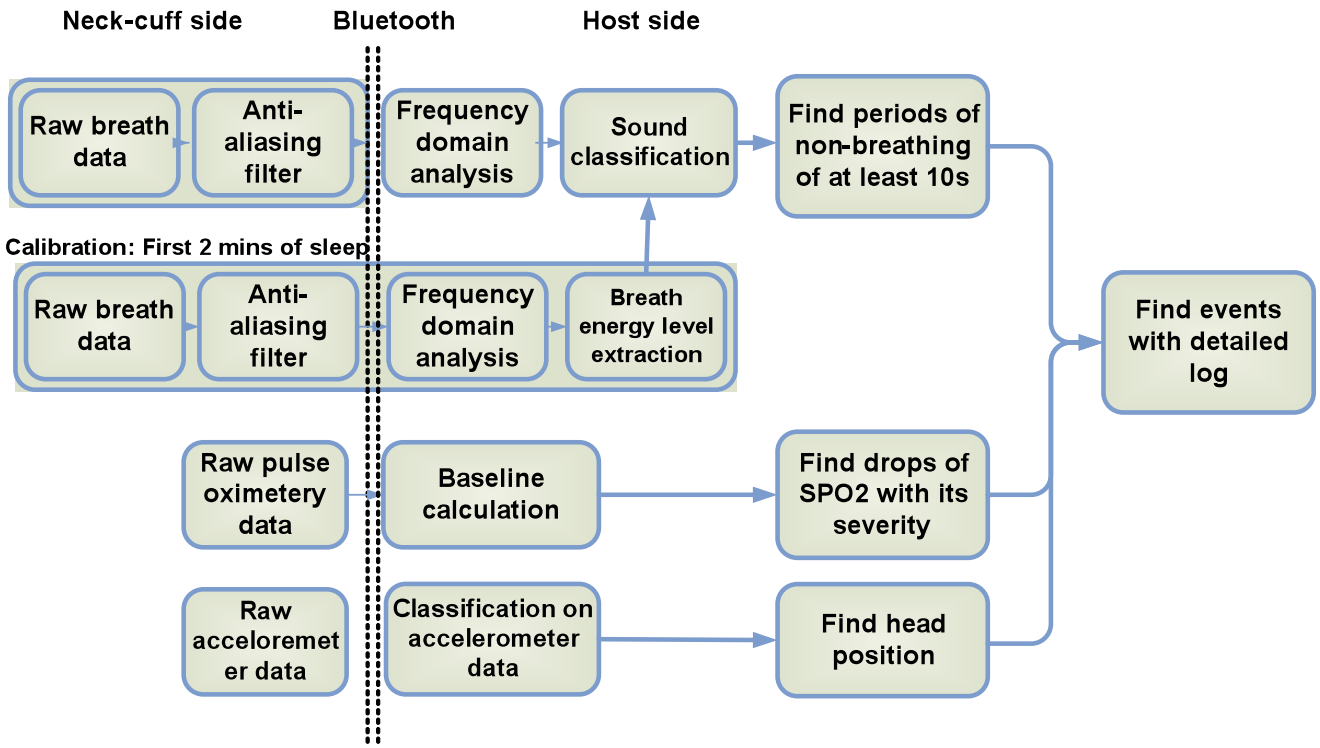

Figure 2.9: Signal Processing

evaluated. A baseline calculation is performed on a moving average window on the data. Any drop in SpO2 values below this baseline of a minimum of 4 % are recorded together with the amount of drop and also the duration. These parameters determine the severity of apnea events. Figure 2.10 shows a recorded drop in SpO2 readings of a subject.

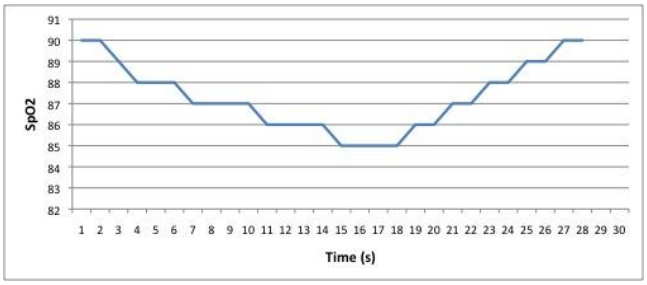

Figure 2.10: SpO2 Drop During an OSA Event

By computing acceleration magnitude from a three axis accelerometer, head movements can be captured and head position can be determined. Head position is classified into three poses of left, supine and right. In the case of an event, head position is recorded in the log. Figure 2.11 shows head positions of a subject through a session of data acquisition.

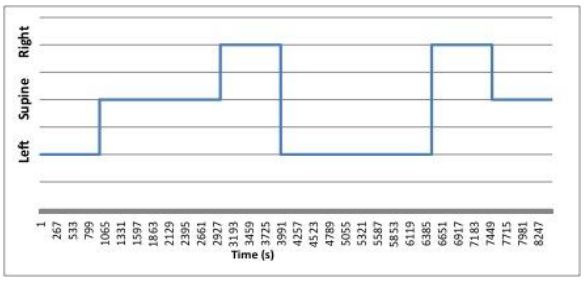

Figure 2.11: Head Position Classification using Accelerometers

In the next stage, all sensor data analysis is combined to determine events. Any changes in oximetry values that coincide with a movement are eliminated. This phase would remove most false positives in our detection mechanism. Then all drops of 4% or more in oxygen saturation level which coincide with non-breathing periods of at least 10 seconds are recorded as apnea events. An AHI index is calculated. Exact time of apnea event, duration, amount of drop in SpO2 and head position during the event of apnea is recorded in the summary.

2.4 Experimental Results

An AHI index of 5-15 typically categorizes mild OSA; 15-30 indicates moderate OSA while AHI index of more than 30 is an indication of severe OSA. Three volunteer subjects wore the neck-cuff overnight at their homes for sleep monitoring. The result of the OSA evaluation together with AHI indexes is presented in Table 2.1.

Table 2.1: Sleep Diagnosis Results

Subject	**AHI**	**Apnea**
1	23	Moderate OSA
2	2	No OSA
3	6.5	Mild OSA

In addition, subject 1 previously went through a full-night PSG study. The result of the full-night PSG also indicated moderate OSA with an AHI score of 29. This was the only system-wide ground truth we had access to in addition to the stated accuracies of the sensors. Table 2.2 shows part of the sleep summary of the system for subject 1. In the sleep summary, information on exact

time of events is provided. Information such as amount of drop in SpO2 value, duration of non breathing event which is useful in determining the severity of events, is also provided.

Table 2.2: A Section of Sleep Summary Information for Subject 1

Event	**Non-breathing period(s)**	**Amount of SpO2 drop %**	**Time of Event**	**Body Position**
1	12	8	22:42:45	Supine
2	20	6	22:50:24	Left
3	12	7	22:52:35	Left
4	15	4	23:00:15	Left

2.5 Conclusions

In this Chapter we developed a non-invasive wearable neck-cuff system which is capable of performing real-time monitoring and visualization of sleep data. The system is composed of several physiological sensors integrated in a comfortable soft neck-cuff which is worn by the patient in their home during sleep. Sleep data is sent wirelessly via Bluetooth to a nearby cell phone for processing and storage. This data is useful for sleep disorder analysis, disease candidate selection and building a collection of sleep data used for further analysis and to establish a wellness baseline. We demonstrated the use of the neck-cuff system in the possible detection of obstructive sleep apnea.

CHAPTER 3

Methods for Quantifying Medical Diagnosis Through Palpation

The sense of touch is used by physicians in different diagnostic scenarios to enhance their perception of a medical condition. It is used in palpating arteries, cysts, tumors, monitoring progress of medical conditions (such as thyroids) and etc. However palpation measurements are subjective and results may differ among different physicians and can change with experience. In this chapter I have looked at designing new sensor systems that would enable quantifying the sense of touch in a stable and accurate manner.

Designing low cost systems is also a major key technological constraint in designing wearable medical systems. For these systems to be widely exploited at large populations, inexpensive systems that are sometimes even disposable due to hygiene constraints need to be designed. The main limitation in designing low cost medical systems is their need for producing accurate and reliable measurement. This can be solved by either taking advantage of sensors already existing on hand-held devices that people carry with the addition of minimal add-ons or using inexpensive material for system production but takes into account the inaccuracies at different levels of system design.

Vision-based systems provide the advantage of increasing sensor density to pixel level and also provide the opportunity of reusing on-device camera sensors available now days on nearly all hand-held phones. I show that our system can be constructed with the addition of an inexpensive add-on part to mobile phones equipped with camera.

3.1 Quantifying Palpation

The sense of touch is used by physicians to diagnose and understand medical conditions in various scenarios. This procedure is called Palpation. Palpation is used as part of the physical examination

to determine the spatial coordinates of an anatomical landmark, assess tenderness through tissue deformation and determine size, shape, firmness or location of an abnormality in the body through the tactile sensing of elasticity modulus differences. It can be used in finding tumors, arteries, moles, etc. It can also be used to diagnose edema and to measure pulses.

However, palpation is a subjective procedure which can be extremely dependant on the level of expertise of the physician performing it. The results of palpation are not necessarily consistent over multiple measurements by the same physician. All these make this procedure prone to error. In order to enable consistent tactile measurements and provide quantifiable data, we propose devices and accompanying software that are able to capture and demonstrate the sense of touch (haptics) in a quantifiable manner. Such systems have many applications from medical diagnosis to aid in teaching palpatory diagnosis, tele-medicine and medical documentation. We will provide more detail on different applications of such systems in Section 3.2.

The goal is to design low cost devices that enable real-time visualization and processing of the haptic sense of elastic modulus boundaries. This modulus is essentially the tissue deformation caused by a specific force. Within the system, images are captured that describe the 3D position and movement of underlying tissue during the application of a known force - essentially what a physician feels through manual palpation.

Our proposed device and supporting software enable the visualization and documentation of the equivalent of 3D tactile input from a known applied force. This system can eliminate the subjective analysis of physical palpation examinations and give more accurate and repeatable results, yet is much less expensive to implement than MRI, ultrasound or similar techniques. The proposed system enhances the information obtained during physical examination by transforming this qualitative exam into a quantitative diagnostic procedure. The force and displacement data collected with the proposed system can be used to model the actual tissue displacements encountered during the palpation examination.

Based on the mentioned advantages of such a device, it is important to design a device which captures accurate information that the haptic sense of human administered palpation would. In this chapter we describe two systems that would enable this, in a non-invasive, low cost and easy to

use and learn approach. We also provide a case study of use of this device for pulse palpation in detecting arterial pressure pulses. There are many methods for measuring the 3D topography of a surface. Recently, optical techniques have become widely used. Gelsight [JA09] is an example of an optically based sensor for acquiring microscopic texture and shape.

3.2 Applications of Quatifying Palpation

The range of applications that would benefit from quantifiable measurements of the sense of touch is not limited to medical. Such systems have potential applications in various domains such as designing natural human computer interfaces. However, the main focus of this thesis is on medical applications of such systems. In addition to the mentioned goal of the system to provide quantitative measurements of palpation to enhance the diagnostic procedure for example for palpating masses such as cysts and abnormalities for cancer detection and assessment of Thyroid [RSS07], the proposed system can also be used for the below applications:

3.2.1 Teaching Medical Palpatory Diagnosis

An important application of such devices is in teaching medical palpatory diagnosis. Recently, new haptic technology is becoming promising in medical training. As an example the Virtual Haptic Back (VHB) is a virtual reality tool of the human back for teaching clinical palpatory diagnosis [HL4]. With the help of devices that would quantify the sense of touch, less experienced physicians or medical students can enhance their palpation perception by comparing their assessments with accurate quantitative assessments.

3.2.2 Arterial Pressure Pulse Palpation

An Arterial Pressure Pulse waveform is considered to be a fundamental indicator for diagnosis of several cardiovascular diseases. An arterial pulse waveform can be acquired by palpation on different areas on the body such as finger, wrist, foot and neck. Different features of the waveform such as shape can be indicators of specific conditions. For example it can indicate the decrease in

the compliance of small arteries and the elasticity of blood vessel wall [Zho94]. The waveform acquired by palpation is considered to offer more information than the single pulse waveform from an electrocardiogram (ECG) [Xu08]. In addition, pulse palpation has been used as a fundamental diagnostic method in Traditional Chinese Medicine (TCM) [Xu08]. Diagnostic features such as width, strength (amplitude), pulse rate, pulse length and shape (amplitude vs. time) variations can be extracted through pulse palpation on a location situated next to the prominent bone on the wrist.

3.2.3 Telemedicine

Haptic sensing devices can also help move towards virtual palpation. Such systems can be used to develop applications such as remote diagnosis of medical conditions for use in rural locations. The practitioner at the rural facility can palpate the patient using the proposed device. The data is transmitted to a medical center where experienced physicians are available. A physician can then observe the 3D constructed image of the palpated surface. In addition, haptic surfaces can be constructed using actuators to simulate the change in the surface so that the physician has the ability to feel what the practitioner felt while palpating.

3.2.4 Medical Documentation

Data processed in addition to captured images are a good means for documentation for patient records and recording medical assessments. This way, physicians may also be able to objectively measure change over time by comparing past data. By incorporating image registration techniques [Bro92], accurate assessment of change over time is possible. Physicians can also share extracted features of abnormalities, etc. together with captured images and data among other physicians for further research.

3.3 Medical Palpation Systems

In this section we propose two devices and associated algorithms that can be used for quantifying the sense of touch. We provide these systems in two categories. The first category provides a more

accurate method for quantifying touch but requires more complex settings. In the second category, we propose a system that provides the same functionality but use simpler systems which are easy to build and can be used by individuals in simpler settings. We also show how the second category of devices can be built on mobile phones. The choice of system is based on application requirements such as accuracy, portability and etc.

3.3.1 Photometric Stereo-based Approach

Photometric stereo is a method for estimating local surface orientation by using multiple images taken from the same viewpoint but under different illumination directions [Woo92]. We use this method to design and develop a system that can perform 3D reconstruction of the shape of objects pressed against it. Different elements that compose this device are: 1) A deformable membrane 2) Camera 3) Multiple LED light sources 4) Micro-controller (See Figure 3.1).

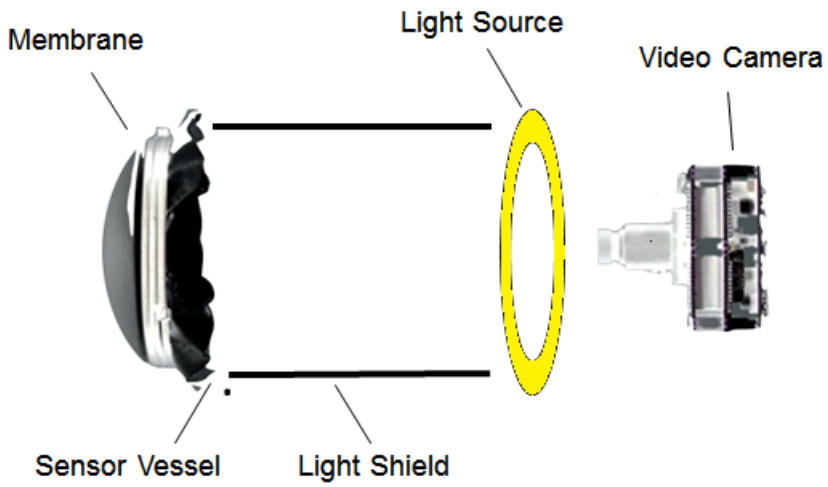

Figure 3.1: Photometric Stereo-Based Approach

The idea is to capture multiple images while holding the viewing direction constant with different light sources to reconstruct the 3D shape of the object pressed against the membrane of the system. An object of interest is pressed against the membrane and multiple images with different light sources on, are taken consecutively by the camera. The micro-controller is in charge of turning on/off LEDs consecutively and grabbing images for each light source. In our current prototype, eight light sources are used; however this method will work with a minimum of three light sources.

More images would enable more accurate shape reconstruction.

In this method the change of the intensities in the images depends on both local surface orientation and illumination direction. In taking multiple images with different lighting directions, since there is no change in imaging geometry, all picture elements (x,y) correspond to the same point in all images. The effect of changing light direction is to changing the reflectance map. Therefore surface orientations and albedos can be estimated uniquely from three images assuming a Lambertian surface. This is shown in Equation 3.1.

$$I_1(x, y) = R_1(p, q)I_2(x, y) = R_2(p, q)I_3(x, y) = R_3(p, q) \tag{3.1}$$

In diffuse reflections the above equations can be written as $I = k_d N.L$ where k_d is the albedo. With more number of light sources the reconstruction results are more accurate. In our current prototype shown in Figure 1 we use 8 light sources arranged in equal distances from each other.

In order to show how the system works, we demonstrated the functionality of the system on reconstructing a plate with 4 equal spheres placed within equal distances. This slide is shown in Figure 3.2.

Figure 3.2: A 4-Sphere Plate

The result of the implemented photometric stereo 3D reconstruction is shown in Figure 3.3.

3.3.2 Single Light Source Approach

The photometric stereo based approach described in the previous part, provides an accurate way to reconstruct 3D surfaces produced by objects pressed by the membrane of the system. In this section we describe another approach which provides a simpler way for palpation: the Haptic

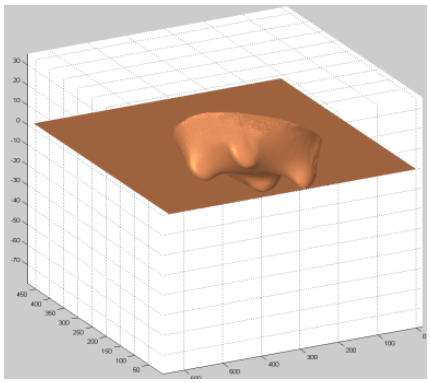

Figure 3.3: Photometric Stereo Surface Reconstruction on a 4-Sphere Plate Pressed Against the Membrane

Lens [Sin97]. Figure 3.4 shows the structure and different parts that compose the Haptic Lens: a white deformable membrane, isotropically died elastomer or liquid; a clear rigid face plate; an illumination source; and a camera.

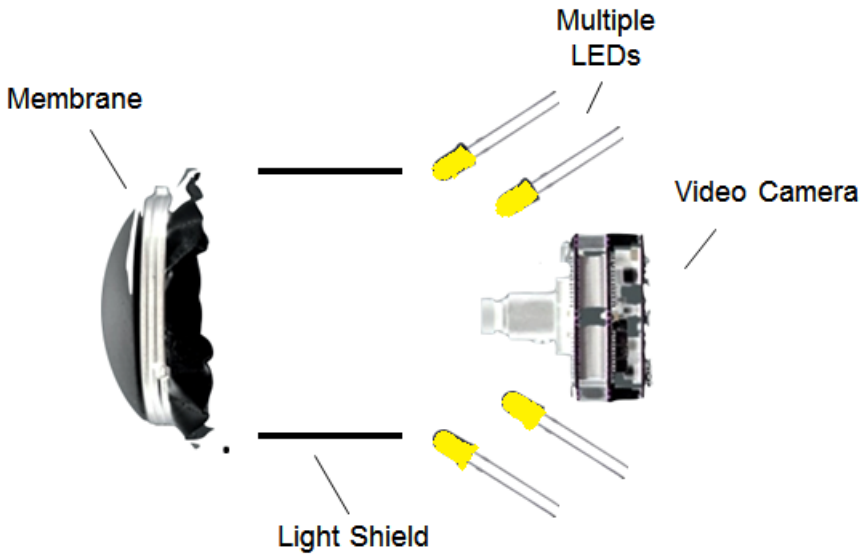

Figure 3.4: Single Light Source Approach Components

The Haptic Lens functions in the following way: The object of interest is pressed externally against the white membrane of the Haptic Lens. This results in the 3D deformation of the membrane and the contained dyed elastomer and finally in the grayscale image representing the 3D depth map of the applied object captured by the camera. Different parts of the object are deformed at different depths from the faceplate, proportional to the local applied force and inversely by the object's modulus. This 3D deformation of the optically attenuating elastomter causes the illumina-

tion to pass through varying thicknesses and hence varying attenuations as seen by the camera. The less the distance of elastomer the light has to travel through, the lighter it appears. Therefore positions on the reflecting white membrane which are deformed to be nearer to the face plate appear lighter than positions further away. This results in a function that maps membrane deformation -heights- at each pixel location to the camera's grayscale intensity value at that location. This is a sensor that acts like a real-time 3D surface digitizer. It should be noted that a dyed liquid can be used in place of the elastomer.

This system can be implemented on a mobile phone setting and resuse the image sensor (camera) available on the phones with the addition of minimal add-ons. It can take advantage of the flash light available on hand-held devices equipped with cameras as the light source. The add-on part consisting of the membrane would be placed on the cover/case of the phone which would go on top of the camera/flsh of the mobile phone, providing a low cost method for palpation. Figure 3.5 shows the mobile implementation of the single light source approach. The add-on part is composed of the membrane with died liquid with the addition of a ring of 8 LEDs that provide uniform light to the interior part of the lens. These LEDs are powered by a battery located in the add-on part.

Figure 3.5: Mobile Prototype of the Single Light Source Approach

3.4 Arterial Pressure Pulse Case Study

In this Section, a case study on using the Haptic Lens in palpating arterial pulses is presented.

3.4.1 Pulse Wave Analysis

The study of the Arterial pulse and its characteristics has been considered important in clinical medicine for a long time. For example, pulse palpation has been used as a fundamental diagnostic method in Traditional Chinese Medicine (TCM) [Xu08]. Different features of the waveform such as the shape and peaks can be indicators of specific cardiovascular conditions. Pulse Wave Analysis (PWA) is the study of the waveform characteristics of pressure pulses and can provide various information on central blood pressure and arterial stiffening, which are associated with aging and hypertension. Pressure pulses can be measured through different invasive and non-invasive techniques. In this work, we focus on a non-invasive method for PWA which does not require medical knowledge. Current non-invasive methods for PWA include Doppler ultrasound and photoplethysmography. Our method using the Haptic Lens is considered a tonometer-based system as it requires the device to be in direct contact with the skin while pressure is applied.

The cardiac cycle is composed of events related to the flow or blood pressure that occurs throughout a heartbeat. The term heart rate is the frequency of the cardiac cycle. During a cardiac cycle the heart goes through systole and diastole phases which in turn refer to the contraction and relaxation of the heart muscles. The arteries in human body function by expanding and absorbing and releasing energy during systole and diastole. This process produces a pulse wave comprising a sharp rise and a near exponential pressure decay of the wave [OG96]. Figure 3.6 shows an example shape of a typical pressure pulse waveform. The shape of an arterial pulse wave is dependent on several arterial wall properties such as arterial stiffness. The pulse wave shape can be affected by various physiological conditions such as age, diet and gender [OPJ01]. The pulse wave contour can vary based on ingestion of food and drinks, age and body height. For example, shorter subjects in terms of body height experience larger augmentations compared to taller subjects.

Recent studies indicate that increased Pressure Pulse (PP) is an important independent risk factor for cardiovascular diseases [SGW00, HL991]. Measurement of central pressure is important as it directly affects the target organs [HKO06].

Figure 3.6 shows a phenomenon called wave reflection at an arterial branch which is responsible for the shape of Figure 3.6. At locations such as arterial branches and arterial-arteriolar

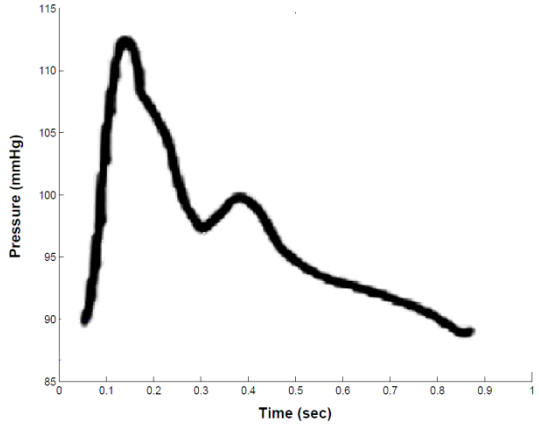

Figure 3.6: An Example Pressure Pulse Waveform

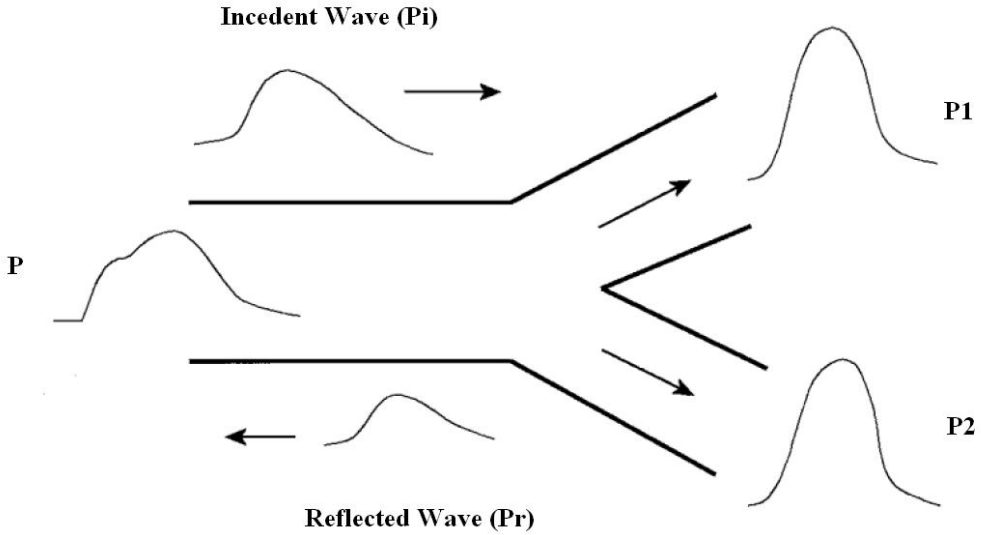

Figure 3.7: Pressure Amplifications at an Arterial Branch (from [HKO06])

junctions, the forward pressure wave in an artery which is transmitted from the central aorta is reflected back towards the periphery. Therefore the pressure waveform recorded can be described as the sum of both forward and reflected pressure waves. In young people, these reflected waves arrive at the heart during late systole or early diastole and therefore does not affect the aortic and brachial PP. In stiffened arteries the diameter of the arteries are reduced earlier and therefore wave reflection happens at an earlier time. In this case, the reflected wave arrives at the heart closer to systole which augments the aortic pressure. In Figure 3.7, the backward pressure wave (Pr) is superimposed with the forward pressure wave (Pi) and results in P.

The augmentation index (AIx) which is defined as the magnitude of wave reflection divided by

PP is a representative of wave reflection. In other words it is a measure of the amount of reflection that the pressure wave experiences. AIx can be measured as the difference between first and second Systolic peak as a percentage of ascending aortic pulse pressure [Dav03].

PWA has been linked to many arterial diseases such as *Hypertension*, *Chronic Renal Failure (CRF)* and *Arteriosclerosis*. Hypertension is an abnormal increase in the systolic, diastolic and/or mean arterial pressure which is due to increased arterial stiffness and can be monitored using PWA [OPJ01]. Different parameters available from PWA such as AIx and Time to Reflection (RF) have proved to be effective in the assessment of CRF [Sav]. Arteriosclerosis which refers to the thickening of the arterial wall can result in an increase of 40-50mmHg to systolic pressure in the central arteries [OPJ01] which can be detected by PWA. In addition Diabetes Mellitus (Type I and II) has been associated with an increase in arterial stiffness [OPJ01].

PWA is currently available only through expensive apparatus and trained operators. This prevents PWA to be used by large populations compared with the conventional blood pressure measurements. PWA is an indicator of several cardiovascular conditions and can assist the physician in assessing the effect of drug therapy. In this chapter we use the methods discussed in the previous section to enable in-expensive while accurate PWA. Our approach is based on tonometry of the radial artery. It requires an individual without any specific medical knowledge to hold a device against the radial artery.

3.4.2 Related Work

Different acquisition systems and devices have been developed for measuring human cardiac signals. The Doppler ultrasound sensor uses reflected sound waves to monitor blood flow through blood vessels [EM00]. Wu, et al [WCJ07] uses a laser triangulation method to detect skin vibrations. Other methods such as thermal imaging [CFE07], pressure [CL11] and acoustic-based [Wan98] sensors have also been explored. The main disadvantage of most of the aforementioned methods is that they involve relatively large devices for capturing pulse waveforms and require a person with knowledge about the system to work with them. Our approach is very similar to the natural palpation procedure where fingers are pressed into the palpatory area. The device is pressed

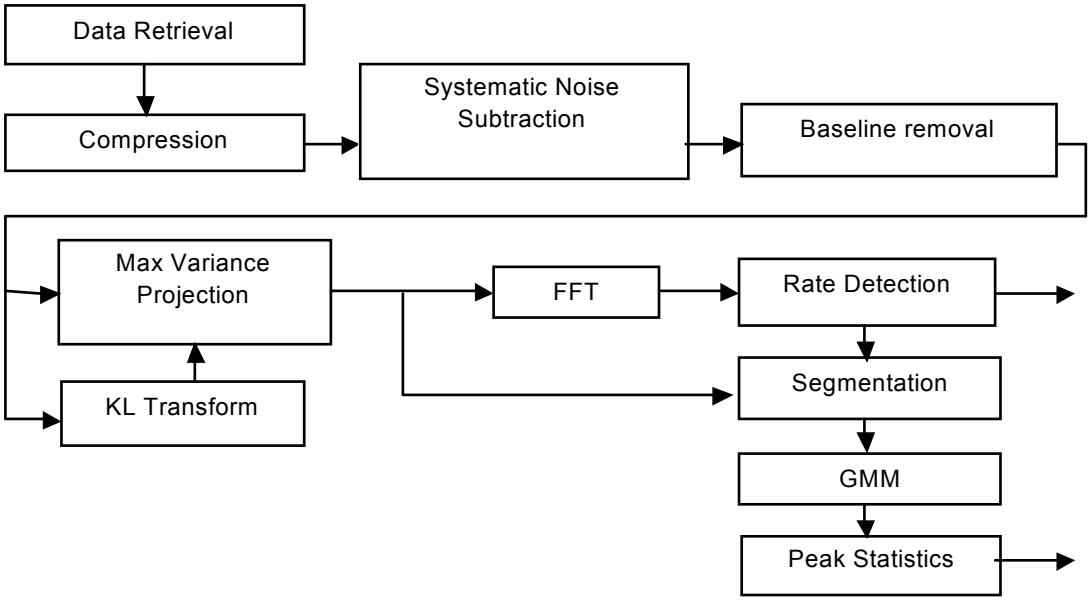

Figure 3.8: Signal Processing and Feature Extraction

against the palpatory area and the pulse signal is immediately visualized so that the individual can reposition the device until a clear pulse is captured. In addition, when comparing with pressure sensor based methods which use either a single sensor or sensor arrays (9 sensors in [CL11]) our approach increases the spatial accuracy to the pixel level. Our proposed method is also portable, non-invasive and low cost.

3.4.3 Signal Processing and Feature extraction

Figure 3.8 shows the overview and different components of signal processing performed on data from the device to detect arterial pressure pulses. Data is collected from the image sensor at a rate of 60 fps, with a frame resolution of 640 by 480 pixels. In the interest of lowering the computational complexity of the algorithm, the frame size is down-sampled to 128 by 96 pixels. Furthermore, an initial empty frame is used to subtract unwanted artifacts from the images.

In the next step a 3D baseline removal procedure is performed. Baseline drift is visible in raw data. This is due to applied pressure variation from human movement. Multiple schemes are available for advanced baseline removal procedures, however it was experimentally determined

that a simple time domain high pass filtering with a cut off frequency of 0.5 Hz can perform reasonably well under slow movement conditions.

This filtering will not remove sudden movements which are in the pass-band. Slower baseline variations such as those induced as a result of breathing movements are removed by the filter.

Let us denote the compressed image data at frame n by $X_c^t(m,n)$, where $X_c^t(m,n)$ represents a 128 by 96 matrix of grayscale pixel data. The output of the baseline removal block is then represented as a convolution shown in Equation 3.2.

$$X_t^{BC}(m,n) = \sum_{\tau=0}^{t} X_c^{\tau}(m,n).h_{HP}(t-\tau) \tag{3.2}$$

Where X_{HP}^t is the impulse response of the high pass filter. We next aim to extract a 1D function of time $x(t)$ from the three dimensional $X_{BC}^t(m,n)$ image data. Proposed is a scheme utilizing the Karhunen-Loeve (KL) transform to obtain $x(t)$ as shown in Equation 3.3:

$$x(t) = w_1^T.\tilde{x}_{BC}(t) \tag{3.3}$$

where $\tilde{x}_{BC}(t)$ is a vector obtained by columnization of the matrix $X_{BC}^t(m,n)$, and w_1 is the first eigenvector of the covariance matrix $C_{\tilde{x}} = E\left\lfloor \tilde{x}_{BC}, \tilde{x}_{BC}^T \right\rfloor$ corresponding to the largest eigenvalue. Implied in this scheme is the modeling of video data as a stochastic process in time, where projecting the frames onto the first orthonormal basis image w1 obtained by the KL transform maximizes the variance of the output process $x(t)$. Also implied is the treatment of variance as a measure of information.

It is notable that while simpler approaches such as a simple summation over the image may be feasible in many instances, there are cases where these approaches will not provide sufficient precision. Such is the case where an increased pressure on the membrane of the apparatus causes the liquid to be shifted from one location to another, resulting in a near-zero net pixel brightness effect on the entire frame image. The KL approach in such cases ensures that the relevant data is captured appropriately by assigning negative weights to some of the pixels. The KL transform also emphasizes the image locations where most of the variation is happening, mostly discarding

areas unaffected by the heartbeat pulses. Figure 3.9 shows a Haptic Lens sample frame compared to the primary basis image obtained by KL transform used for data extraction. It is also worthy to mention that the KL transform will not provide the desired results without a proper baseline removal scheme.

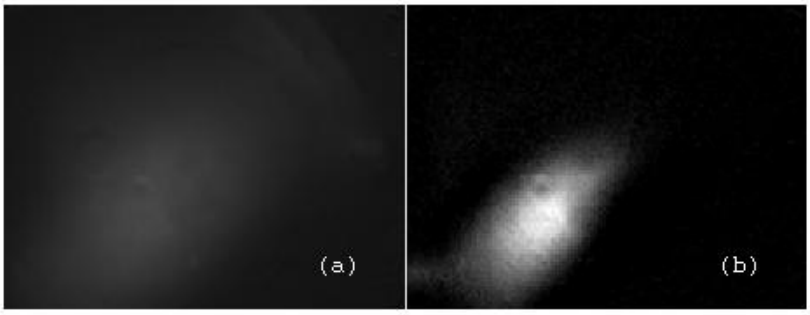

Figure 3.9: (a) Location of Impact in a Sample Frame (b) Primary Basis Image Obtained from KL Transform

In the following phase the heart rate is derived by first performing a Fast Fourier Transform, followed by a peak search in the interval of 0.7 to 2 Hz (see Figure 3.11). Utilizing the heart rate, the $x(t)$ signal is then divided into segments representing each heart beat (see Figure 3.12).

The segment separation is performed by finding consecutive minimums separated by heart beat period intervals - as derived from the FFT phase described above - with a tolerance of 10 percent. The segments are next averaged and fitted to a set of Gaussian Mixed Models with multiple peaks, with each set representing one of the pulse models:

$$\bar{x}(t) = \sum_{N_m}^{k=1} \alpha_k . e^{\frac{-(t-\mu_k)}{\sigma_k^2}} + v_m(t) \tag{3.4}$$

In the above equation $\bar{x}(t)$ represents one heart beat segment obtained by averaging over the individual segments obtained from $x(t)$, Nm is the number of peaks in the m'th pulse model, α_k, μ_k and σ_k are the optimization variables in the fitting process, and finally $v_m(t)$ is the error signal. The fitting procedure is performed using Nelder-Mead iterative method (see Figure 3.13). The mean square of error obtained from each fitting result is computed and compared to decide the pulse model. Figure 3.10 shows an individual using the Haptic Lens to capture their left hand pulse.

Figure 3.10: An Individual Using The Haptic Lens

Figures 3.11, 3.12 and 3.13 show the different stages of the data processing on an individual's pulse measurement.

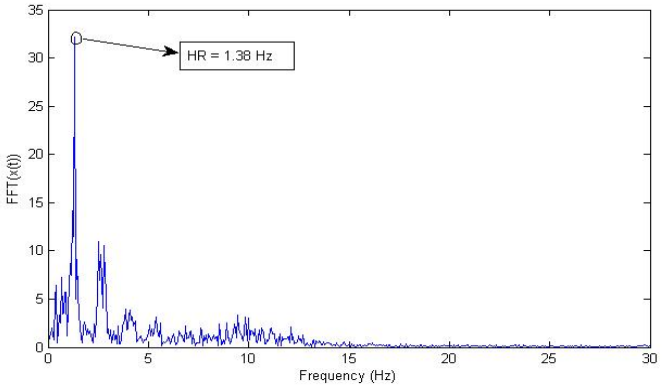

Figure 3.11: Detecting Pulse Rate from Frequency Information in x(t)

Figure 3.17 shows the frequency domain analysis and curve fitting procedures for three different measurements.

3.4.4 Experiments and Results

In order to validate the device as a palpation tool for arterial pulse sensing we used the system on 10 subjects (5 female, 5 male). The subjects age was in the range of 26-39 years. We performed simultaneous measurements of arterial pulse wave on both wrists using two devices: (a) Haptic Lens and (b) SphygmoCor System (AtCor Medical) which is commercially available and is FDA

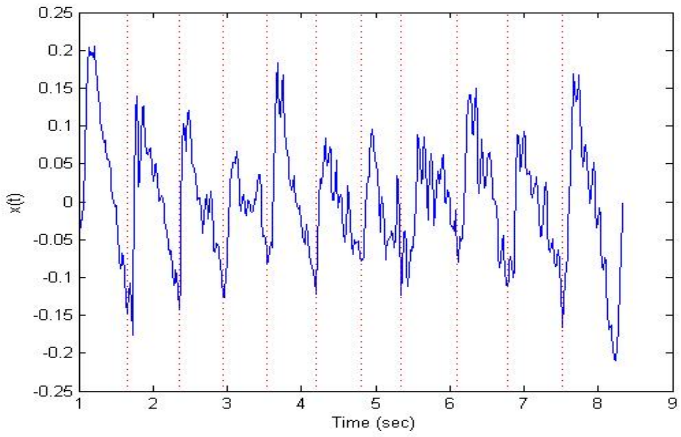

Figure 3.12: Segmented Signal x(t) Obtained by Projecting Frames onto the Primary Basis Image

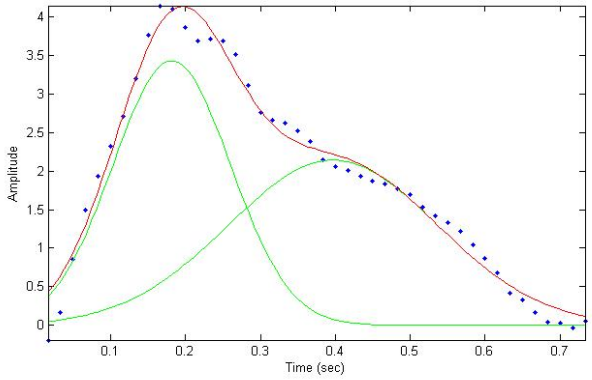

Figure 3.13: Fitting Pulse Segments into a Two-Peak GMM Model.

approved. The Haptic Lens measurement was performed by an individual without any medical knowledge. SphygmoCor measurements were obtained by a trained individual. The Haptic Lens system was explained to users as a device for palpating arterial pulses. The device was pressed on a position on the wrist until a pulse-synchronized in the image shown on the computer screen could be observed. Once the pulse could be observed in the image, data was recorded for 20 seconds without moving the location of the device.

The quality of the extracted arterial pressure pulse signal mainly depended on the correct placement of the device on the wrist and applying constant pressure during the 20 seconds of data collection. In a good quality signal each of the segmented pulses should be as closely correlated to the next as possible. Figure 3.14 shows three segments of final arterial pressure pulse of a subject

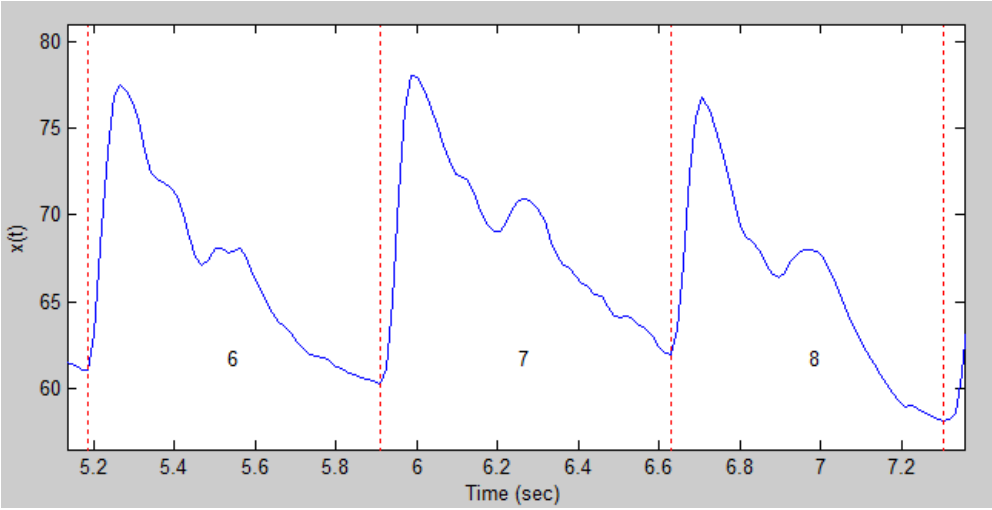

Figure 3.14: Haptic Lens Readings

which had a good overall pulse-to-pulse correlation of 81%

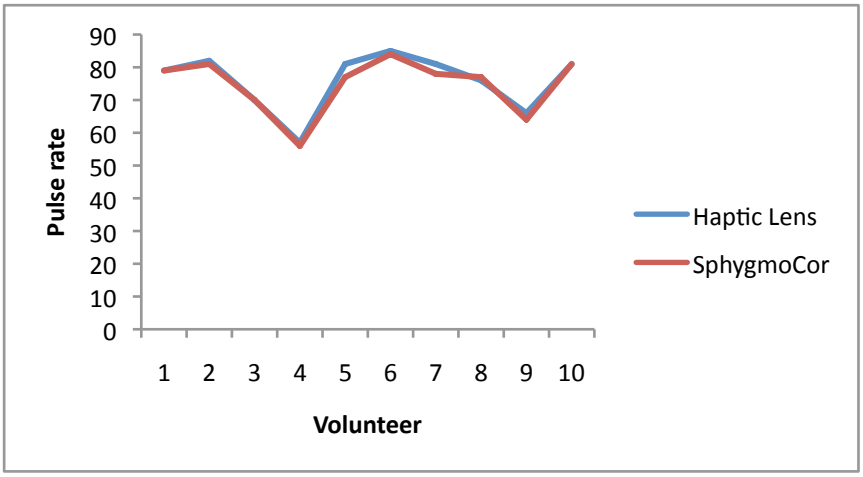

Figure 3.15: Pulse Rate Comparison for 10 Subjects for both methods

We performed comparison on the accuracy of the extracted pulse rate from our method and the SphygmoCor system method. Figure 3.15 shows pulse rates for 10 individuals using both methods. Figure 3.16 shows the pulse wave shape derived from both devices for the subject of Figure 3.14. The SphygmoCor measurements required the operator to move the device and perform multiple measurements until a representative pulse could be extracted for an individual. For this reason, although we started taking measurements at the same time using both devices, in some of the situations there was a maximum delay of 30 seconds between each of the measurements. Although this time delay is insignificant it might explain some of the differences in the pulse rate

measurements.

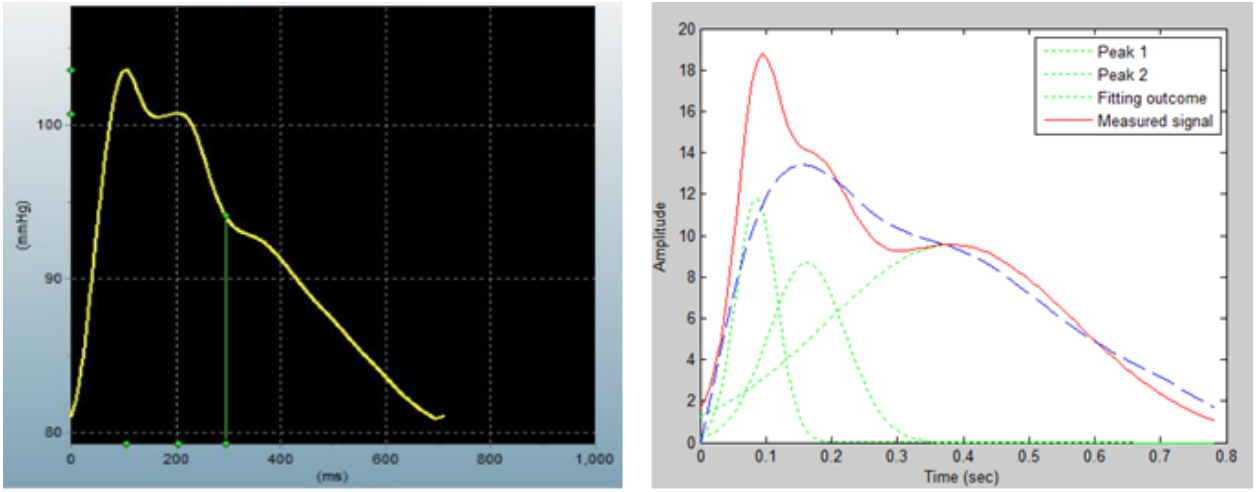

Figure 3.16: Arterial Pressure Pulse. SphygmoCor system (left), Haptic Lens (right)

3.5 Conclusion

In this Chapter we proposed and demonstrated methods for quantifying palpation in medical diagnosis. Our proposed system enhances the information obtained during physical examination by transforming this qualitative procedure into a quantitative diagnostic procedure.We proposed two prototype systems enabling quantifying touch. We proposed algorithms that show significant pulse information can be extracted from the measurements from the Haptic Lens. To show the correctness of the measurement we compared the pulse characteristics with ones measured by the SphygmoCor device.

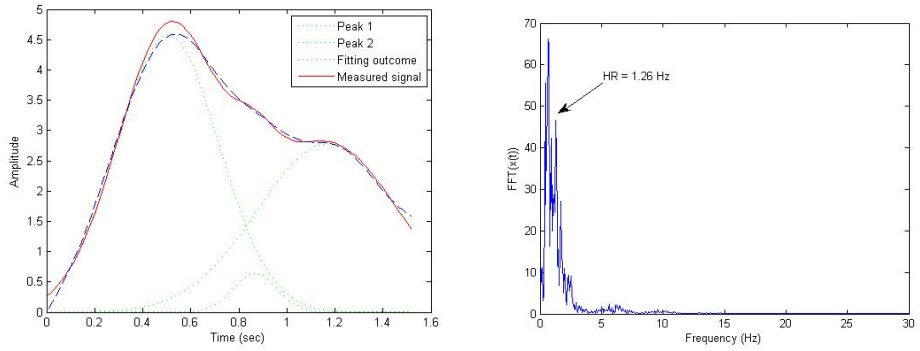

(a)

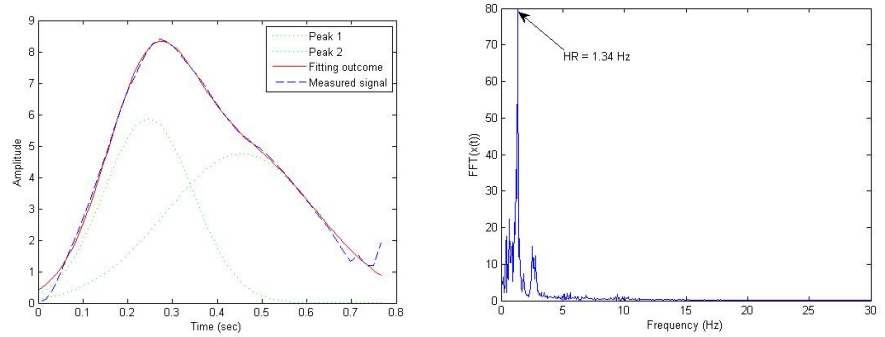

(b)

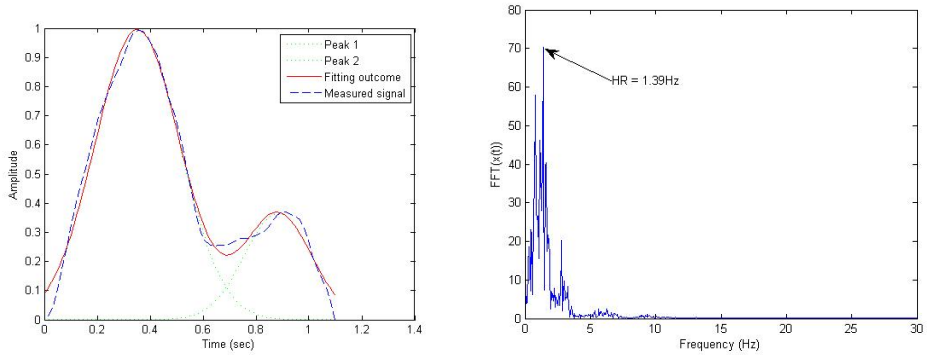

(c)

Figure 3.17: User Results. Measured Pulse Rates: (a) 1.26 Hz (b) 1.34 Hz, (c) 1.26 Hz.

CHAPTER 4

Energy Harvesting in Medical Monitoring Systems

Sensor-based medical equipment is on a brink of revolutionizing many tasks in diagnosis, tracking, treatment, rehabilitation and many other medical activities [PLH09, SRN09]. These systems provide unprecedented comprehensive and real-time data collection with high convenience and reliability. However, there are several major obstacles for their more widespread application. Among them, energy supply is one of the most acute constraints. In a sense, energy harvesting is an ultimate solution. Unfortunately, the current generation of energy harvesters is rarely capable of collecting adequate amount of energy and providing sufficient power.

We focus on energy harvesting in medical shoes with an objective to create and position a single mechanical piezoelectric harvester in such a way that we collect the maximal amount of energy and/or maximize the highest available energy while specified maximal voltage is achieved. The backbone of the approach can be summarized in the following way: We first analyze the pressure sensed at large number of points in the medical shoe during walking trails. Both the collected energy and the maximal achievable power are functions of the pressure. The key trade-off is that high pressure at a particular moment enables higher total energy if collected. This value is the function of the maximal pressure. However, in order to collect a large amount of energy it is not only sufficient to aim for a high pressure; we also need a large force, i.e. , relatively large force over relatively large area. Therefore, it is essential to select size and location of a piezo-electric energy harvester to achieve a quality trade-off between collected energy and maximal collected energy and hence, maximal achievable voltage.

In addition to the first quantitative and optimization intensive treatment of energy harvesting in Medical Shoes our main contribution is a new algorithm for optimization under uncertainty. The algorithm is named scenario-based because it uses a combination of statistical and combinatorial

optimization techniques to find and evaluate the maximal energy harvesting problem in sensor shoes. The key idea is to select a small number of time samples and conduct optimization using only these samples. Once the solution is generated, we evaluate it by calculating the interval of confidence within learn-and-test or re-sampling paradigm. The approach is also applicable to a customized shoe for a particular subject as well as its generic version. All results are obtained using data from BioFoot medical shoe [MCP07].

4.1 Related Work

In the last two decades a large variety of medical shoes with a variety of sensors and interfaces have been designed and evaluated [LIS09, PHB00]. Recently, they have been used in conjunction with artificial intelligence techniques for a variety of tasks ranging from event detection to new types of user interfaces (e.g., computer mouse) [YXL05, CHX08]. More importantly, they have proven invaluable in many medical tasks [HBB06]. Our main novelty is that we use sensing data and sensor location not for data collection but for optimized energy harvesting. During the same period, energy and power emerged as premier design and operational metrics for many systems. A very attractive way to solve energy supply problem is to harvest (scavenge) environmental energy [RWR04, PS05, EH305]. Numerous approaches emerged ranging from photovoltaic and vibration to human activity-based techniques to use of environmental electro-magnetic and nano-scale sources [SIP05, Pri07, SR07]. In [SP01] the authors have investigated power-harvesting from running shoes for generating power for wearable electronics.

4.2 Preliminaries

In this Section we review preliminaries covering information on medical shoes, specifically BioFoot [MCP07] which we use for collecting samples. We also present information on energy harvesting and battery and capacitor models.

4.2.1 Medical Shoes and Datasets

With the advent of micro-system technologies, in-shoe plantar pressure measurement systems have become feasible. These systems are currently employed by clinicians and researchers to assess dynamic plantar pressures. TekScan F-Scan, Novel Pedar and IVB Biofoot are examples of such systems [MCP07, EH1b, EH1a]. For this study we used plantar pressure measurements from BioFoot (IBV [MCP07]). The system consists of two flexible, 0.7 mm insoles. Each insole has 64 small size piezoelectric sensors and has a round $5mm^2$ diameter shape. The output signals are amplified and sent through the wireless transmitter attached to the subjects waist. The system allows measurements in 200m of distance, therefore subjects can freely move around. The sampling rate for our measurements is 100Hz. Figure 4.1.a shows the BioFoot shoe.

4.2.2 Energy Harvesting Model

Electrical power can be harvested using multiple conversion mechanisms such as thermoelectric, electro-magnetic and piezoelectric. Energy harvesting using piezoelectric conversion mechanism converts mechanical strain into electric current or voltage. This process can be described with charge displacement and can be modeled by a linear consecutive equation. According to [WK08], the energy stored in a parallel plate capacitor and corresponding voltage across piezoelectric (V_s) can be expressed as Equations 3.2 and 4.2 respectively:

$$W_{out} = \frac{1}{2}(\frac{\varepsilon_0 \varepsilon_r A}{T})V_s^2 \tag{4.1}$$

$$W_s = (\frac{K_{33} F T}{A})\sqrt{\frac{1}{Y \varepsilon_0 \varepsilon_r}} \tag{4.2}$$

In these equations, ε_0 and ε_r represent free space permittivity and relative permittivity (8.85e-12, 200 to 1350) respectively. In addition, T is thickness (191 um), K_{33} is Electromechanical coupling coefficient (0.69) and Y is Young's modulus (63 GPa). Cross-sectional area of the piezoelectric material and applied force are represented by A and F respectively. Equations 3.2 and 4.2 show that the generated voltage is proportional to the amount of pressure applied $\frac{F}{A}$ while the

generated energy is proportional to $\frac{F^2}{A}$.

4.3 Battery and Capacitor Models

The instantaneous power generated using piezoelectric harvesters might be relatively small depending on the amount of energy required to perform certain tasks, such as wireless transmission. Therefore it is necessary to somehow aggregate the energy before using it, either using capacitors or batteries. Recently there have been several attempts in designing power harvesting circuits. Figure 4.1.b shows a simplified power harvesting circuit [SIP05]. As shown in the figure, in order to aggregate energy continuously the generated voltage needs to get higher as more energy is accumulated. One solution for this is to use multiple small batteries and charging each battery separately. Using a single battery, due to cost consideration requires intelligent energy harvesting mechanisms that produce high voltages.

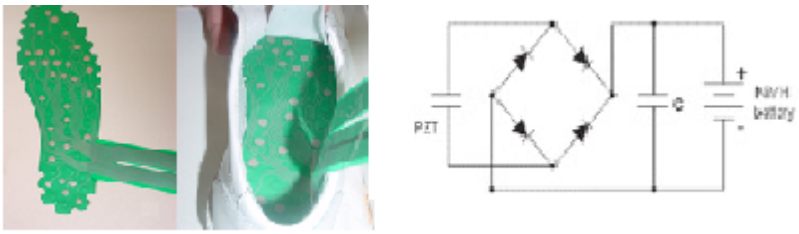

Figure 4.1: (a) BioFoot (b) Schematic of Energy Harvesting Circuit [SIP05]

4.4 Energy Harvesting

In this Section, we formulate the problem of Maximal Energy Harvesting (MEH) and show that this problem is NP-Complete by transforming maximal clique problem. We then propose our scenario approach for this problem in Section 4.4.3.

4.4.1 Problem Formulation

In order to design self-sustainable shoe systems, careful examination of pressure distribution during movement is needed. We use the data from plantar pressure distribution of subjects during

walking trails, to find best location to place energy harvesters. Due to cost considerations, we only look at a single harvester placement problem and find the location and size of the harvester. Therefore, the MEH problem can be defined as selection of shape/size of a single energy harvester in such a way that the amount of generated energy is optimized. The problem can be viewed from another perspective. When considering a case where restoring energy for later burst use is needed, the goal is to optimize for energy optimize for energy considering produced voltage levels.

We solve the MEH problem for two platforms: customized and generic. People have different walking patterns; therefore in order to maximize the amount of energy generated, customized platforms can be developed for individuals by studying their walking patterns. Figure 4.2 shows maximum pressure of different locations during walking, in four different individuals, where black represents maximum pressure. These images show how the pressure distribution is different among individuals; which in turn effects the decision of the location of energy harvester. Generic platforms can be also developed by considering most common features in different people.

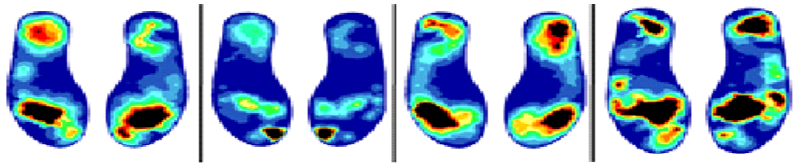

Figure 4.2: Maximum Pressure Distribution in Different Subjects

4.4.2 Problem Complexity

At the intuitive level the MEH problem may be defined as selection of piezoelectric material shape and size so that total collected energy is maximized. There are two primary sources of difficulty in solving this problem. The first is its statistical non-determinism and the second is its combinatorial structure. The first problem is due to uncertainty about future actions of the subject. Although the former is dominant in practice, the latter is a formidable obstacle since it is associated with solving a computational intractable problem. We can formulate a very simplified version of the MEH problem in the following way:

Problem: Deterministic Maximal Energy Harvesting (DMEH)

Given: An undirected graph G (V,E) with a set of vertices and edges, time slots T_1, .. , T_n and pressure $P_{i,j}$ at each vertex i for each T_j.

Objective and constraints: Select a set of time slots T_t and vertices so that the total sum of pressures is maximized and in all selected time slots the pressure is at least P.

In order to prove that the DMEH problem is NP-complete we transform an arbitrary instance of one of 21 initial problems, maximal clique, into DMEH. We start with a graph GG which has the same set of vertices V as graph G. Next, for each edge between vertices V_p and V_q in GG, we create a time slot in DMEH where only corresponding vertices have pressure P and all other vertices have zero pressure. Now, it is easy to see that if and only if graph GG has a clique of size K, we can collect total energy corresponding to sum of pressures $K \times P$.

4.4.3 Scenario Approach

We use a scenario-based approach to find the best location and size of an energy harvester. The proposed algorithm uses a combination of statistical and combinatorial optimization techniques to find and evaluate the maximal energy harvester. The scenario approach uses walking samples from individuals. A small number of samples are chosen as input to a constructive iterative optimizer which finds the best location for the harvesters. This solution is evaluated through calculating the interval of confidence within a learn-and-test paradigm and more experiments are conducted if necessary. Figure 4.3 shows the flow of the scenario approach.

The algorithm starts with randomly choosing a small subset of samples of multiple people. Specifically, K randomly selected samples are used as input to our constructive iterative optimizer (Algorithm II). The optimizer results in a single location for the placement of an energy harvester. We run the optimizer m times, where m is the number of scenarios (Algorithm I, lines 4-7), each time with K random samples and build an interval of confidence for the solution of the optimizer. If the interval of confidence is too small to accept the solution, we repeat the above process, by increasing the number of samples: that is with a larger K (Algorithm I, line 9). The above steps are repeated until an acceptable interval of confidence is found (Algorithm I, line 3). The solution of the constructive iterative optimizer at this step is presented as the final solution of the placement

of a harvester.

Algorithm I: Scenario Approach

```
1:  Input: Randomly selected Samples.
2:  Output: A single location for placement of a generator.
3:  While ( interval-of-confidence < 90%)
4:   for ( int i = 0 ; i< m; i++)
5:        Select K randomly selected Samples
6:        Location = Optimizer (samples)
7:   end for
8:   Calculate interval-of-confidence
9:   if (interval-of-confidence<90%) K+= K_CONSTANT
10: end while
11: return Location
```

Figure 4.3: Algorithm I for Scenario approach

The constructive iterative optimizer (Algorithm II) works as follows: It starts with a single location l_i to place a harvester. It checks to see if it satisfies problem constraints. If yes, it accepts it as a solution. In the next step it forms another solution called $l_{i'}$ by combining l_i with one of its geometric neighboring locations. It then decides to choose $l_{i+1} = l_i$ or $l_{i+1} = l_{i'}$ based on the solution that optimizes the objective. These steps are performed until all locations have been explored. In Figure 4.4, Algorithm II describes the details of the constructive iterative optimizer. It starts with the smallest location generating the highest energy. Next, neighbor locations that can be merged to give a better energy value and satisfy voltage constraints are merged (lines 5-8 in Algorithm II). Then the merged location is added to the potential result list (line 9 in Algorithm II). This process is continued until there is no merging possibility. Finally the location with highest energy is returned.

Algorithm II: Constructive Iterative Optimizer

```
1: resultList <= Highest energy single location
2: locationList <= All available locations
3: while (change in resultList size)
4:    curr <= resultList.removeFirstItem();
5:    for each (location "l" in locationList)
6:       if (curr.isNeighbor(l))
7:           merged <= merge(l, curr);
8:           if(merged.energy>curr.energy && merged.satisfyVoltage())
9:              resultList.insertLastItem(merged);
10:    end if / end for / end while
11: result <= maximumEnergy (resultList);
12: return result;
```

Figure 4.4: Algorithm II for Constructive Iterative Optimizer

As shown in Figure 4.1.b, in order to aggregate energy continuously, a relatively high generated voltage is needed to be able to accumulate energy. Therefore optimizing only for energy is not sufficient as a certain voltage level needs to be met to be able to store energy. The amount of voltage required is dependent upon many factors such as the amount of energy stored and the amount of energy consumed. Therefore in our approach we use a voltage/energy pareto technique, where we optimize for energy considering satisfying voltage requirements. Specifically, we consider a voltage level and require the voltage generated to meet this level by a percentage at all times. We use the same scenario technique described to find the best location of harvester to satisfy each voltage level.

4.5 Simulation Results

In this Section we present experimental results on using the described scenario approach. We use walking samples from 30 individuals to find the position for placing a single generator that would maximize the amount of energy generated and stored. The data is 6 seconds long for each individual. Here, due to space limitations, we only show the data from 5 users.

4.5.1 Optimizing for Energy with Different Generator Sizes

Based on our proposed approach the amount of energy consumed per second in a generic platform, optimizing just for energy is $3.29\mu J$. To show the effectiveness and accuracy of our approach, we compare our results with two methods: 1) choosing smallest size generator at the location of maximum pressure ($0.89\mu J$) and 2) choosing a large generator to cover all the locations that sense pressure ($2.53\mu J$). The results show that choosing a large area piezoelectric to cover all points or a small area piezoelectric at the position of maximum pressure are not correct choices. The interval of confidence for optimizing for energy is $(3.29 \pm 0.15\mu J)$ with probability of 91 % .

Figure 4.5 shows the maximal amount of energy generated per second with different generator areas in both a customized and generic platform. As shown, if the goal is to only maximize the amount of energy generated, a generator with equivalent sensor area of 12 should be chosen for

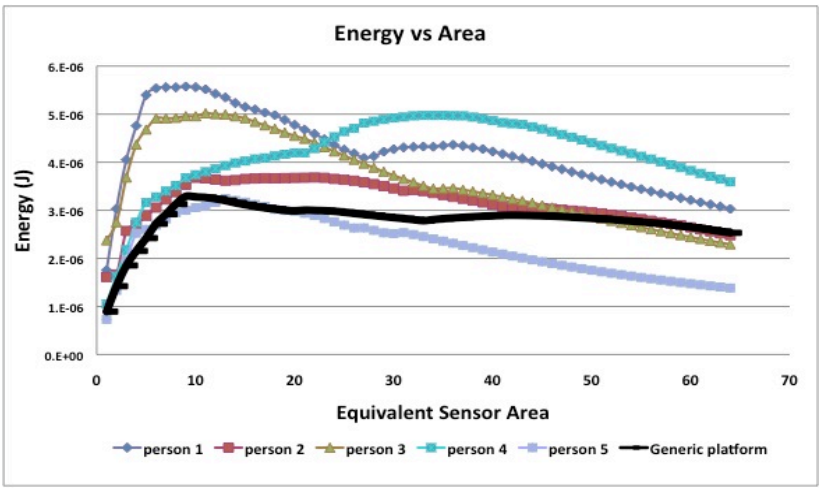

Figure 4.5: Energy vs. Generator area, Customized and Generic Platforms

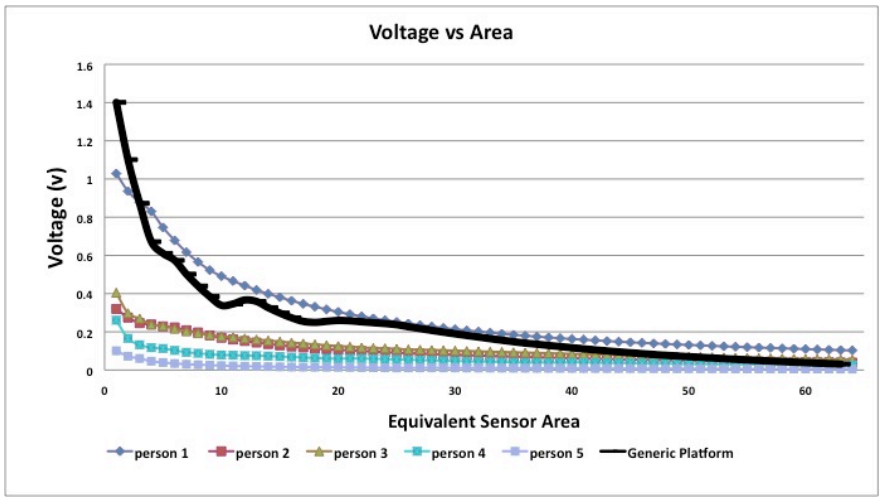

Figure 4.6: Voltage vs. Generator area, Customized and Generic Platforms

the generic platform. We also show customized results for 5 of the individuals.

4.5.2 Optimizing for Voltage with Different Generator Sizes

Figure 4.5 showed the maximal amount of energy generated per second with different size generators. However as discussed in Section 4.4, high voltages are also desired when generating energy, specifically for storing energy. Figure 4.6 shows the maximal amount of voltage generated per second in different generator sizes for the same subjects in Figure 4.5. As expected, according to Equation 4.2, smaller area generators generate more voltage. With the increase in generator area,

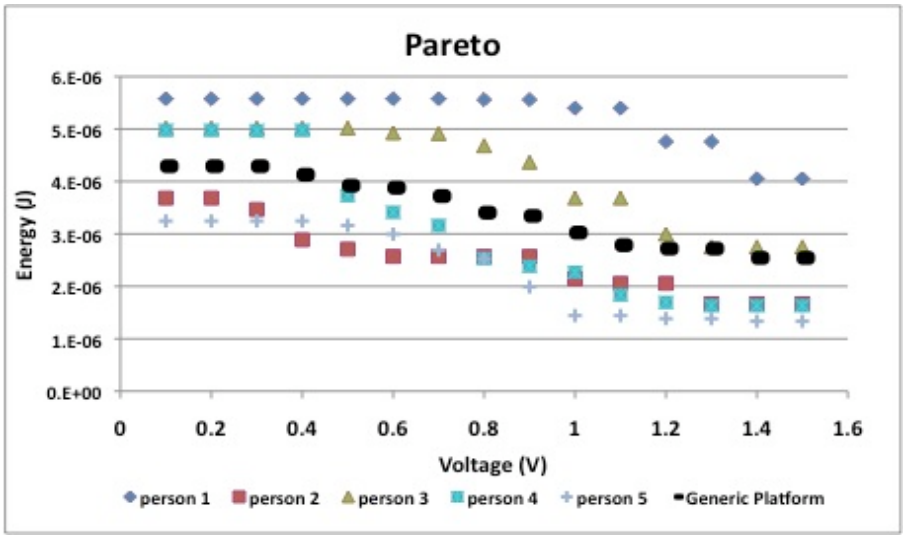

Figure 4.7: Pareto vs. Generator area, Customized and Generic Platforms

the amount of voltage generated becomes smaller.

4.5.3 Optimal Energy-Voltage Points

According to Figure 4.1.b, in order to aggregate energy continuously, the generated voltage needs to be relatively high as more energy is accumulated. Therefore optimizing just for energy or just for voltage is insufficient. We use a voltage/energy pareto technique, where we optimize for energy while at the same time satisfying specific voltage requirements.

We consider a specific voltage level and require the voltage generated to satisfy this level by a specific percentage at all times. Figure 4.7 shows optimal energy-voltage points in both customized and generic platforms. Each point shows the maximum amount of energy generated, while satisfying a specific voltage value for at least 60 % of the time. Therefore each of the found voltage/energy optimal points can be chosen based on different design parameters such as battery specification and application needs or user defined constraints. The result of the optimal location of a generator for a generic platform that produces maximal energy savings over all individuals is depicted in Figure 4.8.

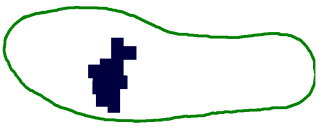

Figure 4.8: Positon of Single Energy Harvester in the Generic Platform

4.6 Conclusion

We developed an optimization intensive approach for energy harvesting in medical shoes. We used readings from 64 pressure sensors of 30 subjects. Using this information and a proposed scenario approach we found size and location for placement of piezoelectric transducer in both common and customized platforms, optimizing for maximal amount of collected energy and maximal amount of collected energy with a specified voltage achieved.

CHAPTER 5

Ubiquitous E-Textile Monitoring Systems

In this chapter the design, architecture and applications of a flexible haptic sheet made from E-textiles is described. This sheet consists of an array of pressure sensing elements and is capable to capture events (pressure asserted at different locations) and perform object localization on objects placed on it. This sheet is made from E-textile material which gives the touch and feel of normal fabric. This feature enables the widespread use of this surface in wearable contexts as a non-intrusive monitoring system in Wireless Health applications.

5.1 Applications

As discussed, the flexibility and wearability of the textile makes this a good platform to be used in wearable systems. This sheet can either be used as a 2D surface for different applications or it can be placed on an individuals hand or used as a glove. There exists a diverse range of applications that can leverage this platform. Below we discuss some of these applications. [Pa02] also provides a list of possible applications for smart skins which can be applied to this context as well.

5.1.1 Bed Sheet

A smart sheet capable of performing real-time object recognition has several applications in health care: One example is a bed sheet sensor. Mobility measurement during sleep is an important consideration in assessing subject's health and quality of sleep [HSM00b]. For example, body movements can be indicators of physical and mental health [DK57]. This information can also be used to monitor patients during long term illnesses. Our proposed smart sheet can be used as bed sheets to offer such real-time measurements and assessments. Smart Textile Surface, being

made of fabric, will have no different feeling compared to normal sheets, but will be capable of performing a vast range of analysis.

Each human body part can be considered an independent object (e.g., head, hands, arms, legs, etc.). The location and orientation of each object corresponding to each human body part can be monitored during a subject's sleep. This information can enable body movement identification [Nes], posture tracking [BMY01], sleeping pattern identification [Taf09], sleep quality assessment [WC84] and monitoring of specific body parts, e.g., Head movement caused by respiration to classify respiration status. Currently there are application specific products targeting a human body part. For example in [HSM00b] they use a sensor pillow system to monitor respiration and in [RSB11] where a neck-cuff system monitors respiration, blood oximetery and head movement during sleep. An additional benefit of such system would be its fabric structure which allows non-intrusive measurement.

5.1.2 Walking Mat/ Shoe Insole

A pressure mat provides an easy way for obtaining a plantar pressure image of a subject's feet which can be used in gait analysis. It can enable detailed analysis of pediatric foot function and gait. This information can be useful in identifying areas of potential ulceration, diagnosis of imbalance, identifying differences in left and right feet pressure profiles and monitoring improvement over time. Alternatively it can be used as an insole inside shoes. Patients can wear the shoe and perform daily activities. At the same time all the aforementioned parameters can be monitored.

5.1.3 Smart Floors for Ambient Intelligence

The haptic sheet can also be used in smart floors, used for monitoring elderly living alone. The floor can be covered with the textile sheet which allows identifying the location and status of multiple subjects (walking, standing, not moving, falls, etc.) at any time without being intrusive. In the US nearly 1/3 of seniors above 65 will experience falls and 9500 of them will die as a result [T25]. A similar product to this is the Smart Carpet [T26]. In addition for health monitoring, the smart floor can be used in smart houses where different appliances or environmental features such as

light, temperature, music and etc, can be automatically adapt to users preferences or different user activities.

5.1.4 Tabletop Interfaces

There are several related platforms for tabletop interfaces. These interfaces allow user interaction by means of predefined gestures. In addition, some provide support for object recognition. Most of the object recognition methods require an external object to be placed on the object under test, such as tags, visual markers or etc. Microsoft Surface [KW09] is a recent tabletop interface that detects objects using markers called Dotcode and some vision algorithms. [SSL02] uses load sensing for performing object recognition. Using the haptic sheet will allow object recognition using the object features such as shape and weight. This method does not require the placement of any additional tags.

5.1.5 Marketing

The haptic sheet can be helpful in advertisement and marketing. By monitoring subject behavior around locations that products are placed, important marketing information can be gathered. Using shape and weight analysis of foot/hand pressure maps, information on age group, and weight of subjects can be extracted. It can be helpful to study different subject behavior in reaction to different advertisements in order to find the most effective ones.

5.1.6 Smart Objects

Use of a haptic sheet on objects that subjects interact with, can provide smart objects which are capable of understanding human emotions and behaviors and therefore interact with the user. [Pa02] suggests that by analyzing grip forces or object handling behaviors, we can make interactive devices that respond to humans, just like humans would. This functionality is called emotional intelligence.

5.1.7 Gaming for Health/ Virtual Reality

Haptic sheet can be used in human computer interaction and in virtual reality. It can be used in the form of a glove and can be applied to rehab exercises. Different games can be designed to improve motor abilities for post stroke patients using the glove. In addition, all the aforementioned platforms, for example the pressure insole in the shoe can also create gaming platforms.

5.2 E-Textile technology and Sensor Modeling

E-Textiles are composite yarns made of fibers coated with conductive polymer. Their natural structure is loose and inside fibers are air gapped. The initial throughout resistor between the top-bottom surfaces is pretty low. When extra pressure actuates on the surface, the intra fibers are squeezed together and the throughout resistor becomes smaller which is inversely proportional to the pressure imposed. Their foldable characteristic make them suitable for many portable and wearable applications including smart medical shoes, smart bed sheets, E-textile data gloves and etc. Below we describe how pressure sensors can be instrumented using E-textiles and then we model their characteristics in the presence of pressure.

5.2.1 Sensor Fabrication

An E-Textile based sensor has a three-stacked layer structure. The sensing material is sandwiched within two conductive pads. In this sensor, E-Textile acts like a pressure sensitive resistor. When force is applied, the resistance of E-Textile will decrease. The conductive layer can be made of conductive fabrics, copper foil tape or conductive threads. In order to maintain the flexibility of the sensor and textile feel we use conductive thread and conductive tape for the conductive layer. Figure 5.1, shows two of these sensors using different conductive material.

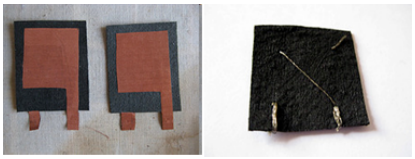

Figure 5.1: The Basic Sensor Structure

In the following part we model characteristic of sensors fabricated using E-Textiles.

5.2.2 Sensor Pressure-Resistance Characteristics

In different applications based on the domain of use, forces applied to E-Textile sensors are different. In this section we model the force-resistance relationship in a sensor made with the structure described earlier. Figure 5.2 shows the curve for forces below 10Ns for a 2cm*2cm sensor. [Pa02] performs a detailed study on metrological properties of E-textiles and provides similar curves for other E-Textile material tested.

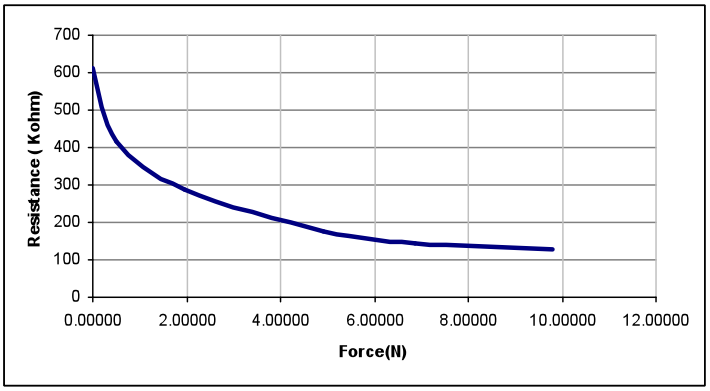

Figure 5.2: Resistance Response Based on Applied Force

5.2.3 Sensor Sensitivity with Distance

In fabricating a sensor array, to make design easy for mass production, a single sensing layer (middle layer in the three-stacked layer structure) is shared among all array sensors. This will be described in more detail later. The result of this design strategy is a dependency of sensors to each other. When applying force on one sensor, the effect would be inevitably posed on its surrounding sensors on account of mechanical linkage. We define the accumulating pressure sensed on each location due to forces applied not directly to itself but to its surrounding locations, the neighboring effect.

5.3 Sensing System Design

The main concern here is to create a sensing architecture that guarantees to capture all events and requires minimal energy. It is tempting to design a sensor array in which a single sensor is assigned to each sensing location with its own dedicated signal line. However, huge energy savings may be accomplished for some of alternative sensing architectures.

Considering an n by m sensor array, the trivial method where each sensor has its own signal line, requires m*n sensor readings in order to conclude the location of asserted pressure. An alternative design mechanism is one in which sensors on the same row/column share the same wire. In this design methodology, a voltage is applied at the column of interest and the current at each row is measured. Using this reading mechanism the entire array is scanned column by column. This design scheme makes the routing much simpler but still needs n*m readings.

In addition to the aforementioned sensor array designs, we propose a multi-layer design in which each layer consists of several sensing elements. The sensor array is constructed by placing the layers on each considering the virtual locations of each sensor in other layers. Pressure asserted at the top layer is sensed in the layers below due to the nature of E-textiles. Calibration can be performed to obtain equivalent pressure at all levels. In addition, sensors in each layer can be combined to form different size sensors. This enables reconfigurable design based on application needs. Figure 5.3 shows this multi-layer design with k layers and the potential of maximum m*n sensors in each of the layers. However based on different design constraints and needs, sensors in each layer can be combined to enable different sampling schemes. They can be combined to produce coarse grain sensing at locations where detailed data is not needed. Figure 5.3 shows some examples of sensor combinations.

To better elaborate this we describe the above design in a two layer structure example. Figure 5.4 shows one way of constructing this structure in which each layer sensing elements are combined into parallel sensing elements. This figure shows a higher level view of sensing elements in each layer. In reality, each sensing element here is the combination of multiple square sensors in one line. The placing of two layers is in such a way that the sensing elements on the layers become orthogonal to each other. The touching layer of these sensors, are connected to Vcc

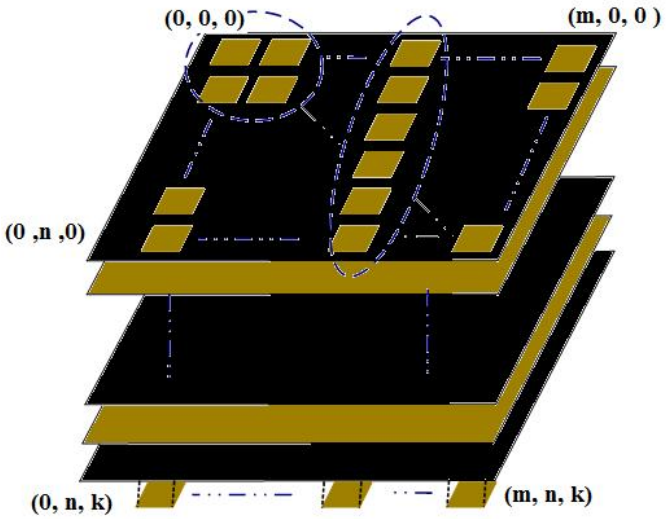

Figure 5.3: Sensor Array Design

and signals are read from each of the sensors on each layer. This design mechanism gives us the ability to create a sensing circuit with more sensing locations per sensor element and therefore requires fewer readings. In this example for n vertical and m horizontal sensing elements, only n+m readings will be required for n*m sensors.

The spacing between sensing elements can be chosen based on desired effect of sensors on each other. Distance between sensors can be chosen in such a way that, neighboring effect is negligible or chosen in a way that only first neighbors of the sensor are affected. Sensing elements can be either drawn or sewed on to the virtual locations. The inclusion of additional layers can either enable additional information processing techniques or provide features such as reliability for the sensing system. However the design and decisions on combining sensors in each layer is not trivial due to geometric constraints such as preserving the neighboring arrangement of sensors.

5.3.1 Group Sensor Readings

In the aforementioned design, each sensor would have a dedicated signal for reading from it which is multiplexed and then read through A/D converters. However, in some situations it might be beneficial to combine sensors in groups and read through one A/D converter in order to save energy. One situation for this was described above. Other cases are when group readings can enable us

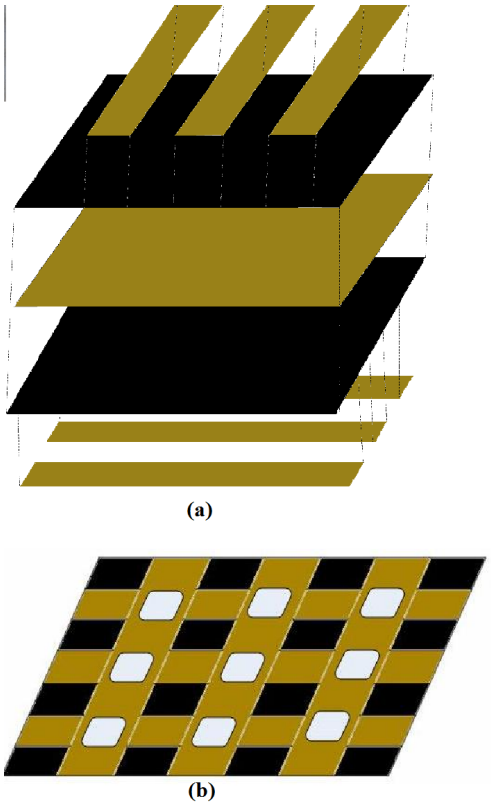

Figure 5.4: Two Layered Design (a) Layer Arrangement (b) Virtual View of Sensing Array and Sensing Locations

to organize effective queries by allowing readings from a combination of sensors. To enable this capability, sensor readings can be combined as needed using electronic switches. We show how our proposed interleaved and coordinated sampling and data processing scheme leverages this. This is done by using summing amplifiers or other components.

5.4 Sensing Strategies

Sensing strategies are different based on nature of applications and events. Some events occur at known times and therefore can enable optimal sampling schedules. On the other hand, detecting events on some other applications might be complex. From another aspect, based on applications needs capturing information about the occurrence of an event and location of event might be sufficient for processing. But other applications might require additional data on characteristics of events such as duration, amplitude and etc. In this section we first introduce the notion of decou-

pled event detection and identification. Once an event is detected, for identifying the location of an event a method is presented the next section. Please note that this method is only for identifying the location of event and not for extracting amplitude information on the event.

5.4.1 Decoupled Event Detection and Identification

Separating concerns both at conceptual and implementation level is considered important in design of systems [28]. This approach, namely layering, helps in managing complexity. We use a similar strategy in decoupling event detection from event identification. Without this, in order to find the location(s) of asserted pressure, a reading of all sensor values at each sampling period is required. This in turn consumes a large amount of energy in applications where extremely fast sampling rates are required in order not to miss any events.

With the use of group sensor readings described earlier, we can create event detection sensors where readings from all sensors are combined. With this, only one reading is required at each sampling period. Additional sensor readings are only performed in the case of the occurrence of an event. Note that in this scheme the energy saving come from reduced samples (use of A/D converters) and that the energy consumed at sensing sub-circuit remains the same.

It was mentioned in the previous section that our architecture enables the inclusion of additional layers to the sensing circuit. Another approach to event detection is the inclusion of an additional sensing layer. To elaborate, the design in example of Figure 5.4 would change to a three layer design where the third layer is a single sensor with the size of the whole sensing array. However in this approach, pressures asserted not directed at sensing locations are also detected as events and additional processing needs to be performed on the event identification part to distinguish them from pressures asserted directly on sensing locations. In the next section we propose methods that would reduce energy consumptions in the event identification part.

5.4.2 Interleaved and Coordinated Sampling and Data Processing

The key question in designing real-time mobile sensing systems is how to organize measurements in such a way that all timing constraints are satisfied and yet leverage remaining time in optimizing

the measurements. Here based on a new paradigm of interleaved and coordinated sampling and data processing we obtain flexibility in managing sampling strategies to optimize energy consumption.

To avoid building complex system of equations and to enable fast and robust reasoning, we use a binary sensing scheme. Our sensor architecture enables us to conduct processing using only binary information about sensor readings due to an experimentally confirmed sensing model. Therefore, for event identification we use combinatorial search that rapidly eliminates possibilities that are inconsistent with the measurements, from further consideration.

In the mentioned sensing model, based on the distance of sensing elements from each other, only a number of sensors detect pressure changes. We perform a binary mapping from sensed values using a platform dependant threshold. Values above this threshold are mapped to 1 and the remaining values are considered 0.

As discussed before, our sensing model enables group readings of sensors. A group reading of n sensors after the binary mapping stage, will result in a 1 if one of it's n sensors is equal to 1. In other words, a group reading of n is an OR of its n inputs. We take advantage of the above discussed group reading ability and binary representation of sensors to minimize the number of queries needed to identify events.

For each event detected by the event detector, depending on the available time to perform processing, the number of sensor readings can be reduced. To elaborate, if the available time allows two epochs (units of time) for processing, using group readings, we can narrow down the search space by a factor of two, three or more in the first epoch and then perform search in the reduced search space in the next epoch. This strategy can be extended to more epoch calculations with the same reasoning. Therefore in each stage information is reused from previous stage and measurements are performed in stages. Figure 5.5 shows an example of two epoch processing of 8 sensors in the case of a single event. In the first epoch, we perform a single group reading of 4 sensors. If the result is 1 we conclude that the activated sensor is within that group. Similarly if its 0 it should be in the other group. Based on this result we perform search only on a group of 4. So in this example instead of performing 8 measurements we only perform 5. Further savings can

result in different combinations and more epochs available.

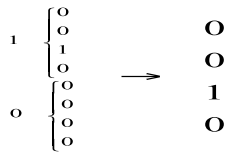

Figure 5.5: Two Epoch Processing Example

Here, the question that arises is how we can determine the number of available epochs for measurement and reasoning. This number depends on the event detector sampling mechanism. In an extreme case, a very fast sampling in the event detector sensor will capture events early enough to enable multiple epoch processing. On the other extreme, sampling at a very slow rate that is only fast enough to capture the presence of events, would allow one epoch processing. This can be further explained with the example in Figure 5.6. This figure shows an event happening in the event detection signal where point C is the end of the event. If the event detector sampling can assure the discovery of an event at an early point such as A, the time available for event identification is t_{AC}. However if the event detector sampling is only fast enough to guarantee to capture events at late points such as B, the remaining time for event identification becomes only t_{BC}.

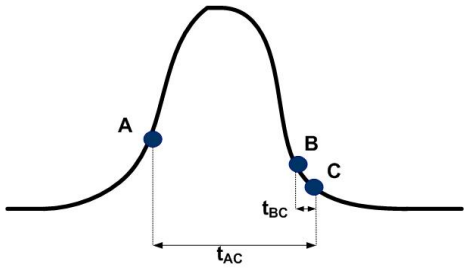

Figure 5.6: Sampling Points on Event Detection Signal

Therefore in order to minimize the overall energy consumption of the system, we need to solve an optimization problem. More epochs available, enable more optimized measurements and therefore less energy consumption in the event identification phase. On the other hand increasing the number of epochs requires a higher sampling rate on the event detection sensor and therefore higher energy consumption in the event detection phase. This optimization problem can be solved depending on different parameters and constraints of applications.

5.4.3 Exploiting Domain Specific Information

Adding semantic interpretations to sensor data can enable optimizations both at architecture and algorithm design levels. Domain knowledge provides information on rate of events, duration of events, location of events, conditional probabilities of events and etc. Rate of events determine how often the event detection sensor needs to sampled. This information together with the duration of events shows how much processing time is available to perform interleaved sampling and data processing. Conditional properties of events provide information on how the sensor groupings can be performed. Location of events on sensing array can determine the sensing circuit design. In addition, studying user activity patterns can also provide information to optimize querying mechanisms.

Examples of semantic knowledge in a mobile textile medical shoe system [NDM10] are information in walking speeds, time that foot is on the ground, etc. In a textile bed sheet system, geometric information on area of body part locations and movements can help in organizing sampling strategies.

Customization can be considered as semantic information that is related to a specific user. Using semantic information we can utilize user dependent information in order to optimize sampling strategies and save energy.

5.5 Case Studies

In this section we demonstrate two built applications using the haptic sheet. The first one is smart keyboard which demonstrates most of notions on sensing system design, sensing strategies and use of domain specific information that we covered in the previous sections. The second application demonstrates a smart surface which accounts for some of the uncertainties present in the haptic sheet. Before describing each application, we provide an overview of our prototype system in these applications.

5.5.1 Prototype Description

Figure 5.7 shows the framework used for our prototype system. The system is composed of a client part and a host part. In the client part, the pressure sensor array is scanned with the use of multiplexers. After the sensing data is acquired by the micro-controller, it is packaged and transferred to the host receiver side through wireless RF circuit. The micro-controller we chose is MSP430f2274. The A/D converter's resolution is 10 bits, and the sample rate is 10 Hz. The communication protocol used to transfer the data is SimpliciTI and CC2500 is used for the wireless chip. SimpliciTI network protocol is a proprietary low-power radio frequency protocol targeting simple, small RF networks. This network protocol can be considered a complement to ZigBee (suitable for larger networks). The client is connected to the sensing circuit described in the previous section. Typing information is transferred wirelessly to the host side potentially a smart phone, PDA or a laptop where it is received by the RF chip.

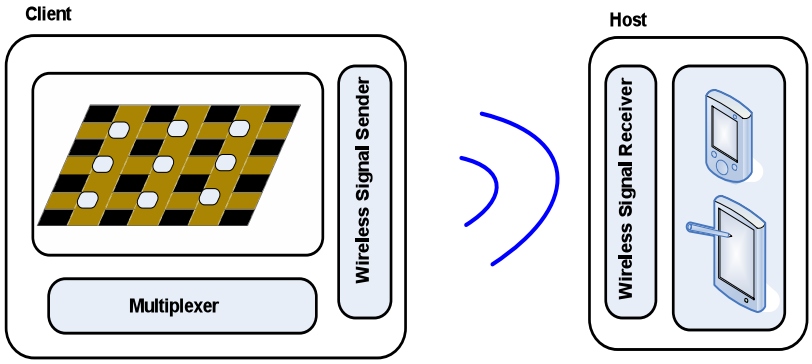

Figure 5.7: System Prototype

Since the applications of this system and similar systems would be in portable/wearable devices we chose, low power, lightweight components for our prototype design. Figure 5.8 shows the EZ430-RF2500 module from Texas Instruments that we chose for our processing and data transfer.

The prototype is powered by two AAA batteries. A UART to USB converter (based on MP2010) is designed for interface compatibility. We have also implemented Bluetooth data transfer which can be used to directly connect to cell phones using serial port, but all our experimental results are based on SimpliciTI protocol.

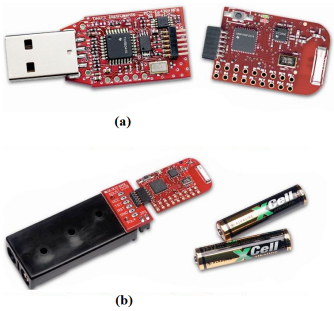

Figure 5.8: EZ430-RF2500 Module

5.5.2 Smart Object: keyboard

Pressure sensors and smart E-Textiles provide a starting point for a wide spectrum of interesting smart objects including smart shoes, smart bed sheets, instrumented gloves, medical canes and smart dressing items [32,33]. An example of such application is a portable keyboard which is designed to be used with small wireless devices such as personal digital assistants (PDAs) and smart phones. Using keyboards with adequate keys to support applications such as writing emails, editing documents and etc. for mobile applications has received a great deal of attention [30,31]. The productivity of the user can be greatly improved by providing full scale and customizable keyboards that are light, low cost and easy to transport and deploy. In addition to enabling the user to use the same keyboard while interacting with a various devices, there are other important advantages. For example, a large number of diseases are transferred using hand contact. Therefore, shared keyboards such as one used at airports for passenger checking, pose significant health risks that are completely eliminated by E-textile keyboards. In addition, E-textile keyboards enable much better security and user authentication. Finally, the new keyboards can also collect a variety of statistics about the user that can be used for improving productivity and even detection of health induced irregularities. In prototype keyboard that we design here has 102 keys.

5.5.2.1 Power Consumption Model

In this section we derive a power consumption model for the system described above. The total power consumption is composed of the power consumed in the sensing circuit and the transmission sub-system shown in Equation 5.1.

$$P_T = P_{Sens} + P_{Com} \tag{5.1}$$

The sensing power (P_{Sens}) is composed of the power driven by the sensing circuit and sampling power. The former is calculated using resistance in the face of asserted pressure while the later is proportional to the power consumed by ADCs as each sensor reading is through a 10-bit ADC. As it can be seen in Table 1, P_{Sens} is dominated by ADC power. This is why group readings are beneficial as they only consume one ADC unit. In the event of group readings the power consumed by summing amplifiers which is in the same order of sensing circuit are also added. Table 5.1 is calculated according to datasheets [34, 35].

Table 5.1: Energy Consumption of Sub-Modules

Sub-module	**Energy (J)**
ADC(per sample)	9*E-9
Data Transmission(per sample)	7.2*E-9
Sensing circuit (average per sensor)	4.8*E-10

From data transmission power which is in the order of ADC power we see that localized processing is a must and that minimizing the number of sensing readings dominates overall energy consumption.

5.5.2.2 Sensing Architecture Design

Using a two-layer design described in Figure 5.4 for our prototype keyboard we would need 17 columns and 6 rows to cover all keys. With this design scheme, rows and columns can be scanned simultaneously to identify the location of the pressed key. To perform architecture exploration we simplify the querying mechanism to consider the extreme case of requiring one epoch (unit of time) for each reading. In this case, the number of queries becomes linear to the number of sensors at each vertical and horizontal side. Therefore, either columns or rows will dominate the querying time depending on the number of sensors they possess. In the case of our current prototype which needs 17 columns and 6 rows, the querying is dominated by the columns. Another advantage of balanced architecture is in terms of sensing. With 17 columns and 6 rows, 23 readings are needed,

whereas in a more balanced architecture of 9 and 12, only 21 readings are needed.

From the above discussion we conclude that a balanced architecture, in terms of number of columns and rows would be more beneficial. For 102 keys (17*6), the most balanced architecture would imply 10 and 11 columns and rows respectively. However due to geometrical constraints such as the need to preserve the neighboring arrangement of each sensor, a balanced design of 10 and 11 is not trivial. In Figure 5.9 we show the sensor arrangements of 9 and 12 columns and rows that produce a fairly balanced architecture. Figure 5.9.a shows the arrangements of 12 rows instead of the original 6 rows. This layer would become the bottom layer of the keyboard. Note that this arrangement results in a unique pair of sensors for each key.

Similarly Figure 5.9.b shows the arrangement of 9 columns. Imagining a virtual line in the middle of the layer, each two sensors from each side are merged to create one sensor. This imaginary line is aligned with the line breaking the 6 rows in 12 rows in the bottom layer. Therefore from Figure 5.9 we can see that since 17 is odd we have 8 columns of 12 rows and 1 column of 6.

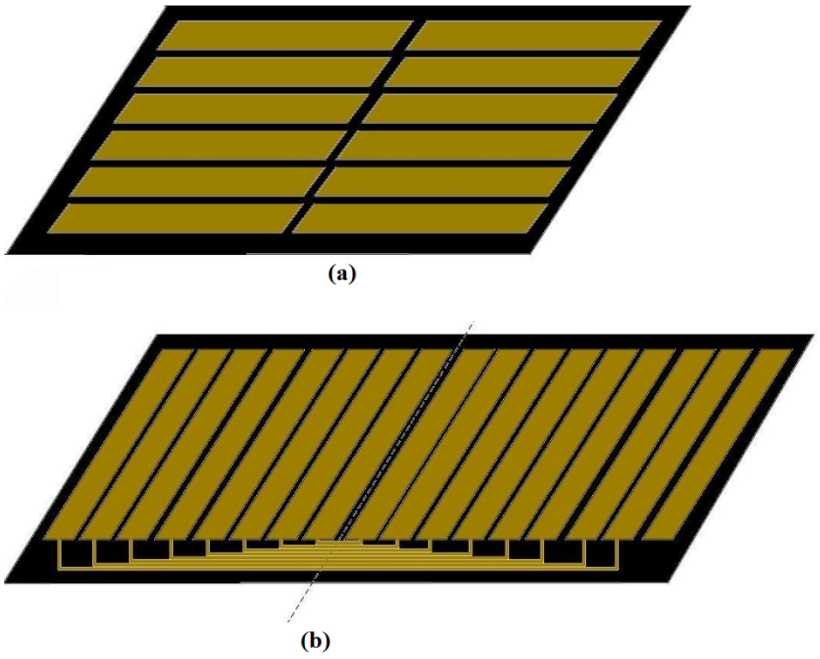

Figure 5.9: Balanced Sensor Array (a) Rows (b) Columns

The widths of the sensing elements are chosen similar to available keyboards (around 1.3cm).

However the choice of the distance between parallel sensing elements is important due to its effect on our detection algorithms. Earlier we described the neighboring effect inherent in sensing elements that share their sensing layers. We choose the distance between consecutive sensing elements in such a way that the neighboring effect is observable on its neighbor sensor but no further. To elaborate, in this design a key press, would result in value changes on 6 readings (3 columns and 3 rows). By conducting experiments we found that placing the center of sensors within 1.5 cm spacing will produce the desired neighboring effect. The detection mechanism that leverages this design is described later in this Chapter. One obvious improvement is that we read 21 (12+9) signals instead of 23 (17+6).

5.5.2.3 Decoupled Event Detection and Identification

Based on the two layer proposed architecture described in the last section, using a summing amplifier we add all the signals from the columns to create an event detector signal. Figure 5.10 shows the event detector signal together with two other columns. The sampling is performed only on this signal and further analysis on key identification is performed only in the case of an event. Sensed values which are larger than a platform based threshold are considered as events. The main concern here is to capture events early enough to allow time for event identification.

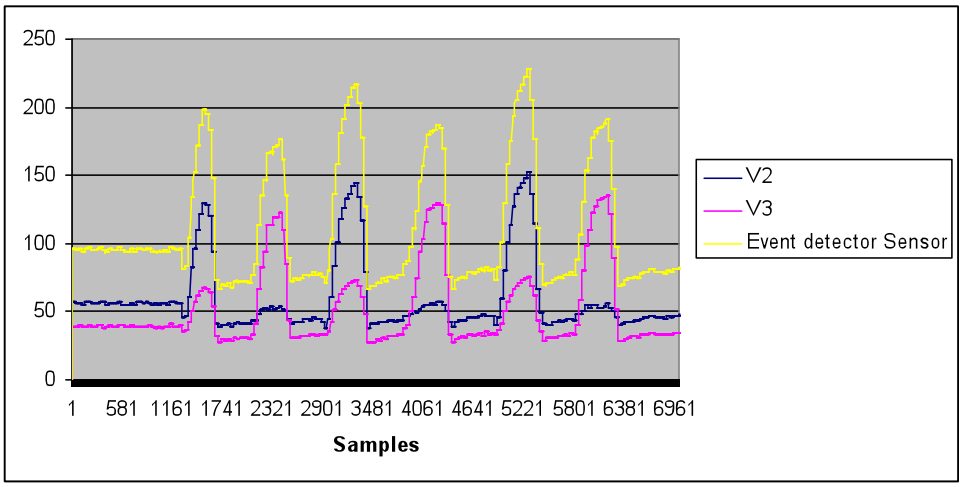

Figure 5.10: Detector Sensor, column 3 and 4 Readings while Pressing 'A' and 'S' keys Consecutively

Once there is no event detected by the event detector sensor for a specific amount of time (in

our case 5mins), the keyboard is considered idle and thus the event detector sensor stops sampling to save energy. For using the keyboard again after an idle period, the user should press an activation button on the keyboard.

5.5.2.4 Interleaved and Coordinated Sampling and Data Processing

As discussed, our prototype keyboard uses a sensing model where only the closest sensor and its two neighbors detect pressure change. Figure 5.10 shows two adjacent columns on the keyboard (V2 and V3). In the scenario shown, keys 'A' and 'S' each on one column, are pressed consecutively. Due to the sensing model, in the case of activation on V2, a relatively smaller activation is observed on V3 and vice versa. Therefore based on our sensing model, after applying the binary mapping stage, a single key press will result in either a pattern of three consecutive '1's or two consecutive '1's at the boundaries. This is shown below, where we show the binary representation of 9 columns in the presence of a single key press at two different locations.

000011100: Event on 6th column

110000000: Event on 1st Column

Here, using the interleaved sampling and data processing method described, if the available time restricts all the reasoning to be performed in one epoch, instead of performing n sensor readings to find a key press among n sensors, reading every other sensor (plus 1, to cover both boundaries in case of even number of sensors) will suffice ([n/2]+1). For multiple epoch processing, this can be done in the last step. For example for two epoch processing, after the search space is reduced by the order of two, three or more in the first epoch, in the second epoch sensors can be measured in the every other pattern. Here since we have 1 MIPS processor, we assume all the computations necessary for key identification to be performed in one epoch.

We show the efficiency of group readings and multiple epoch processing in improving the expected number of readings, in the below example of 4 sensors with the below configuration:

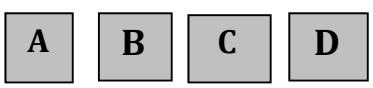

Figure 5.11: Four Sensor Example

In a 3 epoch available time we arrange our readings as below:

In epoch 1 if the group readings of sensors A and B results in a '0', considering the neighboring effect we can conclude that the pressed key is D and we are finished in the first epoch. However, if it results in '1' we proceed to epoch 2 and perform a reading on sensor D. Remembering measurement results of epoch 1, a '1' reading from sensor D means that sensor C should be the pressed key since we sense it's neighboring effect on it's surrounding sensors. Therefore in the case of C being our pressed key, readings terminate in epoch 2, otherwise we proceed to epoch 3 where we perform a reading on sensor C. With similar reasoning a '0' and '1' reading will indicate sensors A and B as the pressed keys respectively. Therefore the expected number of readings using this method will reduce to 2.25 using the below calculation.

$$E(Readings) = \frac{1}{4} \times 1 + \frac{1}{4} \times 2 + \frac{1}{2} \times 3 = 2.25$$

Without the use of this method and calculating everything in 1 epoch would need 4 readings. Using multiple epochs but no group readings will result to the expected value of 2.5 readings. Therefore with this small example we can see the advantages of using both multiple epoch processing and group readings.

Using similar reasoning we have calculated using a one time static exhaustive algorithm, the optimal number of readings with group reading arrangements for different epochs for both rows and columns of our prototype keyboard. The expected value of number of readings required for rows and columns are shown in Table 5.1 .

Table 5.2: Combinatorial Search Method for Columns and Rows

Epochs	**Number of Readings for Columns (9)**	**Number of Readings for Rows (12)**
1	5	7
2	3.55	4
3	3.22	3.66
4	3.22	3.66

The sampling mechanism in the event detector sensor will determine the number of epochs available for processing. We set the longest interval without sampling in such a way that the time is minimal, but sufficient for both event detection and additional measurements required for key identification. To formulate this, if TS represents time of typing session and TP is considered

minimum duration of a typing pulse, we can approximate the number of samples needed to be performed by the global event detector sensor as shown in Equation 5.3. In this case depending on different choices of available time ($T_{Available}$) different stages can be chosen from Table 5.2 to identify the pressed key.

$$N_{Samples} = \frac{T_s}{T_p - T_{Available}} \tag{5.2}$$

The method described above is for single key presses at a time. In some situation a user may press two or more keys simultaneously. We can address the situation when two keys are pressed using an optimal algorithm, similar to the case when single key is activated. Resolving situation when three or more keys are simultaneously pressed induces high energy overhead. Since it happens rarely in actual use of keyboard, we leave this up to the typist to correct such instances. Here we show why an arrangement of 12 and 9 is more beneficial than the original 17 and 6. Table 5.3 shows combinatorial search methods for 17 columns and 6 rows.

Table 5.3: Combinatorial Search Method for Unbalanced Architecture

Epochs	**Number of Readings for Columns (17)**	**Number of Readings for Rows (6)**
1	9	4
2	4.70	2.66
3	4.23	2.66
4	4.17	2.66

In comparing this table with Table 5.2 we can easily see that Table 5.2 is better in the first epoch. It might not be clear to see why Table 2 is better in other epochs as well. The reason for this is that in calculation we should consider we actually have 8 columns of 12 and 1 column of 6 sensors. Using the calculations in Table Table 5.3 for 6 sensors we can easily see that a 12 by 9 arrangement is better than 17 and 9 overall. Even a better saving can be achieved if we change the column connection, by splitting one column to create 7 columns of 12 sensors and 2 columns of 9 which saves even more energy.

5.5.2.5 Exploiting Domain Specific Information

In this section we show how the use of semantic information can optimize our sensing strategies and how we can perform customization using this.

Domain Specific Information: We exploit semantic information of typing language in order to further reduce the system energy consumption. Results presented in Table 5.2 in the previous section, assumes equal probabilities of events per sensor. However, using semantic information of the language one would see that columns and rows have unequal probabilities of being activated. We leverage this property to modify our querying scheme to find more likely events at an earlier time and thus reduce the total expected number of readings required. To elaborate this, we revisit the example of Figure 5.11. In this case if different sensors have different probabilities of being pressed, it is beneficial to place the key with highest frequency in location D so that only one reading is required to identify it. Similarly the next key with highest frequency would be places in location C and so on.

We used relative frequency of letters in English from [29] to calculate probabilities for rows and columns on our prototype keyboard by adding probabilities of keys in each row/column. Using this frequency information we found the optimal sampling strategy for different epochs available using the same strategy. The results for this are shown in Table 5.4 . This method can be adapted to other languages as well and we can make customized keyboards for languages.

Table 5.4: Combinatorial Search Method with Semantic Information for Columns and Rows

Epochs	**Number of Readings for Columns (9)**	**Number of Readings for Rows (12)**
1	5	7
2	2.92	2.49
3	1.68	1.58
4	1.68	1.58

Table 5.4 shows better savings accomplished in the rows compared to columns. The reason for this is considering the standard layout of keyboards and our sensing architecture keys are better distributed in the rows in term of their frequency of occurrence relative to columns. In addition,

similar to above, we can consider conditional frequency of letters to each other to calculate search strategies.

Customization: Customization can be considered as semantic information that is related to a specific user. Users of keyboards have different typing-level proficiency and typing characteristics. This information can be used in order to perform customization on the sampling strategies used in the keyboard. Information gathered from customization does not affect the event identification but can vary the event detection phase. In this section, we perform customization in two ways. First we exploit typing speed information to adjust the event detection sampling and second, we leverage customized information about latency of the next event as conditional value that depends on the previous event.

The minimum time between consecutive activations of two characters is beneficial in adjusting the event identification sampling. For example, for a typist with the speed of 1 char per second there is no point in sampling every 0.1 second or less. We collected data for minimum time between two consecutive key presses for different people using our prototype keyboard. For the people we tested the results showed different values from to 399 ms to 699 ms. We noticed relatively slower typing speeds on our prototype keyboard compared to standard keyboards.

The second component is a conditional measure of the minimal time of an event after a known event. This minimal time guides our sensor querying (sampling) schedule. We use this information to create customized sampling schedules. We measured the minimal time of an event after each of the alphabet characters. Figure 5.12 shows the minimum, median and maximum of this value over five participants.

Figure 5.12 is interesting from two aspects. First, that some characters have relatively longer delays after them, over all users and second that delays after characters are different among users. To better see this we show the data for two of the users in Figure 5.13.

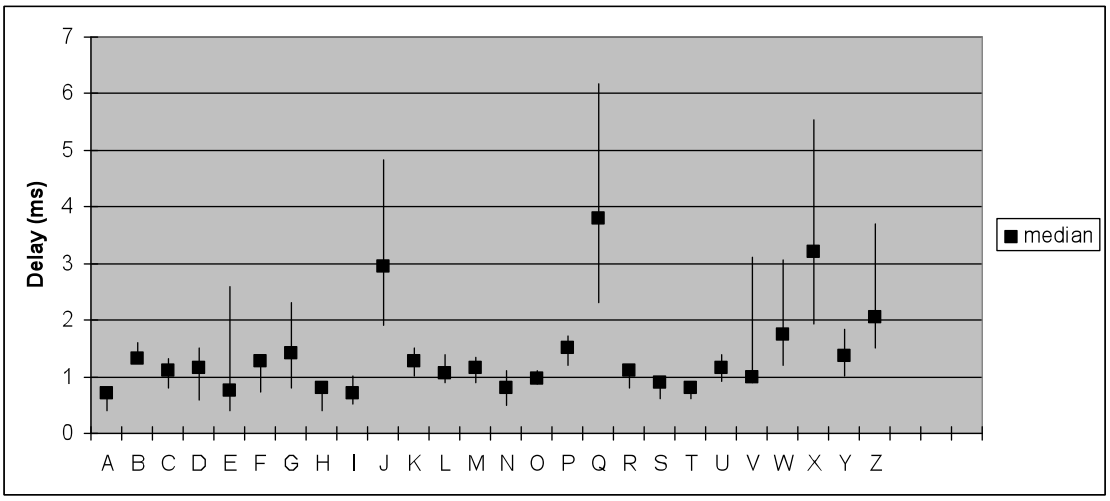

Figure 5.12: Conditional Measure of Minimal Time of an Event After a Known Event

5.5.2.6 Experimental Results

In this section we show the energy savings resulting from sampling and processing strategies described. We gathered typing data from different people and performed statistical analysis to find the necessary parameters for our proposed sampling scheme. One of these parameters is the duration of a key press pulse. This amount is different among different people and is also different for the same person in different situations and different keys. A direction for future work can be studying these pulses under different typing situations (e.g., stress) and use it in customization. Here, we only consider the minimum pulse duration we found over all people which is 250 ms. We use this parameter in determining the sampling frequency of the global sensor detector using Equation 5.3.

We compare 4 different strategies. Method 1 is energy results for using non-intelligent sampling of all sensors at 10 Hz sampling intervals for key identification. However this method is still better than a trivial non optimized method since it uses a near optimized sensing architecture which only requires n+m readings for n*m keys. Method 2, uses statistical information on duration of typing forces to reduce sampling intervals on the optimized sensing architecture. In Method 3 we use our proposed combinatorial search in binary representation of signals with epoch time intervals. In Method 4 we integrate semantic information to our combinatorial search mechanism together with statistical information about type force durations on our near optimized sensing structure. The time

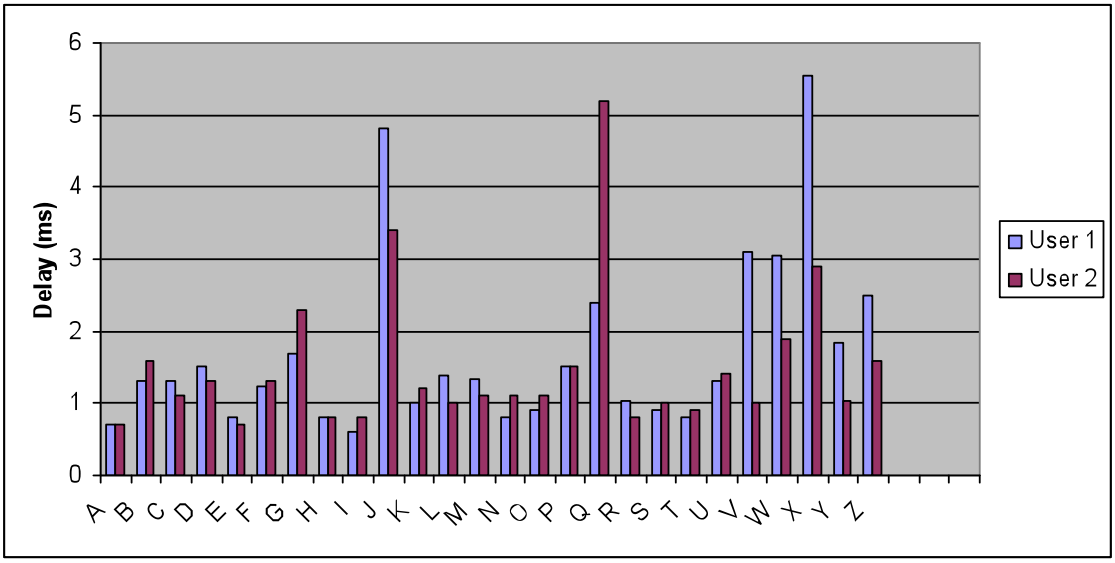

Figure 5.13: Conditional Measure of Minimal Time of an Event After a Known Event for Two Users

of session in the below experiments is 20 seconds. This information is presented in Table 5.5.

Table 5.5: Energy Consumption of sampling techniques (nJ)

Typing Speed (chars per sec)	**Method 1**	**Method 2**	**Method 3**	**Method 4**
1.75	41.4	15.12	2.89300	1.7199
0.5	41.4	15.12	1.34500	0.9864
2.2	41.4	15.12	3.45028	1.98396
5	41.4	15.12	6.91780	3.627

To show the efficiency of our combinatorial search sensing we show the different situations of Method 3 and 4 based on available epochs and their energy consumptions in Tables 5.6 and 5.7.

As Table 5.5 shows using our most optimized version that uses semantic information with 4 epochs we are able to achieve savings from 12x to more than 42x in energy consumption depending in typing speeds compared to the non optimized version (Method 1). Comparing to Method 2 which uses statistical data of typing force durations we achieve 4x to 15x savings in energy consumption. As expected, if the user is excellent typist the savings are minimal and if the user is slow typist the savings are very significant.

Our most optimized version is when we consider, customization in our sampling. We show

Table 5.6: Energy Consumptions for Combinatorial Search in Binary Representation (nJ)

Typing Speed (chars per sec)	1 Epoch	2 Epochs	3 Epochs	4 Epochs
1.75	4.5	3.10114	2.89300	2.89594
0.5	1.8	1.40239	1.34500	1.34794
2.2	5.472	3.71269	3.45028	3.45322
5	11.52	7.51789	6.91780	6.92074

Table 5.7: Energy Consumptions for Combinatorial Search Using Semantic Information in Binary Representation (nJ)

Typing Speed (chars per sec)	1 Epoch	2 Epochs	3 Epochs	4 Epochs
1.75	4.5	2.4151	1.7289	1.7199
0.5	1.8	1.1979	0.9954	0.9864
2.2	5.472	2.8533	1.9929	1.98396
5	11.52	5.58	3.636	3.627

two different customization techniques. First we use minimum delay between characters for each person. This customization has its most benefit in slow typists (Customization A). In this method we consider both the duration of typing pulses and minimum delay between key presses. In the second customization we go further to use information from conditional measure of the minimal time based on characters identified (Customization B). The saving from customization is because of more efficient sampling in event detection. Event identification energy remains the same. Below in Table 5.8 we show the result of customization on three of the users and compare it with Method 4 which was the more optimized method we had achieved before customization.

Table 5.8: Energy Consumption of Customization Sampling Techniques (nJ)

Users	Typing Speed (chars per second)	Method 4	Customized A	Customized B
1	0.599	1.6612	1.24172	1.11039
2	0.398	2.16	1.892261	1.62537
3	0.699	1.54386	1.08137	1.00050

Results of Table 5.7 indicates that we can achieve up to a further 1.5x savings compared to out most optimized version before customization. Therefore considering altogether savings, we achieve up to compared to 63x compared to the non optimized method and 23x compared to Method 2 which uses intelligence on typing force durations.

The lifetime of the system using the most optimized sensing mechanism is more than 500 hours with two AAA batteries. This is significant energy reductions comparing to current available foldable keyboards [36, 37] which offer 90 hours life time.

5.5.3 Smart Surface

In this section we focus on one of the mentioned capabilities of the haptic sheet which was object localization and recognitions. As mentioned earlier, this feature is helpful in many applications such as bed sheet, table to interfaces and etc. Using the haptic sheet object localization is possible without the use of RFID tags placed on objects. Pressure map based object recognition is a complementary way of image processing based recognition. However, using cameras and images for performing object recognition is not used here in order to limit the system's knowledge to specific objects. Cameras will provide unlimited knowledge about the under test environment, whereas the Smart Textile Surface limits the system's knowledge to specific objects that are introduced to the system, not violating privacy. Therefore the level of privacy can be controlled in such system based on application needs. Blocked object recognition is a challenge in image processing; however our approach can obtain information about blocked objects based on weight information.

However, one of the problems which makes object recognition not trivial is the present of the neighboring effect between sensors. In the last section, in the smart keyboard application, we leveraged this effect to be able to sense more locations per sample. But here since object recognition is based on weight and shape features, accurate sensor data is needed in order to be able to perform accurate weight calculation.

5.5.3.1 Smart Surface Algorithms in the Presence of Interference and Uncertainty

Not considering different sampling mechanisms and how all the data is gathered, each surface reading is a two dimensional array of values between 0-255 representing the pressure map of the objects placed on it. This is very similar to the input of many computer vision algorithms, processing images for object recognition.

The idea of directly applying existing computer vision algorithms is attractive but there are

significant differences between the two that requires major modifications in the algorithm design. The most important difference is sensor uncertainty and error existing in the system. Although errors of such are also apparent in images, however due to different sources and nature of errors the algorithms dealing with them are completely different. Sensor errors may present significance importance in cases where each sensor area is big relatively to the object's area. Therefore, in this section we first derive a model of the errors in the system and then present modified algorithms using this model. One assumption made here is that the textile surface is much larger than the objects placed on it.

5.5.3.2 Uncertainty and Interference

In this section we use an experimental approach to model interference existing in the system. This interference is mainly due to the neighboring effect which is described below. As discussed, a single sensing layer is shared among all the array sensors, and sensors are within certain spaces to each other. When applying pressure on one sensor, the effect would be inevitably posed on its surrounding sensors on account of mechanical linkage. Here note that the mechanical linkage between the sensors is minimal if they are not adjacent. We define the accumulating pressure sensed on each location due to forces applied not directly to itself but to its surrounding locations, the neighboring effect. The experimental set-up is as follows: a range of weight scales were applied to one sensor location (X in Figure 5.14) and all the values read from its 8 neighbors (N1 to N8 in Figure 5.14) were recorded.

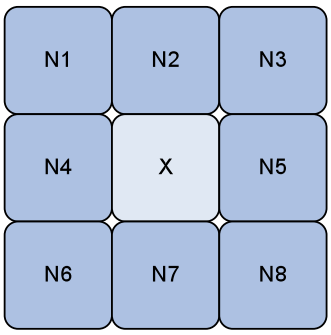

Figure 5.14: Neighboring Effect

Below in Tables 5.9, these values are shown for weights 50g - 250g for each of the neighbors.

Note that the values shown for X are sensor reading and not weights.

Table 5.9: Neighboring Effect on 8 Neighbors for Weights 10g to 1.5kg

Value read from X	**N1**	**N2**	**N3**	**N4**	**N5**	**N6**	**N7**	**N8**
10	1	4	2	6	6	1	5	1
18	1	7	2	8	8	2	7	0
29	1	11	3	10	11	1	12	2
34	1	14	2	12	12	2	14	1
46	3	18	3	15	15	2	18	2

From Tables 5.9, we can see the neighboring effect of locations N2, N4, N5 and N7 (above, left, right and below X) are similar to each other, and different from locations on the diagonal positions. This is better shown in Figure 5.15, where similar locations are grouped together. Values in Figure 5.15 correspond to objects with weights in the range of 50g-1kg.

We performed linear regression on each set of data. Equations 5.3 and 5.4 show the corresponding relationships together with square R for each set of locations around X.

$$y = 0.0006x^2 + 0.2257x + 2.2443 \qquad R^2 = 0.97 \tag{5.3}$$

$$y = 3E - 05x^2 + 0.0478x + 0.0896 \qquad R^2 = 0.79 \tag{5.4}$$

5.5.3.3 Algorithm Overview

Weight and shape are the two main features we use to recognize objects. The weight of the object is assumed to be consistent throughout time. But depending on the 3D shape of objects, they can be placed from various directions on the surface. Therefore the attributes we use to save information about objects are weight and a series of edges that represent objects shape. The system has two phases: a) Learning and b) Recognition. In the learning phase objects are placed from every possible stable position on the surface. The shape of the object is determined through an edge detection algorithm described later. This information together with the object weight is stored in the database for that object.

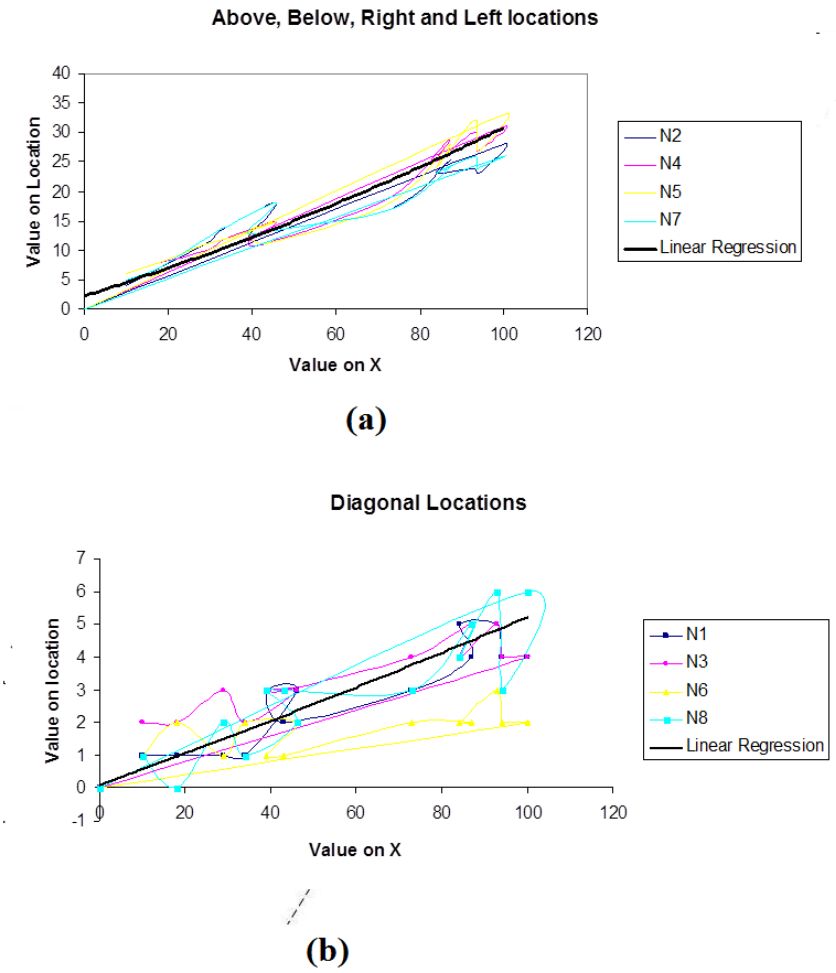

Figure 5.15: Linear Regression

In the recognition phase, various objects are placed on the surface. Our proposed edge detection algorithm determines boundaries of each object together with its weight. This information is searched in the database to find the best match to the measured data. Note that, at this stage we assume non-overlapping objects as inputs of the edge detection algorithm.

5.5.3.4 Computing with Uncertainty

Finding the object's shape is based on edge detection. Without the presence of uncertainty in sensor data, edge detection is a straightforward task. A binary mapping is done from the value of each location based on a threshold value. Locations having a value higher than the threshold are set

to 1 to represent object area, while other locations below the threshold are set to 0. The boundary that separates the 0 and 1 locations is identified as object's edges.

However, due to the presence of uncertainty and interference as described earlier, this process is prone to error. Therefore prior to edge detection we perform another mapping that accounts for the neighboring affect. Figure 5.16 depicts the mapping process.

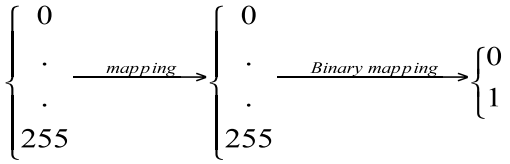

Figure 5.16: Stages for Edge Detection

Figure 5.17 shows the proposed algorithm for thresholding and edge detection in the face of interference. Steps 1-3 in this algorithm perform the first mapping in Figure 5.16 while step 4 performs the binary mapping in Figure 5.16. In summery the algorithm starts at the location with minimum weight. This is because this location has the least effect on its neighbors. Note that our main goal in the binary mapping step is to find correct object area and not an exact pressure value of locations.

Note that in each location analysis we only consider its 8 neighbors. Although more distant locations might also have effect on location X's data, we consider their affects recursively onto X's 8 neighbors when processing X. The algorithm above assumes single object detection on the surface. In case of multiple non-overlapping objects, a segmentation phase needs to be also added. In line 2 the reason for choosing $w_{mij} + \Delta$ is to not calculate the effects of locations with similar values on each other. Here, Δ is the sensor error. A simple thresholding method can be to make values higher than 0, 1.

In our proposed Smart Textile Surface we enable an architecture that allows sensing of objects with weights in different ranges. This can be done using multiple layers of different sensing material which we will not describe its details here. However, with the presence of uncertainty, there is a lower bound in being able to discriminate between objects of same shape and area. This lower bound gives a measure of the accuracy of the system. The weight of an object can be calculated from Equation 5.5:

1. We first sort the locations based on their weights from small to large. Let w_{mij} be the minimum weight location in the surface. Consider a 3x3 window around it.
2. For each location ij, consider the 8 surrounding neighbors (3 or 5 neighbors for corner and edge locations).
   Calculate the accumulating neighboring effect based on rules in part A for neighbors with larger values than $w_{mij} + \Delta$ (where $\Delta \leq sensor\ error$)

   $$\text{Neighboring Effect (Ne)} = \sum_{i=0}^{8} N_i$$

   Make the new value of w_{mij} be $w_{mij}' = w_{mij} - Ne$

   Any negative value will be mapped to zero.

3. Let w_{mij} be the next smallest weight location in the list. Go to 2 until all locations have been processed.
4. Once all locations are processed perform thresholding on all locations.
5. For performing edge detection, for each location, if any of its eight neighbors are 0 that location is marked as an edge.

Figure 5.17: Modified Thresholding and Edge Detection Algorithm

$$2 + 1w_x = \sum a_{ij} \times w_{mij} \quad , \quad a_{ij} = \begin{cases} 0 & \text{if } location\ ij\ is\ 0 \\ 1 & \text{if } location\ ij\ is\ 1 \end{cases} \tag{5.5}$$

In the above equation w_{mij} is the measured weight of location ij after the algorithm in Figure 5.17 is applied and aij is determined by step 4 of the algorithm (thresholding). However there are multiple sources of uncertainties in the above formulas. One source of uncertainty is sensor uncertainty (Δ) which is due to manufacturing and sensor degradation in time. The ADC resolution limitation is another kind of inherent systematic error. For example, the quantization error of 8-bit ADC is 0.39 %. Another source of uncertainty is due to interference modeling. As described before, linear regression is used to derive equations 1-2. Linear regression is not accurate and suffers from error. This error affects weight computation since the wmijs used in Equation 5.5 are computed by using the below formula. Here wm is the measured weight read from the sensors.

$$w_{mij} = w_m - \sum_{i=0}^{8} N_i \tag{5.6}$$

And each of the N_is in this equation suffers from regression error. The R squared values derived before, show this error. Equations 5.7 and 5.8 formulate these uncertainties:

$$w_m = w_{mc} \pm \Delta\%.w_m \tag{5.7}$$

$$N_i = N_{ic} \pm (1 - R^2)\%.N_i \tag{5.8}$$

In the above formulas, w_{mc} and N_{ic} are the correct value of w_m and N_i respectively which is unknown to us. Therefore if we combine, Equations 5.5- 5.8 we will have the worst case uncertainty of:

$$W_x = W_{mx} + \Delta\% \times \sum_{n} w_m + (1 - R^2)\% \times \sum_{8n} N_i \tag{5.9}$$

Here W_{mx} is correspondingly the exact weight of object x. Therefore the difference in weights of two different objects of size n should be at least the value of $\Delta\% \times \sum_n w_m + (1 - R^2)\% \times \sum_{8n} N_i$ in order to be able to distinguish for our system.

5.5.3.5 Experimental Results

The Smart Textile Surface we developed for our experiments is a 16x16 array of 1x1cm sensors with a 50mm spacing. The E-textile used is NW170-PI-10E4 from EEONYX [T10]. Conductive threads were chosen for the conductive part.

We placed several objects of different weights and shapes on the developed Smart Textile Surface. Figure 5.18 shows the output of the user interface GUI developed for the edge detection algorithm.

In order to evaluate the effect of our proposed algorithm for eliminating the neighboring effect

we present the details of our proposed algorithm, by showing each stage of our proposed algorithm on a wire roll object. Figure 5.19.a shows the object under test.

Figure 5.19.b shows this object from top view and how it is located on the surface. The reason for choosing this object is the middle location on the surface which suffers most from the neighboring effect. Figure 5.20.a shows the sensor data obtained from the Smart Textile Surface.

Applying a trivial thresholding and edge detection algorithm on the data in Figure 5.20 will result in a wrong result (29). A trivial algorithm cannot distinguish any differences between value of locations 13 (L13) and L7, L9, L17, L19. But our proposed algorithm applies the Interference rules and from that distinguishes correct area locations. As we see one sensor value has a great effect on the output of our object recognition program. Please note that although the resulting shape is a hollow square instead of a hollow circle, we are able to detect the circular shape of the object by simply using smaller sensor sizes. The current sensor size and objects are used as a proof of concept.

5.6 Conclusion

In this chapter the design, architecture and applications of a flexible haptic sheet made from E-textiles is described. This sheet consists of an array of pressure sensing elements and is capable to capture events (pressure asserted at different locations) and perform object localization on objects placed on it. The flexible nature of E-Textile material enables the widespread use of this surface in wearable contexts as a non-intrusive monitoring system in Wireless Health applications. In this chapter I have looked at efficient sensor structure design that minimizes the number of samples required and therefore increase the life time of these systems have been discussed. I have also looked at designing efficient sampling techniques that use the semantic knowledge about the application to perform less and on-time samplings in such systems.

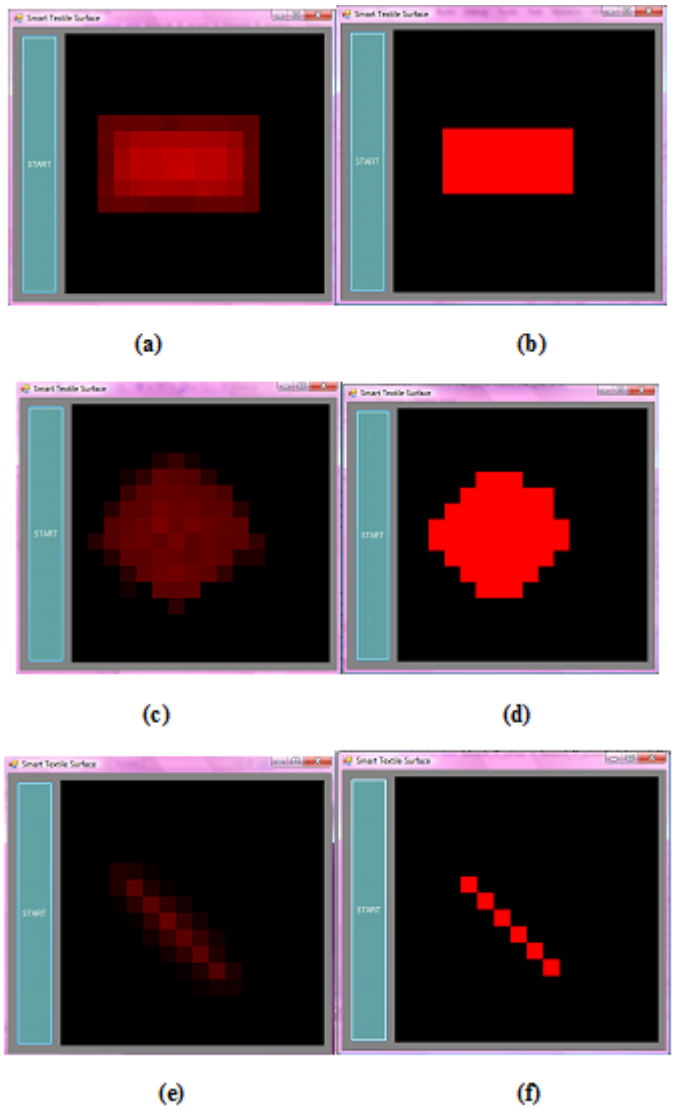

Figure 5.18: Sensor Readings for Objects and Result of Thresholding.(a) Sensor Reading for an iphone. (b) Thresholding Result of an iphone (c) Sensor Reading for a Cup (d) Thresholding Result of a Cup (e) Sensor Reading for a Marker pen (f) Thresholding Result of a Marker

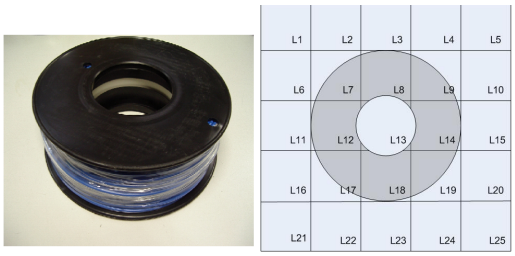

Figure 5.19: (a) Object Under Test (b) Object View from Above

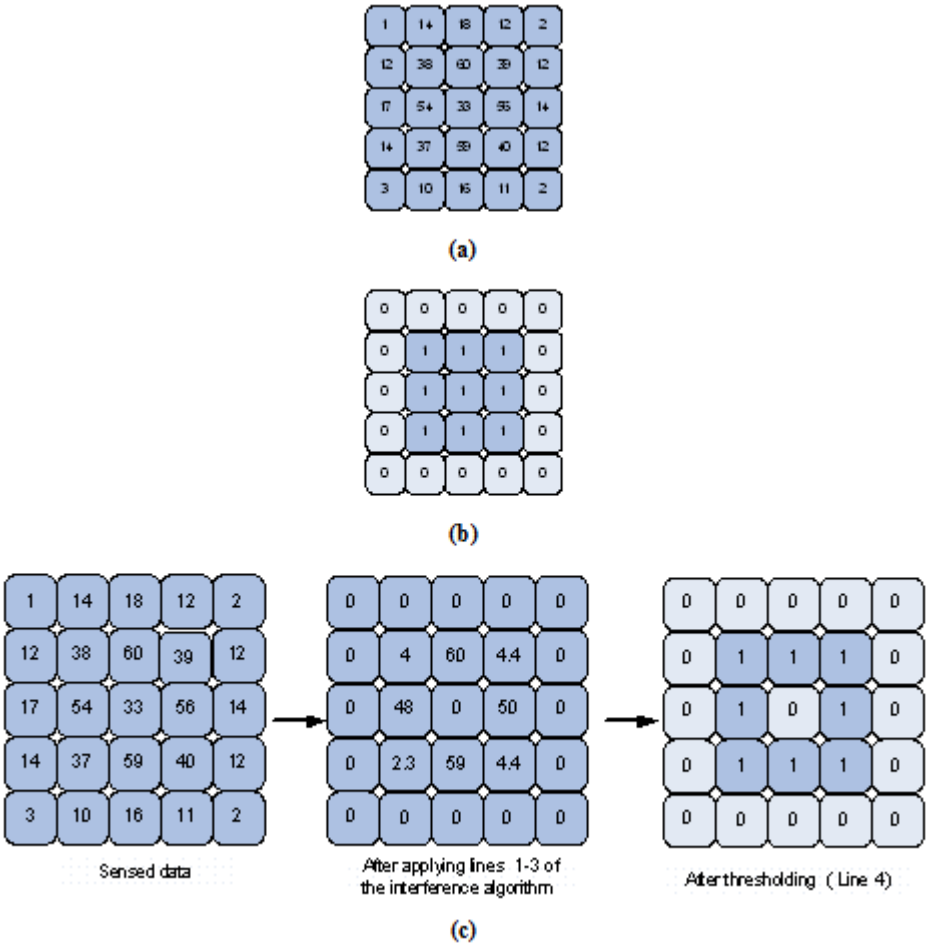

Figure 5.20: (a) Sensor Data (b) Result of a Trivial Thresholding (c) Final Result

CHAPTER 6

Haptic-based Feedback

Haptic feedback provides an effective means of transferring information through tactile stimulation. In this chapter we look into the use of tactors for haptic feedback in body-worn contexts where individuals are allowed to move around. In this context it is crucial to design low power systems that allow the activation of multiple tactors at the same time with limited battery power. We investigate how to minimize tactor power consumption by tuning the characteristics of their excitatory signal and present an activation policy to maximize the number of tactors that can be simultaneously powered by a battery under a tight peak current constraint.

The proposed optimizations reduce power consumption and allow a much higher number of simultaneously active tactors. Furthermore, we provide a design strategy whereby designers can tune the maximum number of simultaneously allowed active tactors based on battery and system requirements.

6.1 Haptic Feedback

Haptic feedback is used as a means of transferring information to individuals using tactile stimulation as an alternative to the traditional methods of auditory or visual feedback. Moreover, it has been deployed in a broad range of applications from biomedical and tele-surgery to robotics and virtual reality [Col70, LB66, KMB03, BF00, SGB01]. Tactile stimulation has been extensively used to provide various kinds of information about the environment and objects to visually handicapped individuals since several decades ago [Col70, LB66].

In the field of virtual reality, haptic sensation provides physical interaction between the subject and virtual environments. For instance, the work in [KMB03] presents a data glove with a built-in

vibratory stimulus device for tactile feedback during virtual reality experiments. This is towards the goal of being able to accurately mimic real-life events and assessing neurological and psychiatric disorders through brain activity. In telesurgery, the surgeon's perception of the patient is limited to visual feedback. There is work investigating the use of haptic feedback to provide the surgeon with tactile sensation of the patient's tissue in several surgery procedures [BF00, SGB01].

A vast range of applications deploy tactile stimulation in body-worn contexts with either single or multiple sources of haptic feedback. Some of these systems only target specific parts of the body, like fingertips, shoulders, wrists, etc. Others cover the whole body through suit-type active clothing. An example of the former group is in [TGY03] where haptic cues are used to draw the individuals attention to a specific area of interest on the body. In some applications, rich information is transferred to individuals by employing a large number of tactors concentrated at high density in one region of the body. In [Col70], 400 tactile stimulators are used in a tactile television system to permit blind to determine the position, size and movements of objects. [JSA10] explores the effect of vibro-tactile biofeedback on body sway in stance in patients with severe bilateral vestibular losses.

In all these fields of application wireless sensor networks and body area networks are getting momentum as enabling technologies in healthcare. Therefore, the integration of actuation capabilities in some of the nodes of a network will enable many interesting possibilities.

In body-worn contexts, many biomedical applications would benefit from allowing people equipped with a large number of tactors, possibly in form of a wireless network of small devices, to move around instead of forcing them to sit on chairs or wear vests with mounted tactors connected to large power supplies. Therefore it is important to design low power systems that provide this capability. This creates the problem of being able to support a high number of tactors with limited power, particularly if equipped with wireless capabilities. On the other hand, providing haptic feedback through vibration implies mechanical movement which requires higher power levels in comparison to other tasks of a mobile application. This problem is even more challenging in the case where multiple tactors are needed.

Batteries have a maximum discharge current which bounds the number of simultaneously ac-

tive tactors driven by it. In a scenario where the current used for stimulation is I_x and the maximum discharge current of the battery used is I_y, a trivial method will allow a number of $\left\lfloor \frac{I_y}{I_x} \right\rfloor$ simultaneously active tactors (assuming the current driven by other parts is insignificant). This number can be as small as 3-4 based on the characteristics of the battery. In this chapter we present a method to allow the increase of this number to hundreds. We also show how an appropriate Ix can be chosen in order to increase this number.

The contribution of this work is twofold: first we formulate the problem of driving multiple motors by a single, power-constrained actuator node as an optimization problem. Second, we propose a strategy to maximize the number of simultaneously active motors that can be driven by a battery-powered node with maximum output current constraint. We also demonstrate the use of the proposed approach on a real-life prototype.

6.2 Related Work

The main approaches for tactile stimulation are electro-tactile and vibro-tactile [PSH03]. Electro-tactile stimulation uses electrodes to produce sensation through electric current. By changing electrode size and the properties of the applied waveform, different sensations can be produced. On the other hand, vibro-tactile stimulation uses mechanical vibrations to trigger the skin mechanoreceptors. It provides fewer control parameters for stimulations but its cost, size and robustness make it a more popular choice in various applications. Several works have focused on power optimization techniques in vibro-tactile and electro-tactile stimulations [TGY03, Per95, PW91, PSH03]. The work in [TGY03] shows that low duty cycle pulses produce the same sensitivity levels as 50 % duty cycle pulses. The power delivered to the frequency region of maximum tactile sensitivity (25-700 Hz) is optimized in [Per95] to minimize the overall power consumption.

However there has been little work done on power optimizations in rotary-motion tactors used in cell-phones (pager motors). [JC07] investigates the relationship between the perceived magnitude of vibrations and its power consumption. The authors show that more power does not always result in higher sensation magnitudes. Voltage is the only control variable used for power optimization in [JC07]. In this work we add another control variable for better optimizations of power

consumption.

6.3 Stimulation Model

The important factors to be considered for the perception of a tactile stimulation are: vibration frequency and amplitude, the location of stimulation on the body and the adaptation behavior. Adaptation in a tactile stimulation is defined as the reduced response to stimulation due to exposure to a continued stimulus [Nun89]. In order to prevent this physiological adaptation effect, a recovery time (a period without any stimulation) is added between two successive stimulations.

Another important aspect of tactile stimulation is the stimulation location. Tactile receptors have higher densities on the fingertips and face and lower densities on the back and legs. Spatial resolution is important in choosing the number and distance of tactors in different body parts.

In our experiments we use the palm of the hand as the stimulation location. Tactors are placed directly on the skin, however clothing can also be worn between the tactor and the skin. In this case, higher stimulation intensities are required to produce the same effect. To provide tactile feedback in body-worn contexts, we use vibro-tactile stimulation through actuators with characteristic similar to vibrators used in cell phones. They are a good choice since they are lightweight, inexpensive and small. We should add that one of the limitations of pager motors is their slow rise-time (100-200ms), therefore for applications requiring very strict timings, they are not recommended, but as far as providing haptic cues, they are sufficient.

The pager motor is composed of a motor with an eccentric mass. Applying voltage to the motor, results in rotation of the motor, which in turn causes stimulation to the skin. Higher voltages result in higher motor rotation velocities which are felt as higher intensity stimulation. This is known as one of the limitations of this type of motors, imposing only one control variable (voltage supplied to the motor) [JC07].

In this work, we produce stimulation through on-off pulses in a square-wave shape. By changing the duty cycle of these pulses we add another control variable to the system and study its effects on stimulation perception, power consumption and deployment in sensor nodes.

In detail, stimulation is produced through trains of rectangular pulses followed by a recovery period. The main characteristics of the excitatory waveform are: applied voltage, pulse frequency, duty cycle and recovery time. The pulse frequency used in our experiments is 150 Hz. Note that this frequency is different from what produces the vibrations in the motor. This is the frequency of the rectangular pulses in the excitatory waveform. In all of the following experiments we keep the recovery time constant at 1 sec. Duty cycle and voltage level are variables in the experiments.

6.4 Characterization and Parameter Optimization

In this section we describe the system prototype and the vibrator motor characteristics. We then give an optimal selection of parameters for minimum power consumption.

6.4.1 System Prototype

Active nodes driving the actuators discussed above usually embed a radio transceiver, a microcontroller, electro mechanical components and a battery to provide power supply for these units.

Using miniaturized nodes to derive vibrating motors (as low-cost tactors), needs good consideration of the power limitations of the battery supply. Additionally, wearability, unobtrusiveness and small size of the system are specific requirements which represent another key challenge to be addressed with integrated and small-sized components. Thus, the node adopts a modular architecture where each functional block is included at design time only if required by the application (e.g. some nodes would be equipped only with tactors and inertial sensors if required on a particular part of the body).

The main control block is based on an ultra-low power RISC microcontroller (MSP430 from Texas Instruments) which provides a good tradeoff between power consumption and performance. The radio section would be designed to meet both low-power requirements and high interoperability with other personal networks. In our prototype, a Bluetooth-based radio has been used, with an average power consumption of 20mW.

Finally an efficient power supply block is important to sustain the peak current requests from

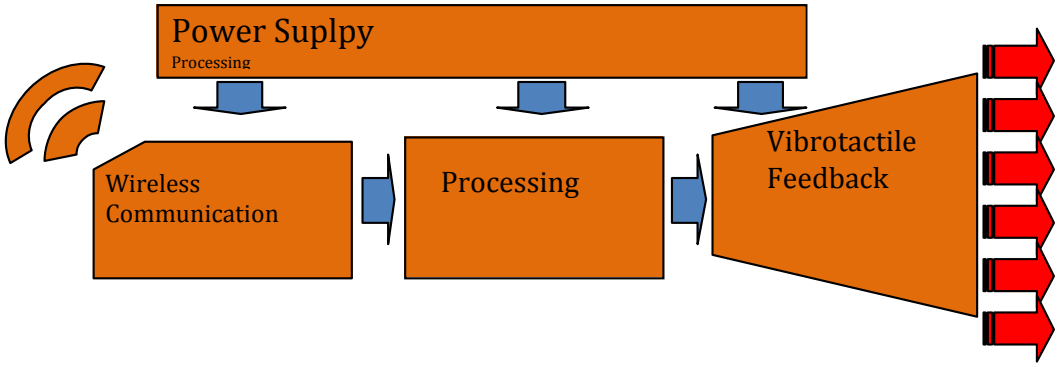

Figure 6.1: Sensor Node Block Diagram

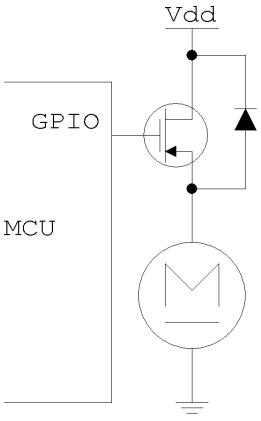

Figure 6.2: Driver Circuit for the Tactor

both the radio and the tactors. Usually a step-up converter is adopted to guarantee a constant supply voltage and to exploit all the energy in the battery, since a DC-DC device can operate also with input voltage of about 1V. Moreover an efficient DC-DC module can be coupled with energy harvesting circuits to collect and extract energy from human motion, thereby extending the lifetime of the system [Par06]. Figure 6.1 depicts the block diagram of our node prototype.

Modularity allows driving several motors. The vibro-tactile device used in our experiments is a 12mm shaft-less vibration motor from Precision Microdrives. It is 1.7g with a nominal speed of 9000 rpm, which means a vibration frequency of 150 Hz. Each motor is controlled by a GPIO signal from the microcontroller which drives a MOSFET able to provide enough current to the tactors. A diode is inserted to protect the circuit by spikes of current generated by the inductive coils of the motor as depicted in Figure 6.2.

6.4.2 Stimulation Waveform Parameter Selection

We studied the effects of changes in duty cycles of the excitatory waveform to the motor described in 4.1. Duty cycles were varied in the range of 5 % to 90 %. At each duty cycle, the applied voltage was changed until it reached the perceived sensation threshold (a threshold which re. Figure 6.3 shows the required voltage in each duty cycle at the perceived sensation threshold in a fixed frequency of 150 Hz. Duty cycles lower than 10 % could not reach the sensation threshold with the motor characteristics used. This is because they require a higher voltage than 5V and therefore are not shown.

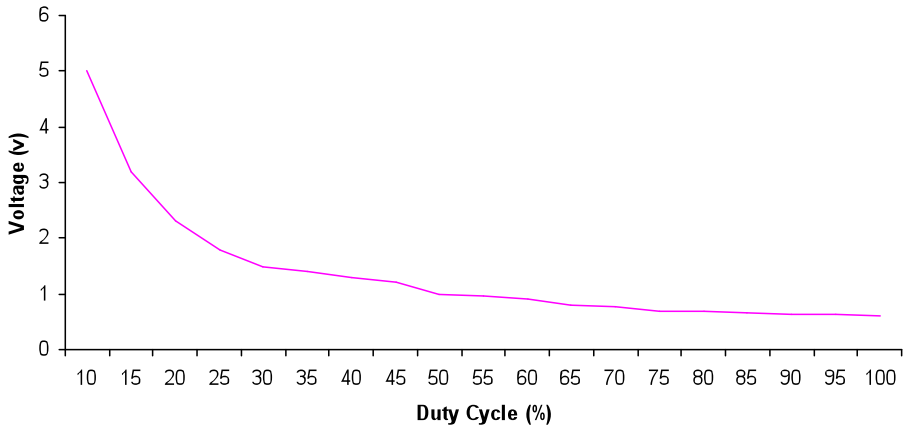

Figure 6.3: Voltage vs. Duty Cycle

In each duty cycle and its corresponding voltage at the perceived sensation threshold, the current values were measured and Power consumption was in turn computed with the $P = I \times V \times DutyCycle$ formula. Figure 6.4 shows the power consumption and current in each duty cycle.

Similar experiments were performed from the frequency perspective which shows that frequency change did not have any significant effect. Therefore the results indicate that a short (low duty-cycle) rectangular pulse is beneficial both from power consumption perspective and the current drawn. The latter is important when these actuators are used in battery-powered nodes. As it can be seen in Figure 6.4, lower duty cycles correspond to lower current values. Section 6.5 describes how lower duty cycle pulses are beneficial in such cases.

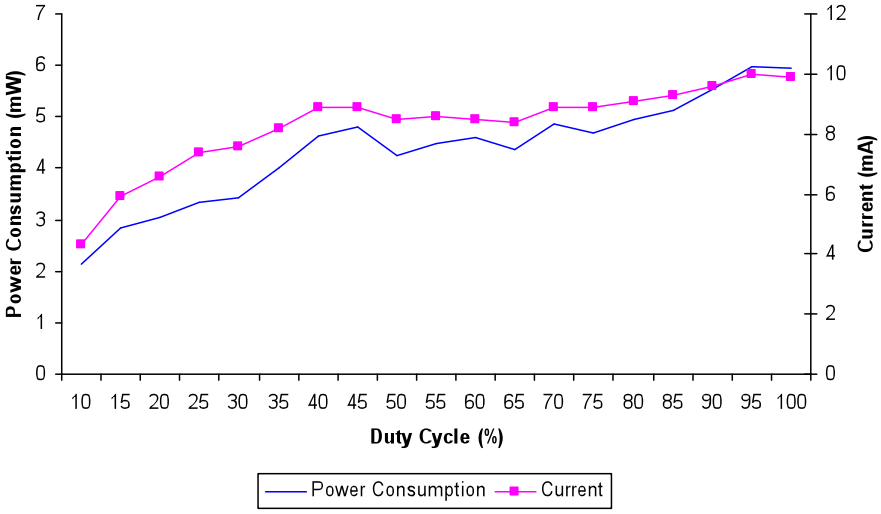

Figure 6.4: Power Consumption and Current vs. Duty Cycle

6.5 Maximizing the Number of Simultaneously Active Actuators in a Sensor Node

Results of Section 6.4 suggest that lower duty cycle pulses utilize less power to reach the perceived sensation threshold. In most applications the use of multiple tactors is required to meet applications requirements. In this section we propose a method to maximize the number of simultaneously active motors derived by a sensor node.

6.5.1 Maximum Number of Actuators vs. Battery Current

Batteries have a maximum discharge current, which is a characteristic of the type and size of the battery used. Therefore, the number of simultaneously active motors supported by a single battery is bounded by its maximum discharge current. The lower the current to drive one tactor is; the higher number of motors can be active at the same time. Here we can see that the lower currents corresponding to smaller duty cycles allow the activity of more tactors simultaneously.

A constant part of the maximum discharge current in batteries is used by the microcontroller on the sensor board. The remaining current bounds the number of active tactors. We call this remaining usable current ($I_{Batt-max}$). The trivial approach to activate multiple actuators would

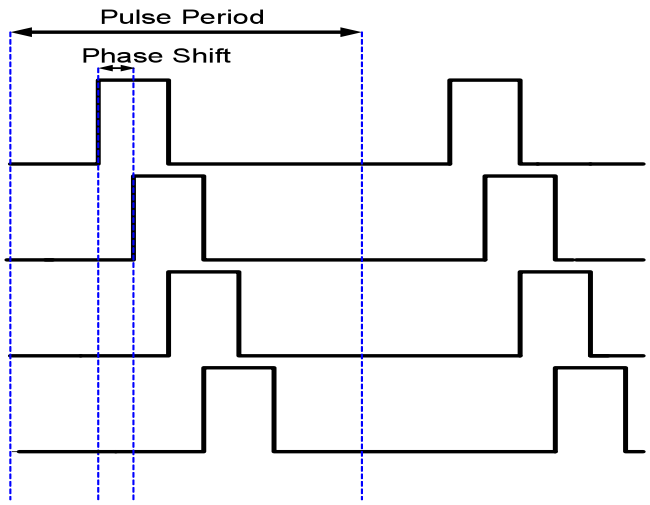

Figure 6.5: Multiple Waveforms with Phase Shifts

activate as many motors at the same time as the maximum discharge current allows. This number is determined by $\left\lfloor \frac{I_{Batt-max}}{I_{Stim}} \right\rfloor$ where I_{Stim} is the current corresponding to the lowest duty cycle resulting in minimum power consumption (duty-cyclemin).

In order to activate the maximum number of possible tactors, we propose a method which makes use of the low signal section of the pulse (when the signal is 0 in a pulse period). We also allow a small delay between the activation of different tactors instead of activating them at exactly the same time.

Figure 6.5 shows how multiple pulses can be overlapped in a pulse period with a phase shift. Note that in this figure each pulse is driving a separate motor. With this activation scheme, the actual stimulation by each motor is not at the exact same time but the maximum delay between two different pulses is at most equal to the pulse period which is insignificant for the human body and it is not perceptible by the user. In this scheme lower duty cycles are not only beneficial in consuming less power but also in using less space in a pulse period and in turn allowing more active actuators.

We performed experiments to measure the perceived delay of stimulations of different motors at various frequencies. The results indicate that for frequencies higher than 30Hz, the subject cannot perceive any delay between stimulations with the maximum phase shifts equal to the pulse period (T).

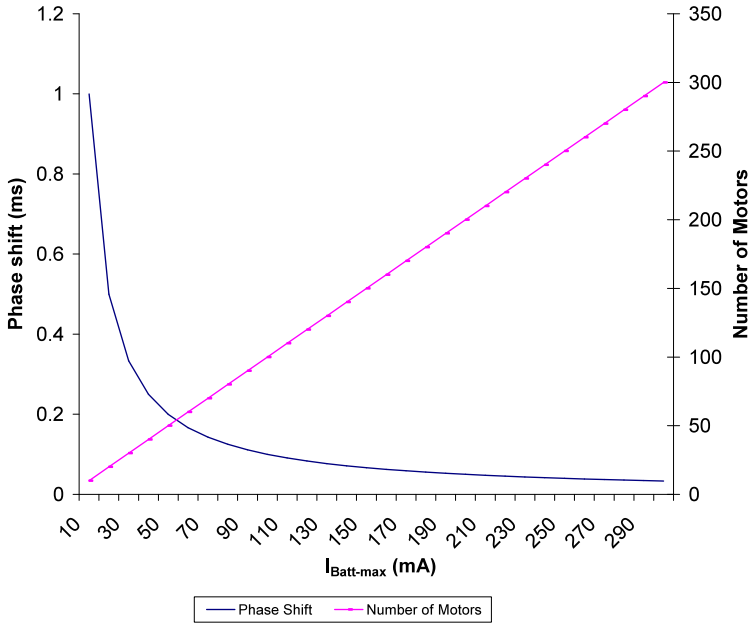

Figure 6.6: Number of Simultaneously Active Motors vs. IBatt-max vs. Phase Shift at Duty Cycle 10 %

As Figure 6.5 depicts the maximum discharge current determines the phase shift required for delays between tactor stimulations. Equations 6.1 and 6.2 show the formula to obtain these parameters.

$$PhaseShift = dutyCycle_{min} \times \frac{I_{Stim}}{I_{Batt-max}} \times T \tag{6.1}$$

$$Numberof\,ActiveMotors = \frac{T}{PhaseShift} \tag{6.2}$$

Figure 6.6 shows how the number of simultaneously allowed active motors changes with the type of battery used in the sensor node with duty cycle of 10 %. Designers can choose their battery based on the specific number of motors required by their applications and accordingly choose the phase shift required. From another perspective, applications determine the battery requirements of a sensor node, and our phase-shift policy makes it possible to use smaller and inexpensive batteries or to avoid the use of expensive super-capacitors while still supporting a large number of simultaneously active motors.

Using this method the number of active motors is increased significantly. In a scenario where the characteristics of the battery and tactor used result in $\left\lfloor \frac{I_{Batt-max}}{I_{Stim}} \right\rfloor = 4$, the trivial method would only activate 4 motors in a pulse period. However according to Equations 6.1 and 6.2, this number increases to 40 (assuming $dutycycle_{min}$ = 10 % as in above) for our proposed method.

6.5.2 Quality of Service

Battery life extension is a key objective in the design of wireless nodes. This is important due to the cost and difficulty to exchange or recharge batteries. In our analysis, we discuss the system from the Quality of Service (QoS) point of view.

Quality of service in applications providing haptic feedback through tactile stimulation in wearable contexts can be defined as a function of number of motors used. Therefore based on the requirements of an application this function can be different. For instance applications requiring exactly a specific number of motors to convey information, would have the QoS vs. number of motors as a step function. On the other hand, in other applications, QoS can linearly increase with the number of motors.

From another perspective, the ideal relation between the battery capacity and its discharge time (t) is $C = t \times I$. In the above formula I is the discharge current. But in reality this equation does not fully hold. Larger discharge currents tend to decrease the battery efficiency. Therefore this equation can be rewritten as:

$$C = t \times I^{\alpha} \tag{6.3}$$

Here, a is the Peukert's value [LR02], which is greater than 1. From above, there is a trade-off associated with maximum active tactors and the battery's lifetime. Figure 6.7 shows this.

Higher discharge rates correspond to a larger number of simultaneously active motors. The product of QoS and battery lifetime represents a trade-off metric that balances between the system quality of service and the lifetime of the battery. The optimum number of motors that maximize this product mainly depends on the shape of the quality of service function which is application-

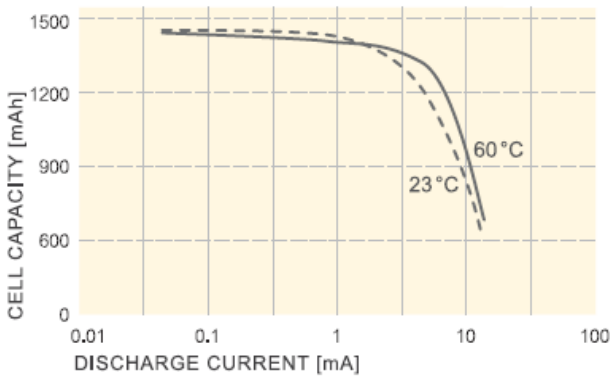

Figure 6.7: Battery Capacity vs. Charge

dependent. Below we show this with an example of two applications with different functions of QoS vs. number of motors. Figure 6.8.a shows this function for each application, while Figure 6.8.b shows the relation of QoS vs. the load current. Figure 6.8.(b) is simply obtained from Figure 6.8.a by using the information from Figure 6.6.

In order to maximize the product described above we need to find the load current and its corresponding number of motors that maximize the graph in Figure 6.9, which depicts this product. In this example the number of motors that maximizes the product of capacity and QoS for application 1 is 50 while it is 10 for application 2. The number of motors is calculated from Equations 6.1 and 6.2 using their corresponding I load as $I_{Batt-max}$ that maximizes the graphs in Figure 6.9.

The number of motors derived from this approach, minimizes the power consumption and prolongs battery lifetime based on the QoS of the specific application. Designers can find this optimum number based on the battery they are using and their applications needs.

6.6 Conclusion

Tactile stimulation is used as a means of transferring information through tactile interfaces. In this Chapter we looked into the use of vibro-tactile stimulators in producing haptic feedback in sensor nodes. We used stimulators similar to the ones used in cell phones. We investigated how the parameter selection of the excitatory signal can affect the power consumption of the system. We then

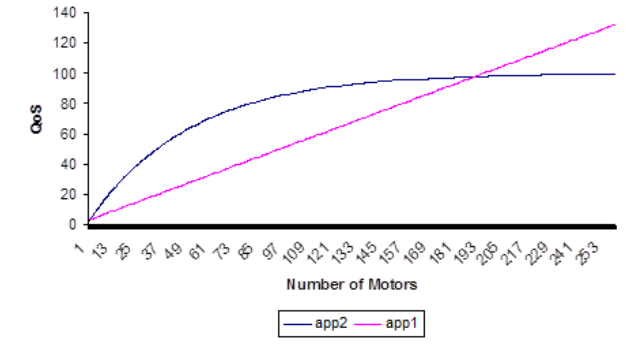

(a)

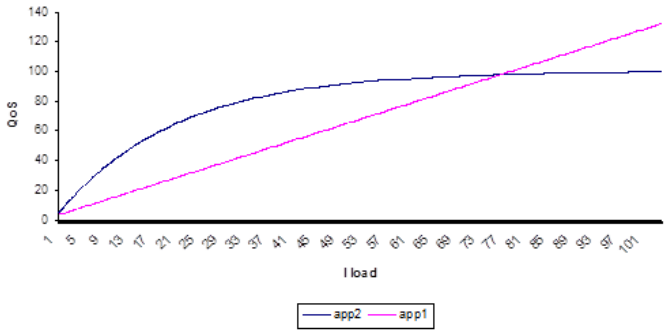

(b)

Figure 6.8: (a) QoS vs. Number of Motors for Application1 and 2. (b) QoS as a Function of Battery Load Current for Applications 1 and 2.

looked into how to choose these parameters in order to maximize the number of simultaneously allowed active tactors derived by a single battery. Results showed that signals with lower duty cycles, result in both lower power consumption and allow a higher number of the overall simultaneously active tactors. The quality of service associated to the use of these tactors in a sensor node was also discussed.

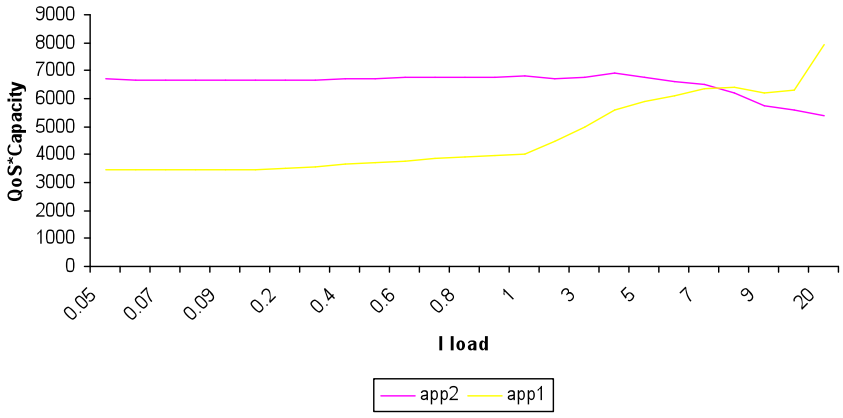

Figure 6.9: Product of Battery Capacity and QoS vs. Load Current

CHAPTER 7

Conclusions

The emergence of low cost micro-electronics and wireless systems has enabled the practical application of wearable monitoring systems that promote health and well-being of individuals. This new area when studied from a computer science point of view requires numerous problems to be solved. There are potentials for inventing new sensor devices and end-to-end systems that serve the needs of the medical community in addition to building systems that monitor different aspects of health, deliver therapies in real time with minimal intrusion and cost. Research effort remains to aim for the most effective applications of home-based and mobile technologies to increase adherence to rehabilitation and medical instructions, enable skills and exercise practice with feedback about performance, reduce muscle wasting in ill inpatients, and improve self-care management of chronic conditions. In this dissertation I discussed challenges associated with design of such systems and developed new methods that can enable widespread use of these systems to address the recently growing demand of accessible health care services. I focused on these challenges in two categories of medical monitoring systems that ubiquitously collect medical data and feedback systems that could enforce awareness, deliver therapies in real-time and increase adherence to rehabilitation and medical instructions. Specifically, I focused on the most significant challenges of these systems which are energy consumption and accuracy vs. cost of these systems.

Most wireless health systems are wearable and therefore operate on battery power. On the other hand, in order to enable real-time monitoring round the clock, long life-time is required. In this dissertation I looked at designing intelligent sampling and data aggregation strategies which are often tied with application level understanding of the semantics of the system in order to minimize energy consumption. In addition, for these systems to be widely exploited in large populations, they need to be designed in-expensively and also sometimes even disposable due to hygiene con-

straints. But the main limitation is the precision levels required by these systems. I looked into this problem by either taking advantage of sensors already existing on hand-held devices that people carry with the addition of minimal add-ons or by using inexpensive material for system production but taking into account the inaccuracies at different levels of system design.

Based on the topics discussed in this dissertation, the future directions of this work can be categorized as below:

7.1 Architecture Stack Design in Wireless Health Monitoring Systems

A future direction for this dissertation is to design, prototype and develop the architecture stack for end-to-end Wireless Health monitoring systems. This stack is shown below in Figure 7.1 focusing on the sensing dimension for the sake of simplicity; other dimensions (e.g. communication and data storage) are not listed.

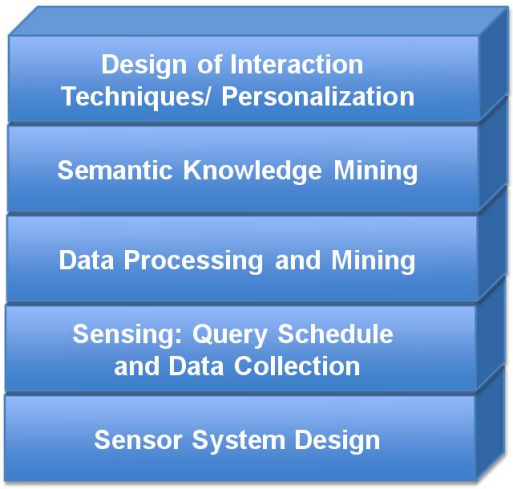

Figure 7.1: Architecture Stack of Wireless Health Monitoring Systems

Personalization of the health-care experience requires studying as it engages individuals in taking control of their own health care. Novel interaction techniques need to be designed to engage people in this process. Gaming for health is a good example for this. New interaction techniques that involve gestures which are more suitable for handicapped individuals need to be addressed. Understanding the semantics of application and behavior, developing new models and identifying diagnostic metrics can have huge effect in intelligent optimized design techniques and savings in

below layers of data processing and collection.

Design of novel sensors for quantifying medical perception potentially by reusing sensor-rich carry-on devices (e.g. , cell phones) as health devices (Example: The phone prototype of Quantifying medical palpation system described in Chapter 3) that are cost effective while reliable and secure enough to satisfy diagnostic metrics specific to the medical diagnosis of interest, is an area with huge potentials. These systems can become reconfigurable to serve different needs.

Providing a balance trade-off between cost and accuracy of medical embedded systems is an area that still requires research. As mentioned the inexpensive platforms that enable the instrumentation of low cost devices sometimes lack the accuracy required by the medical applications that they target (example: E-Textiles). Based on the findings of my current research, new methods need to be developed to account for these inaccuracies in different levels of design such as designing error checking mechanisms at circuit level or high in application level. Application level error checking is only possible by understanding the semantics of the medical application and aiming for optimizing accuracy in detecting the medical features of interest.

7.2 Haptic Diagnosis

Based on the study I presented in Chapter 3, I believe haptic diagnosis is promising in various areas and can have huge impacts. I believe the systems described in Chapter 3 have huge potentials for other new applications and areas of research specifically in the areas listed below:

- Using haptic diagnosis for assessing body tissue stiffness.
- Arterial Pressure Pulse Palpation.
- Teaching palpatory skills to medical students.
- Telemedicine - used in rural locations.
- Palpating masses such as cysts and abnormalities for cancer detection.
- Palpating and assessment of Thyroid.

- To be used in documentation and recording of medical assessments and their progress over time.

REFERENCES

[Aro09] Van Cauter E Tasali E. Aronsohn RS, Whitmore H. "Impact of untreated obstructive sleep apnea on glucose control in type 2 diabetes." *Am J Respir Crit Care Med.*, pp. 507–513, 2009.

[BF00] Schurr M. O. Buess, G. E and S. C. Fischer. "Robotics and Allied Technologies in Endoscopic Surgery." *Arch Surg.*, pp. 229–235, 2000.

[BMY01] Eric R. Bachmann, Robert B. McGhee, Xiaoping Yun, and Michael J. Zyda. "Inertial and magnetic posture tracking for inserting humans into networked virtual environments." In *Proceedings of the ACM symposium on Virtual reality software and technology*, VRST '01, pp. 9–16, New York, NY, USA, 2001. ACM.

[Bro92] Lisa Gottesfeld Brown. "A survey of image registration techniques." *ACM Comput. Surv.*, **24**(4):325–376, December 1992.

[CFE07] Sergey Y. Chekmenev, Aly A. Farag, and Edward A. Essock. "Thermal Imaging of the Superficial Temporal Artery: An Arterial Pulse Recovery Model." In *CVPR*. IEEE Computer Society, 2007.

[CHX08] Meng Chen, Bufu Huang, Yangsheng Xu, and A Motivation. "Intelligent shoes for abnormal gait detection." *2008 IEEE International Conference on Robotics and Automation*, pp. 2019–2024, 2008.

[CL11] Cheng-Chang Yeh Chung-Shing Hu, Yu-Feng Chung and Ching-Hsing Luo. "Temporal and Spatial Properties of Arterial Pulsation Measurement Using Pressure Sensor Array." *Evidence-Based Complementary and Alternative Medicine*, 2011.

[Col70] Compton Collins. "Tactile Television-Mechanical and Electrical Image Projection." *IEEE TRANSACTIONS ON MANMACHINE SYSTEMS*, **MM**(1):65–71, 1970.

[Dav03] Allan D Davies, Justine Ina; Struthers. "Pulse wave analysis and pulse wave velocity: a critical review of their strengths and weaknesses." *Journal of Hypertension*, **21(3)**:463–472, 2003.

[DK57] William Dement and Nathaniel Kleitman. "Cyclic variations in EEG during sleep and their relation to eye movements, body motility, and dreaming." *Electroencephalography and Clinical Neurophysiology*, **9**(4):673 – 690, 1957.

[EH1a] "F-Scan http://www.tekscan.com/medical/system-fscan1.html.".

[EH1b] "Pedar: plantar pressure system. http://www.novel.de.".

[EH305] "Energy Harvesting Projects." *IEEE Pervasive Computing*, **4**:69–71, 2005.

[EM00] D. H. Evans and W. N. McDicken. "Doppler Ultrasound: Physics, Instrumentation and Signal Processing (Second Edition)." *Physiological Measurement*, **21**(3):425, 2000.

[HBB06] H.L.P. Hurkmans, J.B.J. Bussmann, E. Benda, J.A.N. Verhaar, and H.J. Stam. "Accuracy and repeatability of the Pedar Mobile system in long-term vertical force measurements." *Gait and Posture*, **23**(1):118 – 125, 2006.

[HKO06] Kozo Hirata, Masanobu Kawakami, and Michael F O'Rourke. "Pulse wave analysis and pulse wave velocity: a review of blood pressure interpretation 100 years after Korotkov." *Circulation journal official journal of the Japanese Circulation Society*, **70**(10):1231–1239, 2006.

[HL991] "Prevention of stroke by antihypertensive drug treatment in older persons with isolated systolic hypertension: Final results of the Systolic Hypertension in the Elderly Program (SHEP)." *JAMA*, pp. 3255–3264, 1991.

[HSM00a] T. Harada, A. Sakata, T. Mori, and T. Sato. "Sensor pillow system: monitoring respiration and body movement in sleep." In *Intelligent Robots and Systems, 2000. (IROS 2000). Proceedings. 2000 IEEE/RSJ International Conference on*, volume 1, pp. 351 –356 vol.1, 2000.

[HSM00b] T. Harada, A. Sakata, T. Mori, and T. Sato. "Sensor pillow system: monitoring respiration and body movement in sleep." In *Intelligent Robots and Systems, 2000. (IROS 2000). Proceedings. 2000 IEEE/RSJ International Conference on*, volume 1, pp. 351 –356 vol.1, 2000.

[JA09] Micah K. Johnson and Edward H. Adelson. "Retrographic sensing for the measurement of surface texture and shape." In *Computer Vision and Pattern Recognition (CVPR)*, pp. 1070–1077, 2009.

[JC07] Jaehoon Jung and Seungmoon Choi. "Perceived magnitude and power consumption of vibration feedback in mobile devices." In *Proceedings of the 12th international conference on Human-computer interaction: interaction platforms and techniques*, HCI'07, pp. 354–363, Berlin, Heidelberg, 2007. Springer-Verlag.

[JSA10] Maurice Janssen, Robert Stokroos, Jos Aarts, Rob van Lummel, and Herman Kingma. "Salient and placebo vibrotactile feedback are equally effective in reducing sway in bilateral vestibular loss patients." *Gait and amp Posture*, **31**(2):213 – 217, 2010.

[KMB03] Jeonghun Ku, Richard Mraz, Nicole Baker, Konstantine K Zakzanis, Jang Han Lee, In Y Kim, Sun I Kim, and Simon J Graham. "A data glove with tactile feedback for FMRI of virtual reality experiments." *Cyberpsychology and Behavior*, **6**(5):497–508, 2003.

[KW09] K. Meyer K. W. Bollhoefer and R. Witzsche. "Microsoft surface und das Natural User Interface (NUI)." In *Technical report, Pixelpark*, Feb 2009.

[LB66] J.G. Linvill and J.C. Bliss. "A direct translation reading aid for the blind." *Proceedings of the IEEE*, **54**(1):40 – 51, jan. 1966.

[LIS09] Tao Liu, Yoshio Inoue, and Kyoko Shibata. "Development of a wearable sensor system for quantitative gait analysis." *Measurement*, **42**(7):978 – 988, 2009.

[LR02] D. Linden and T.B. Reddy. *Handbook of batteries*. McGraw-Hill handbooks. McGraw-Hill, 2002.

[McC99] Teri L Gibbons LE Kukull WA Bowen JD McCormick WC Larson EB McCurry SM, Logsdon RG. "Characteristics of sleep disturbance in community-dwelling Alzheimer's disease patients." *J Geriatr Psychiatry Neurol*, pp. 53–59, 1999.

[McN00] W. T. McNicholas. "SImpact of Sleep in COPD." *CHEST -CHICAGO-*, **117**:48–53, 2000.

[MCP07] Alfonso Martnez-Nova, Jos Carlos Cuevas-Garca, Javier Pascual-Huerta, and Raquel Snchez-Rodrguez. "BioFoot in-shoe system: Normal values and assessment of the reliability and repeatability." *The Foot*, **17**(4):190 – 196, 2007.

[Mil07] Cappuccio FP. Miller MA. "Inflammation, sleep, obesity and cardiovascular disease." *Curr Vasc Pharmacol*, pp. 93–102, 2007.

[Mol93] Rasmussen LS Jensen PF Pedersen BD Ravlo O Rasmussen NH Espersen K Johannessen NW Cooper JB Moller JT, Pedersen T. "Randomized evaluation of pulse oximetry in 20,802 patients: I. Design, demography, pulse oximetry failure rate, and overall complication rate." *Anesthesiology*, pp. 436–444, 1993.

[NDM10] Hyduke Noshadi, Foad Dabiri, Saro Meguerdichian, Miodrag Potkonjak, and Majid Sarrafzadeh. "Energy optimization in wireless medical systems using physiological behavior." In *Wireless Health 2010*, WH '10, pp. 128–136, New York, NY, USA, 2010. ACM.

[Nes] Sally A. Ness. *Body, Movement and Culture: Kinesthetic and Visual Symbolism in a Philippine Community (Series in Contemporary Ethnography)*. University of Pennsylvania Press.

[NH02] Y. Nishida and T. Hori. "Non-invasive and unrestrained monitoring of human respiratory system by sensorized environment." In *Sensors, 2002. Proceedings of IEEE*, volume 1, pp. 705 – 710 vol.1, 2002.

[Nun89] Jarmul E Lipetz LE Weed HR Nunziata E, Perez C. "Effect of Tactile Stimulation Pulse Characteristics on Sensation Threshold and Power Consumption." *Ann Biomed Eng.*, pp. 423–435, 1989.

[OG96] M.F. ORourke and D.E. Gallagher. "Pulse wave analysis." *Journal of Hypertension*, **14**:147–157, 1996.

[OPJ01] Michael F O'Rourke, Alfredo Pauca, and Xiong-Jing Jiang. "Pulse wave analysis." *British Journal of Clinical Pharmacology*, **51**(6):507–522, 2001.

[Pa02] Thomas V. Papakostas and et al. "5.3: A large area force sensor for smart skin applications." In *SENSORS, 2002, PROC. OF IEEE*, 2002.

[Par06] Joseph A. Paradiso. "Systems for human-powered mobile computing." In *Proceedings of the 43rd annual Design Automation Conference*, DAC '06, pp. 645–650, New York, NY, USA, 2006. ACM.

[Per95] Muiioz P. Perez C.A. "Optimization of the Power Targeted to the Frequency Region of Maximum Tactile Sensitivity." *Medical Progress through Technology*, pp. 67–76, 1995.

[PHB00] Joseph Paradiso, Kai yuh Hsiao, Ari Benbasat, and Zoe Teegarden. "Design and Implementation of Expressive Footwear." *IBM Systems Journal*, **39**:511–529, 2000.

[PLH09] Shyamal Patel, Konrad Lorincz, Richard Hughes, Nancy Huggins, John Growdon, David Standaert, Metin Akay, Jennifer Dy, Matt Welsh, and Paolo Bonato. "Monitoring motor fluctuations in patients with Parkinson's disease using wearable sensors." *Trans. Info. Tech. Biomed.*, **13**(6):864–873, November 2009.

[Pri07] Shashank Priya. "Advances in energy harvesting using low profile piezoelectric transducers." *Journal of Electroceramics*, **19**:167–184, 2007. 10.1007/s10832-007-9043-4.

[PS05] Joseph A. Paradiso and Thad Starner. "Energy Scavenging for Mobile and Wireless Electronics." *IEEE Pervasive Computing*, **4**(1):18–27, January 2005.

[PSH03] C. Perez, A. Santibaez, C. Holzmann, P. Estvez, and C. Held. "Power requirements for vibrotactile piezo-electric and electromechanical transducers." *Medical and Biological Engineering and Computing*, **41**:718–726, 2003. 10.1007/BF02349980.

[PW91] C.A. Perez and H.R. Weed. "Optimization Of The Relationship Between Pulse Width, Pulse Frequency And Sensation Thresholds For Vibrotactile Information Transfer." In *Engineering in Medicine and Biology Society, 1991. Vol.13: 1991., Proceedings of the Annual International Conference of the IEEE*, pp. 1805 –1806, oct-3 nov 1991.

[Rei05] Skatrud JB Young T. Reichmuth KJ, Austin D. "Association of Sleep Apnea and Type II Diabetes: a Population-Based Study." *Am J Respir Crit Care Med.*, pp. 1590–1595, 2005.

[RJ79] Hetzel M. R. and Clark T. J. "Does sleep cause nocturnal asthma?" *Thorax*, pp. 749–754, 1979.

[RSB11] Mahsan Rofouei, Mike Sinclair, Ray Bittner, Tom Blank, Nick Saw, Gerald DeJean, and Jeff Heffron. "A Non-invasive Wearable Neck-Cuff System for Real-Time Sleep Monitoring." In *Proceedings of the 2011 International Conference on Body Sensor Networks*, BSN '11, pp. 156–161. IEEE Computer Society, 2011.

[RSS07] T. Rago, F. Santini, M. Scutari, A. Pinchera, and P. Vitti. "Elastography: New Developments in Ultrasound for Predicting Malignancy in Thyroid Nodules." *Journal of Clinical Endocrinology and Metabolism*, **92**(8):2917–2922, 2007.

[RWR04] Shad Roundy, Paul Kenneth Wright, and Jan M. Rabaey. *Energy Scavenging for Wireless Sensor Networks: With Special Focus on Vibrations*. Kluwer Academic Publishers, Norwell, MA, USA, 2004.

[Sav] Pinder SJ Tomson CR. Savage MT, Ferro CJ. "Reproducibility of derived central arterial waveforms in patients with chronic renal failure.".

[SGB01] D. Salle, F. Gosselin, Ph. Bidaud, and Ph. Gravez. "Analysis of haptic feedback performances in telesurgery robotic systems." In *Robot and Human Interactive Communication, 2001. Proceedings. 10th IEEE International Workshop on*, pp. 618 –623, 2001.

[SGW00] Jan A Staessen, Jerzy Gasowski, Ji G Wang, Lutgarde Thijs, Elly Den Hond, Jean-Pierre Boissel, John Coope, Tork Ekbom, Franois Gueyffier, Lisheng Liu, Karla Kerlikowske, Stuart Pocock, and Robert H Fagard. "Risks of untreated and treated isolated systolic hypertension in the elderly: meta-analysis of outcome trials." *The Lancet*, **355**(9207):865 – 872, 2000.

[Sin97] Michael Sinclair. "The haptic lens." In *ACM SIGGRAPH 97 Visual Proceedings: The art and interdisciplinary programs of SIGGRAPH '97*, SIGGRAPH '97, pp. 179–, New York, NY, USA, 1997. ACM.

[SIP05] Henry A. Sodano, Daniel J. Inman, and Gyuhae Park. "Comparison of Piezoelectric Energy Harvesting Devices for Recharging Batteries." *Journal of Intelligent Material Systems and Structures*, **16**(10):799–807, 2005.

[Sle] "Nonin: http://www.nonin.com/.".

[Sle99] American Academy of Sleep Medicine Task Force. "Sleep-related breathing disorders in adults: recommendations for syndrome definition and measurement techniques in clinical research. The Report of an American Academy of Sleep Medicine Task Force." *Sleep*, 1999.

[Sle09] "Sleep Apnea: What Is Sleep Apnea?" *NHLBI: Health Information for the Public*, 2009.

[SP01] Nathan S. Shenck and Joseph A. Paradiso. "Energy Scavenging with Shoe-Mounted Piezoelectrics." *IEEE Micro*, **21**(3):30–42, May 2001.

[SR07] H.A. Sodano S.R. Anton. "A review of power harvesting using piezoelectric materials." *Smart Mater. Struct.*, **16**(3), 2007.

[SRN09] Myung-kyung Suh, Mahsan Rofouei, Ani Nahapetian, William J. Kaiser, and Majid Sarrafzadeh. "Optimizing Interval Training Protocols Using Data Mining Decision Trees." In *Proceedings of the 2009 Sixth International Workshop on Wearable and Implantable Body Sensor Networks*, BSN '09, pp. 318–323, Washington, DC, USA, 2009. IEEE Computer Society.

[SSL02] Albrecht Schmidt, Martin Strohbach, Kristof van Laerhoven, Adrian Friday, and Hans-Werner Gellersen. "Context Acquisition Based on Load Sensing." In *Proceedings of the 4th international conference on Ubiquitous Computing*, UbiComp '02, pp. 333–350, London, UK, UK, 2002. Springer-Verlag.

[T10] "www.eeonyx.com/.".

[T25] "http://inqri.blogspot.com/2009/10/elderly-fall-injuries-cost-20-billion.html.".

[T26] "http://www.smartcarpet.com/.".

[Taf09] Mehdi Tafti. "Genetic aspects of normal and disturbed sleep." *Sleep Medicine*, **10, Supplement 1**(0):S17 – S21, 2009. ¡ce:title¿The Art of Good Sleep Proceedings from the 6th International Sleep Disorders Forum: Sleep and Society¡/ce:title¿.

[TGY03] Hong Z. Tan, Robert Gray, J. Jay Young, and Ryan Traylor. "A Haptic Back Display for Attentional and Directional Cueing." *Journal of Haptics Research*, **3**:20, 2003.

[Tob02] Batchelder PB Tobin RM, Pologe JA. "A characterization of motion affecting pulse oximetry in 350 patients." *Anesthesia and Analgesia*, pp. 54–61, 2002.

[Wan98] Xiang JL. Wang BH. "Experiment design and power-spectral characteristics of pulse signal." *Chin J Phys Med.*, pp. 158 – 161, 1998.

[WC84] Robert T. Wilkinson and Ken B. Campbell. "Effects of traffic noise on quality of sleep: Assessment by EEG, subjective report, or performance the next day." *The Journal of the Acoustical Society of America*, **75**(2):468–475, 1984.

[WCJ07] Jih-Huah Wu, Rong-Seng Chang, and Joe-Air Jiang. "A Novel Pulse Measurement System by Using Laser Triangulation and a CMOS Image Sensor." *Sensors*, **7**(12):3366–3385, 2007.

[WK08] T Wacharasindhu and J W Kwon. "A micromachined energy harvester from a keyboard using combined electromagnetic and piezoelectric conversion." *Journal of Micromechanics and Microengineering*, **18**(10):104016, 2008.

[Woo92] Robert J. Woodham. "Shape recovery." chapter Photometric method for determining surface orientation from multiple images, pp. 115–120. Jones and Bartlett Publishers, Inc., USA, 1992.

[Xu08] Meng M.Q. Shi C. Wang K.Q. Li N.M. Xu, L.S. "Quantitative Analyses of Pulse Images in Traditional Chinese Medicine." pp. 175–189, 2008.

[YM09] A. Yadollahi and Z. Moussavi. "Acoustic obstructive sleep apnea detection." In *Engineering in Medicine and Biology Society, 2009. EMBC 2009. Annual International Conference of the IEEE*, pp. 7110 –7113, sept. 2009.

[YXL05] Weizhong Ye, Yangsheng Xu, and Ka Keung Lee. "Shoe-Mouse: An Integrated Intelligent Shoe." *2005 IEEERSJ International Conference on Intelligent Robots and Systems*, pp. 1947–1951, 2005.

[Zho94] Zhu DZ. Zhou SH. "The blood dynamics analysis of taut pulse mechanism." *Liaoning Journal TCM*, pp. 49–51, 1994.